NUMERICAL SIMULATION OF IMPACT ROLLERS FOR ESTIMATING THE INFLUENCE DEPTH OF SOIL COMPACTION

A Thesis

by

KUKJOO KIM

Submitted to the Office of Graduate Studies of
Texas A&M University
in partial fulfillment of the requirements for the degree of

MASTER OF SCIENCE

August 2010

Major Subject: Civil Engineering

NUMERICAL SIMULATION OF IMPACT ROLLERS FOR ESTIMATING THE INFLUENCE DEPTH OF SOIL COMPACTION

A Thesis

by

KUKJOO KIM

Submitted to the Office of Graduate Studies of
Texas A&M University
in partial fulfillment of the requirements for the degree of

MASTER OF SCIENCE

Approved by:

Chair of Committee,	Jean-Louis Briaud
Committee Members,	Charles Aubeny
	Mark Everett
Head of Department,	John Niedzwecki

August 2010

Major Subject: Civil Engineering

ABSTRACT

Numerical Simulation of Impact Rollers for Estimating the Influence Depth of Soil Compaction.

(August 2010)

Kukjoo Kim, B.E., Korea Military Academy, Seoul, Korea

Chair of Advisory Committee: Dr. Jean-Louis Briaud

The use of impact rollers has increased for many decades over a wide variety of applications in various parts of the world. Many manufacturers have made claims that impact compaction rollers could have an effect to 1 m or more. In addition, other positive features such as greater depth of influence and faster travel speed than conventional rollers are being reported from the field. However, there is a lack of theoretical explanations or scientific research information for how to operate these rollers. Hence, this study will focus on a geotechnical modeling that describes the behavior of soils during ground compaction using various impact rollers (e.g., triangular, Landpac 3-sided, Landpac 5-sided, and octagonal shapes). In addition, this study will estimate more precisely the depth of influence for impact rollers.

To do so, the general purpose finite element computer program LS-DYNA is used for numerical predictions. The finite element study is carried out with three-dimensional models. A simplified elastic perfectly plastic model with the Druker-Prager

yield criterion is used for soil modeling and rollers are treated as a rigid body (i.e., incompressible material).

The result of this study compares well with existing field experiment data for estimating vertical stress profile and compaction features, and demonstrates that the impact rollers are appropriate for thick layers.

DEDICATION

To my wife, Soonjung Woo and my family with love

ACKNOWLEDGEMENTS

First of all, I sincerely appreciate my advisor Dr. Briaud. He has always inspired and believed in me, and he has given specific guidance to complete my thesis. I also would like to thank Dr. Aubeny and Dr. Everett for providing the guidance in the area of the intelligent soil compaction and for serving on my committee. Secondly, I appreciate my country, the Republic of Korea, and the Korea Army Corps of Engineers. My country and the Army gave me the chance to study geotechnical engineering and also have supported me in many ways. Finally, I sincerely appreciate my wife. She has always been my most important mentor and advisor, and she is the reason I am where I am today.

TABLE OF CONTENTS

Page

LIST OF FIGURES

Page

Page

Page

Page

LIST OF TABLES

1. INTRODUCTION

1.1. GENERAL

Impact compaction was invented in 1949 in order to address the deep compaction problems. Over the last 20 years, the use of impact compaction has grown for a wide range of earthworks projects around South Africa, Australia, and many other countries because roads have to withstand larger truck loads or heavier aircraft than before and many countries are reclaiming land from the sea. In particular, it was used for the construction of the Hong Kong Chep Lap Kok Airport runways which was one of the largest construction projects in the 20th century.

Impact compaction rollers are comprised of non-circular modules rotating due to the frictional force on the ground surface, and they fall to impact the ground dynamically. For example, Landpac has impact rollers with a 3-sided and a 5-sided module, and Bomag has an 8-side module towed at 10-12 km/h. Furthermore, the impact compaction rollers offer an alternative compaction solution that can prove cost-effective. The key feature of impact rollers is that they provide deeper layer compaction because they travel at a relatively high speed compared to conventional machines and impart substantial impact energy into the ground. As a result, the impact compaction rollers have a significantly greater depth of influence than conventional rollers.

However, there is a lack of available verification, scientific research information,

---

This thesis follows the style of *Journal of Geotechnical and Geoenvironmental Engineering*.

and professional guidance in spite of the benefits of deep compaction offered by impact compaction rollers. Consequently, many geotechnical engineers and designers have relied on product marketing documents and reported project experiences.

1.2. RESEARCH OBJECTIVES

The primary purpose of this study is to predict the depth of influence of the compaction process using the different types of impact rollers, to make direct comparison between the impact roller shapes and the depths of influence, and to verify the efficiency of ground improvement. For this purpose, this study is restricted to using identical drum weights and does not include other issues. These issues are the effect of the wave absorption and reflection, water table within the zone of influence of the compaction, and layers. The depths of influence of various rollers are determined by the finite element method (FEM) and are also compared to the results of field data (i.g., Bomag (Wallrath, W., 2004) and Broons field data). To model the soil material, the simplified elastic perfectly plastic model with Druker-Prager yield criterion when the roller compacts the ground was considered.

1.3. THESIS ORGANIZATION

This thesis is composed of five sections. The first section of the thesis addresses the background including the problem statement and research objectives. The second part of the thesis provides a review of the existing knowledge of soil compaction, intelligent compaction, and impact rollers. The third section presents the methodology

such as the FEM modeling process, and the simuluation results. The fourth section describes the results of the comparison with the simulation results and field measurements. The section also illustrates the results of model validations by using field measurement values. Lastly, the fifth section states the executive summary of this research including the findings and limitations.

2. EXISTING KNOWLEDGE

2.1. CONVENTIONAL COMPACTION

For the construction of roads, retaining structures, and embankments, soil or rock fills are used to raise the site level. The soil or rock in the fill can be compacted mechanically and densified with static or vibrating rollers to increase its shear strength and stability, to enhance resistance to erosion, and to reduce its compressibility and permeability. When the compaction work complies with specifications, the soil or rock fill can be used to support structures, such as buildings, pavements, and retaining structures. There are four types of compaction efforts on soil or rock fills: vibration, impact, kneading, and pressure. These four different types of efforts can be divided into two principal types of forces: static and vibratory compaction.

2.1.1. Background of soil compaction

Soil is used in many types of construction to support structures, pavements for highways and airports, and dams and levees to resist water pressure. It is highly important for engineers to understand the properties, characteristics, and behaviors of soil. Raymond R. Proctor (1933) developed the useful knowledge related to the properties and characteristics of soils. To stabilize or improve the engineering properties of soil in the field, the primary method is compaction. The term, “soil compaction”, refers to the method of mechanically and artificially increasing the density of soil. It involves compressing soil particles together and removing air or water from soil void

spaces. Proctor (1933) stated that compaction is a function of the dry density of soil, water content, compaction effort, and soil types, such as the gradation and the presence of clay minerals, etc. Traditionally, soil or rock fills are compacted with vibration, impact, kneading, pressure, and combination effort found in the two principle types of static and vibratory compaction forces.

2.1.2. Static rollers

Static rollers achieve compaction simply by using the deadweight that applies a downward force on the soil surface and compresses the soil particles together without the presence of vibratory motion. For example, kneading and pressure are two types of static compaction. A static roller is shown in Figure 2.1. The steel wheel and sheepsfoot rollers supply pressure, whereas pneumatic tire rollers supply pressure with some kneading.

Steel wheel rollers are used to compact all types of soil in layers from 4 to 12 inches deep depending on soil types and roller weights and should be limited to 4 to 6 inches in a clay layer to avoid the compaction of the top layer only.

(a) Steel wheel roller
(Bomag web site)

(b) Sheepsfoot roller
(Dynapac web site)

(c) Pneumatic roller
(Ammann web site)

Figure 2.1 Static rollers

When compacting cohesive soil, these rollers tend to form a crust over the soil surface that may prevent compaction of the lower portions of the soil left. However, these rollers are effective in smoothing the soil surface that has been compacted by tamping or impact rollers. Sheepsfoot rollers can be used on cohesive soils that respond best to kneading forces and are least efficient in sandy and gravel types. In addition, the compaction depth of a layer of soil is limited to approximately the length of the feet. Pneumatic-tired rollers apply the principle of kneading action and usually have two tandem axles with four to nine tires on each axle. These units are especially useful for any type of soil and final finishes, proof roll subgrades, bases on airfields, and earth-fill dams, but the rollers' weight and tire pressure must be proper for the soil type. Usually, static rollers may be classified by weight in tons. In contrast, pneumatic rollers have at least four methods for classifying compaction ability; these are

1. The gross weight of the unit;
2. The gross weight per wheel;
3. The weight per inch of the tire width; and
4. The air pressure in the tires.

Because the contact area between the soil surface and the tire varies with the air pressure in the tire, it is not enough to indicate compaction ability by the total weight or the weight per wheel only. Figure 2.2 illustrates a graphical method of determining the ground contact pressure for a 13.00 × 24 18-ply smooth compactor tire subjected to varying loads and inflated to varying air pressures. Similar information regarding the tire sizes and loads is available from tire manufacturers. (Peurifoy and Ledbetter, 1985)

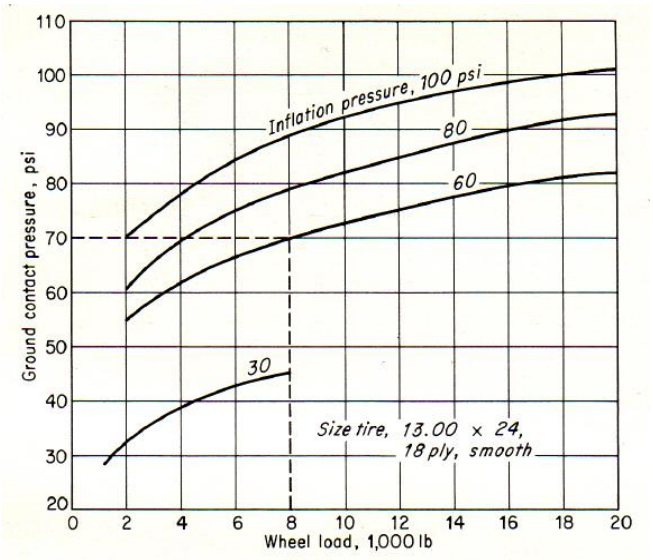

Figure 2.2 Ground pressure at varying wheel loads and air pressures (Peurifoy and Ledbetter, 1985)

Conventionally, the static compaction is confined to the upper soil layers of the material and is limited to any appreciable depth because the effective depth of static compaction is limited.

2.1.3. Dynamic rollers

Dynamic rollers use a vibrating or oscillating mechanism, usually one or more rotating eccentric weights, to create a downward force in addition to the machine's static weight. The dynamically excited rollers deliver a combination force to the underlying soil surface by a rapid sequence of blows. Dynamic forces move through the material and then set soil particles and move them closer together efficiently. These vibrations facilitate the rearrangement of the soil particles into positions that result in lower void ratio and higher density by eliminating the internal friction between the soil particles.

2.1.3.1. Vibratory roller

The most common type of roller is the vibratory roller which has been used for many years, and its design has evolved into many types. The smooth drums are used for the compaction of gravel or rock-fill, and sheepsfoot or padfoot drums are adequate to compact clay and other cohesive materials. The drum of a vibratory roller is excited by the rotating mass connected to the shaft of the drum axis as shown in Figure 2.3. The rotating eccentric mass on the concentric shaft imparts a centrifugal force to the drum, and this dynamic excitation causes the drum to vibrate. The compaction depth effect of vibratory rollers is greatly increased by dynamic excitation beyond the effect achieved by static rollers. During compaction, the motions of a dynamically excited roller changes depending on the travel speed, soil properties, and roller parameters. The variety of significant roller motions is referred to as the operating conditions in Table 2.1 (Adam and Kopf, 2000).

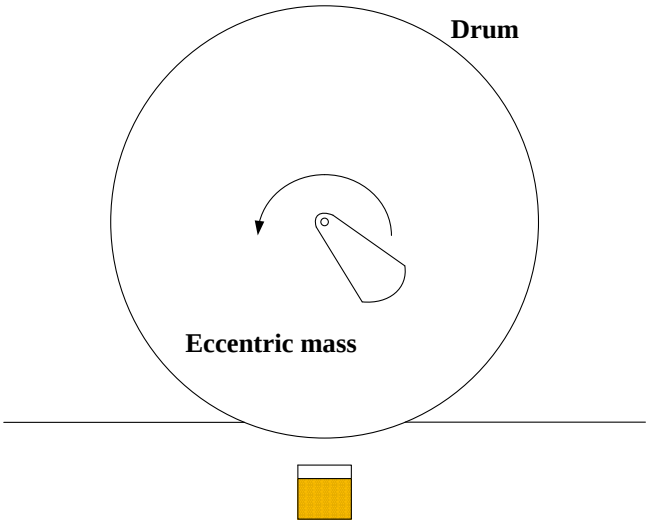

Figure 2.3 Drum of a vibratory roller

Table 2.1 Operating conditions of vibratory rollers (Adam and Kopf, 2000)

Drum motion	Drum-soil interaction	Operating conditions	Eccentric rotations per load cycle	Soil stiffness	Travel speed
Periodic	Permanent contact	CONTACT	1	low ↓ high	high ↑ low
	Loss of contact	PARTIAL UPLIFT	1		
		DOUBLE JUMP	2		
		ROCKING	2		
Chaotic		CHAOTIC	-		

In the contact mode, the drum of a vibratory roller is in continuous contact with the soil surface during dynamic compaction. This mode only occurs in soft soil, with a relatively small eccentric force, a heavy frame mass resting on the drum, and relatively high travel speed. When soil stiffness increases, the operating condition changes from contact to uplift. In this mode, the drum is lifted off the soil and falls back onto the ground with every turn of the eccentric mass, and dynamic compaction takes place for the most part. When the soil stiffness is increased further, the operating condition changes into double jump. In this mode, the drum hits the ground with alternating harder and softer hits and is repeated only every second revolution of the eccentric mass.

Figure 2.4 illustrates the vertical movement of the soil at different depths in the double jump condition. When the soil is very stiff, the vertical acceleration of the drum appears as an oscillation with half the excitation frequency because the additional degree of freedom causes the drum to oscillate to the left and to the right to perform a rocking motion. In the chaotic operating condition, the drum motion no longer shows any periodicity and effective compaction (Adam and Kopf, 2000).

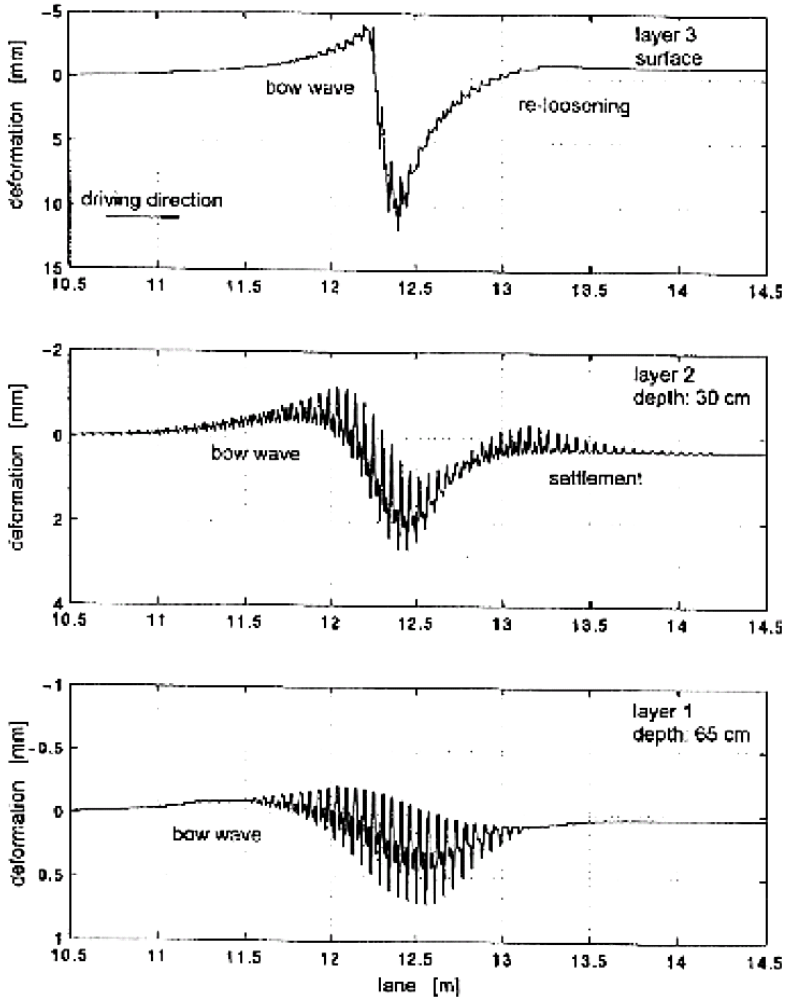

Figure 2.4 Soil deformation at three depths below the impact of a vibratory roller drum operating in the double jump condition (Adam and Kopf, 2000)

2.1.3.2. Oscillatory roller

The drum of an oscillatory roller contains two eccentric masses arranged symmetrically relative to the center as shown in Figure 2.5. When these eccentric masses rotate in the same direction, the periodic torque caused by the horizontal and vertical components of the centrifugal forces makes the drum oscillate torsionally. These horizontal forces cause dynamic shear stresses in the ground, resulting in additional

compaction. The oscillatory rollers are used in the vicinity of sensitive structures, such as the backfilling of abutments and urban underground environments, because the emitted vibrations are typically lower in amplitude and do not reach down very deeply. Moreover, the oscillatory rollers create extremely smooth surfaces and reduce water permeability. Therefore, the oscillatory rollers are used primarily for asphalt compaction and cohesive soils.

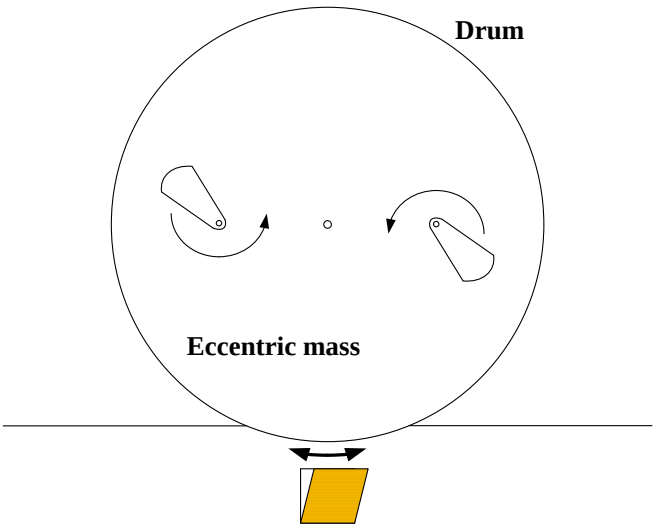

Figure 2.5 Drum of an oscillatory roller

During oscillatory compaction, a variety of different operating conditions occur: stick, slipping, and uni-directional slipping modes. These conditions depend on the friction coefficient between the drum and the soil, soil stiffness, and roller parameters. In the stick mode, the static friction force between the drum and the ground is higher than the ground contact force. This means that the relative dynamic speeds of the drum and the soil are always the same in the interface area. In the slip mode, the ground contact force periodically exceeds the static friction force between the drum and the ground.

This causes the drum to slip across the ground until the difference has disappeared. These periodic slips occur repeatedly in and against the travel direction. The uni-directional slipping mode occurs when there is an uneven distribution of the driving force between the drum and the driving wheels with single-drum compactors. These differences in the propelling effect and in slip may produce an imbalance between the two axles. As a result, the drum may start slipping periodically while it never gets beyond the static friction limit in the other direction. (Adam and Kopf, 2000).

The commonly used conventional compaction equipment with typical sizes, weights, and guidance lists is in APPENDIX A.

2.1.4. Typical compaction thickness

As noted above, mechanical compaction uses various rollers. The pressure of rollers decreases with depth within the layer being compacted. The pressure bulb theory is related to the distribution of a load (Peurifoy and Ledbetter, 1985).

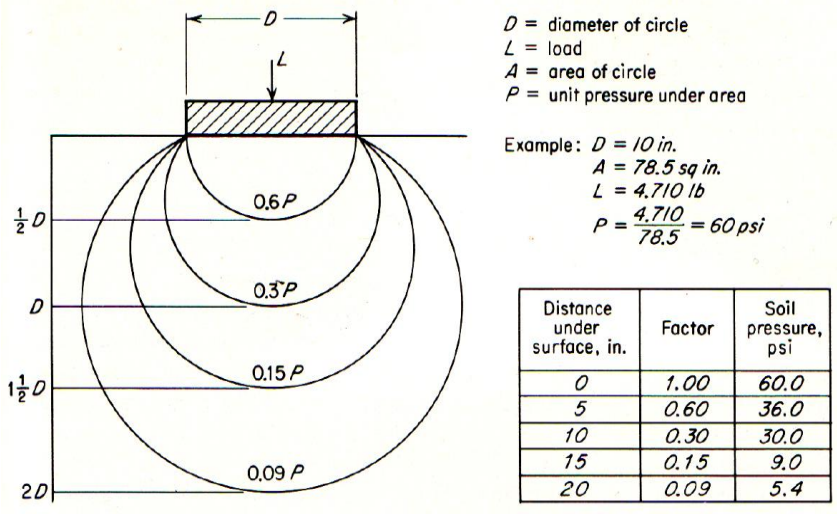

Distance under surface, in.	Factor	Soil pressure, psi
0	1.00	60.0
5	0.60	36.0
10	0.30	30.0
15	0.15	9.0
20	0.09	5.4

Figure 2.6 Variations in pressure with depth (Peurifoy and Ledbetter, 1985)

When the load is applied to the soil, the contact area between a tire and the ground is approximately a circle. That is why the theory can be applied to pressure in the soil under the tires with slight modifications. Figure 2.6 shows the ratios of unit pressures with depth. In addition, Boussinesq's theory is also related to this problem. Although Boussinesq's theory assumes elastic material, the theoretical values are reasonable approximations of true pressure distribution under the roller. By using theoretical equations and field experiment data, Peurifoy and Ledbetter (1985) suggested the equipment suitability for compacting soil. They are listed in Table 2.2.

Table 2.2 Suitability for compacting soils (Peurifoy and Ledbetter, 1985)

Type of Compactor	Soil Best Suited For	Maximum Effect in Loose Lift, inches	Density Gained In Lift	Max. Weight Tons
Sheepsfoot	Clay, silty clay, gravel with clay binder	7-12	Nearly uniform	20
Steel tandem, two-axle	Sandy silts, most granular materials with some clay binder	4-8	Average*	16
Steel tandem three-axle	Sandy silts, most granular materials with some clay binder	4-8	Average*	20
Steel three-wheel	Granular or granular-plastic material	4-8	Average* to uniform	20
Pneumatic small-tire	Sandy silts, sandy clays, gravelly sand, and clays with few fines	4-8	Average* to uniform	12
Pneumatic large-tire	All types	3-6	Uniform	50
Vibratory	Sand, silty sands, silty gravel	Up to 24	Uniform	30
combinations	All	3-6	Uniform	20

2.1.5. Compaction quality assurance testing

During construction of a compacted fill, the quality assurance test provides the quality of the completed fill. The compaction mechanism for different soil types is affected by the following variable factors:

1. Cohesionless soils: (a) Soil gradation and the coefficient of uniformity; (b) Water content; (c) Magnitude of the compactive effort; (d) Thickness of the soil layer being compacted; and (e) Characteristics of the compaction equipment.

2. Cohesive soils: (a) Soil texture including clay content and plasticity; (b) Water content and degree of saturation; (c) Magnitude of the compactive effort; (d) Thickness of the soil layer; and (e) Characteristics of the compaction equipment.

As mentioned above, there are many factors that affect the compaction; however, moisture content is the most critical factor since if soil contains the right amount of water, water will provide a lubricant to allow the soil grains to slide on each other. As a result, the soil layers can be compacted thoroughly and conveniently. This amount of water is called the optimum moisture content. If a soil contains too much moisture, it is likely to become rubbery under a roller. When the roller has passed, the soil particles spring back into their original position by water pressure. Otherwise, if a soil is too dry, it is likely to become loose or powdery under the pressure. It may be firm but not dense as it should be.

To control the compaction quality, the laboratory moisture-density test is performed conventionally, which is used to find the specified optimum moisture content and maximum dry density. These values are convenient compaction control parameters.

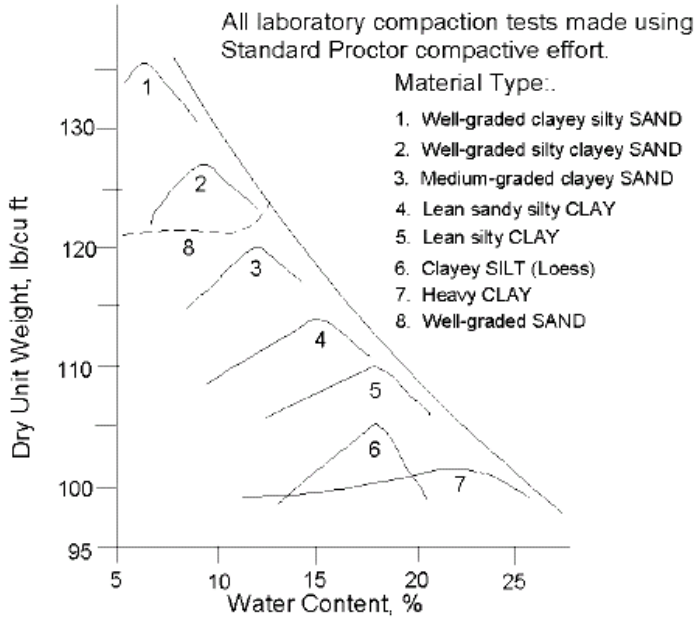

Figure 2.7 Maximum dry density and optimum water content for soils of several textures (Johnson and Sallberg, 1960)

Figure 2.7 shows the relationship between the optimum water content and the maximum dry density with different grain-size distribution. Note that well graded sands (SW) have a higher density than more uniform soils (SP). In cohesive soil cases, the maximum dry density tends to decrease as plasticity increases.

For estimating compaction test data, the zero air void curve, a line connected to all points of 100% saturation, is very important because it is impossible to have a dry density, i.e., a water content point to the right of the zero air void curve. If a test date exists to the right of the zero air void, it has some errors. In addition, it is important to keep in mind the applied compactive effort. If more compactive effort is applied by using heavier rollers or more passes of the same roller, the maximum dry density increases but the corresponding optimum water content decreases. In other words, if the

soil in the field is compacted above its optimum water content, a lower strength will be obtained even though it has been compacted to a higher density. This effect is known as overcompaction (Turnbull and Foster, 1956).

2.1.5.1. Proctor test and modified proctor test

To develop the maximum dry density and optimum water content curve, the Standard Proctor Test developed by R.R. Procter in the early 1930s, a field engineer for the City of Los Angeles, California, is performed.

In this test, a sample of soil is compacted in approximately l liter (0.944×10^{-3} m^3 or 1/30 ft^3). The soil is placed in three layers and each layer is compacted 25 times by using a 5.5lb weight which is lifted through a distance of 12 inches. The compactive effort is 12,375 ft·lb. of energy per cubic foot, determined as follows:

$$\frac{1\,ft.\times 5.5\,lbf.\times 25\,drops\times 3\,layers}{\frac{1}{30}\,ft^3} = 12{,}375\ ft\cdot lbf\ /\ ft^3$$

The sample soil is weighed immediately after the test and then weighed again after drying the soil in an oven. The difference between the wet and dry soil weights is the weight of water and is expressed as a percentage of the dry weight. The procedure is repeated for different amounts of water, and then the relationship between the dry density and the water content is plotted.

The recent trends are to build heavy structures, which demand tougher compaction specifications. For heavy structures, a Modified Proctor Test was developed, which is very similar to the Standard Proctor Test. Table 2.3 illustrates the differences.

Table 2.3 Proctor compaction test methods

Specifications	Standard Proctor Test	Modified Proctor Test
ASTM Standard	D 698	D 1557
Weight of the Hammer	5.5 lb.	10 lb.
Distance of Drop	12 inches	18 inches
Number of Soil Layers	3	5
Number of Drops on Each Layer	25	25
Volume of Test Container	1/30 cu ft.	1/30 cu ft.
Energy Imparted to Soil	12,375 ft.lb. per cu. ft.	56,250 ft.lb. per cu.ft.

2.1.5.2. Field test

To determine the effectiveness of the compaction, the density and water content of compacted fill should be measured. There are two major methods, field density test methods and water content test methods, used for field compaction testing today because the dry density and water content are very convenient construction control parameters and are very easy to correlate with other properties. These major methods also have two basic procedures, direct measurement and indirect measurement.

In field density test methods, the direct measurements are based on the procedure of digging a hole, measuring its volume, and weighing the excavated material. The indirect methods are based on the procedure of passing some energy through the soil and measuring the attenuation energy as a function of the density. In the water content test methods, the direct measurement procedure involves weighing the wet sample, removing the water, and then weighing the dry soil. The difference in weight is the weight of the water in the soil. The indirect method procedure is similar to the field density test. Table 2.4 describes and summarizes these methods' procedures.

Table 2.4 Field density and water content test methods

Test method	Procedures
Field density test methods	
Undisturbed tube sample *ASTM: D 2937*	Driven into compacted layer and retrieved using a thin-wall sampling tube. The soil in the tube is tested.
Sand cone *ASTM: D 1556*	A small hole is excavated (6 inches deep) with the soil carefully retrieved and weighed. The volume of the hole is measured by filling with sand. The volume is calculated by the calibrated sand.
Water balloon *ASTM: D 2167*	A small hole is excavated (6 inches deep) with the soil carefully retrieved and weighed. The volume of the hole is measured by inserting a rubber balloon filled with water. The volume is calculated by the calibrated water.
Nuclear density gauge *ASTM: D2922*	The nuclear meter is placed directly on the soil. Gamma rays from a radioactive source penetrate the soil and reflect back to the surface. The density is calculated by using the returned energy intensity.
Water content test methods	
Microwave oven *ASTM: D 4643*	This method uses a computer-controller standard micro wave to dry a soil sample.
Calcium carbide gas pressure *ASTM: D 4944*	Water in a soil sample combines with calcium carbide in a container. The pressure of the acetylene gas is proportional to the water content in the soil sample.
Rapid heating *ASTM: D 4959*	This method is useful for coarse-grained soils. Soil samples are dried on a hot plate or burner.
Nuclear moisture gauge *ASTM: D 2922*	The nuclear moisture gauge emits neutrons. When the neutrons strike a hydrogen atom,, the velocity is halved. The reduction is proportional to the water content in the compacted fill.

2.1.5.3. Briaud compaction device (BCD)

Briaud et al. (2006) developed the Briaud compaction device (BCD), which is a new instrument to measure a soil modulus in the field and in the lab in only a few seconds. Using the soil modulus, reflects a trend toward an alternative to dry density in compaction control to avoid the undesirable nuclear devices such as the nuclear density gauge and to use a parameter more directly related to limiting deformations which is the design criterion in the field. The BCD consists of the plate, the load cell, the tube, the handle, and the display (See Figure 2.8). The stainless steel plate, 2mm thick and 150mm in diameter instrumented with eight electrical strain gauges, contacts with the surface of the soil to measure the soil modulus.

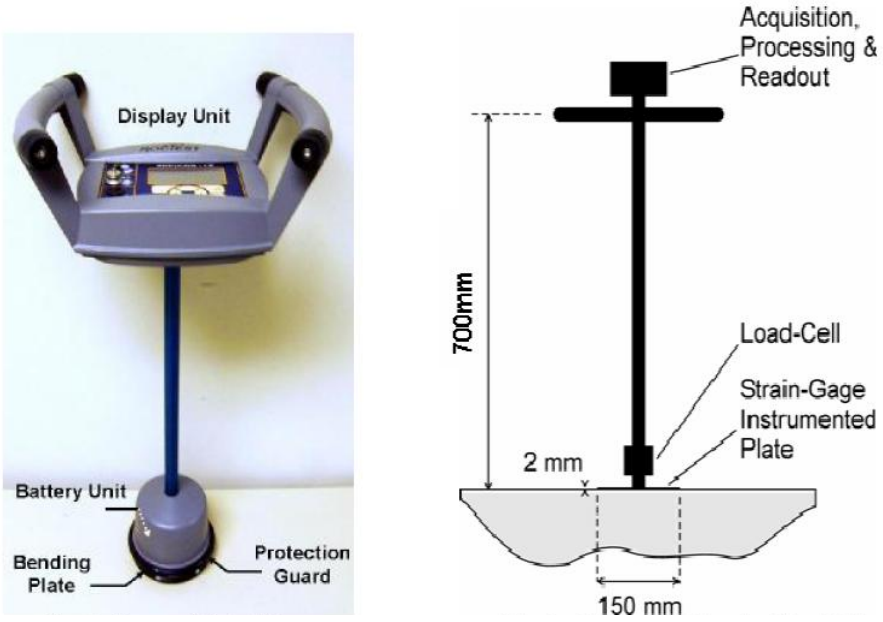

Figure 2.8 Briaud Compaction Device (BCD manual, 2008)

It is of critical importance to establish target modulus values by using a modulus compaction curve in the lab first (much like the dry density compaction curve) and verify the target modulus value achieved in the field because many factors can influence a soil modulus (Briaud, 2001). The BCD is a much faster test, taking approximately 5 s, and the procedure is as follows:

In the field, (1) decide the test spot; (2) place a handful of wet sand on the test location and pat it down firmly and evenly into a 4-5mm thick sand layer; (3) lean on the BCD until the display passes through 223 N perpendicularly; and (4) repeat that step a second time. When the force display passes through 223 N, the modulus is calculated and displayed automatically. Figure 2.9 shows the BCD test procedures in the field.

Figure 2.9 Field BCD Test (BCD manual, 2008)

In the lab, (1) set a modified Proctor Test (ASTM D1557) on a 150 mm-diameter mold; (2) place the BCD plate on top of the soil surface in the Proctor mold; (3) lean on the BCD until the display passes through 223 N perpendicularly; and (4) repeat that step

a second time. Figure 2.10 shows the BCD test procedures in the lab. The BCD modulus is a soil modulus corresponding to the following orders of magnitudes: strain level 10^{-3}, stress level 50kPa, and a time of loading of a few seconds. Typical BCD modulus values fall in the range of 5 to 300 MPa. (Briaud et al., 2006)

Figure 2.10 Lab BCD Test (BCD manual, 2008)

2.2. INTELLIGENT COMPACTION (IC)

Intelligent compaction (IC) started in Europe in the late 1970s and early 1980s with the work of Bomag in Germany, Ammann in Switzerland, and Geodynamic in Sweden. These European companies seem to dominate the market, but US construction manufacturers are also developing IC equipment. Currently, Bomag, Ammann, Dynapac, and Geodynamik manufactured equipment is available in the US.

Intelligent compaction (IC) technology truly is an innovation in compaction control and testing. These pieces of equipment use the accelerometers and machine energy to calculate an index parameter related to the soil modulus or stiffness. This collected information is used by the roller's control systems to optimize compaction by automatically adjusting the different compaction parameters for the roller such as the drum vibration, amplitude, frequency, and working speed. These parameters are used by together to modify the compactive energy delivered by a roller of specific mass and diameter.

Furthermore, IC rollers can provide continuous and real-time verification of in situ soil properties over the entire compaction area to use as quality control (QC) and quality assurance (QA) programs. These rollers are equipped with a real-time geospatial location record and a documentation system that record continuous data in the form of a plan-view, color-coded plot of roller stiffness, and roller pass number. It helps to attain a more uniform compaction which contributes to increased service life time, avoidance of time-consuming field tests such as sand cone and water balloon methods, and elimination of the chance of overcompaction.

2.2.1. Principle of obtaining the soil modulus E

To understand an IC technology, it is necessary to comprehend the related soil properties to evaluate the compaction process such as soil modulus and stiffness. The properties of soils that show elastic and plastic characters are difficult to estimate with the soil modulus. Many different moduli can be obtained from a load-reload stress-strain curve, and they form a consolidation or tri-axial test. Many different soil moduli have been defined in Figure 2.11. For example, the secant modulus is E_s is defined as the slope from O to A. The secant modulus E_s is used for predicting the movement due to the first application of a load. The tangent modulus E_t is defined as the tangent to the point considered on the stress strain curve. The tangent modulus E_t is used to calculate the incremental movement due to an additional load. The unloading modulus E_u is calculated from the slope from A and B in Figure 2.11. E_u can be used to calculate the rebound of a pavement after loading by a truck tire (resilient modulus).

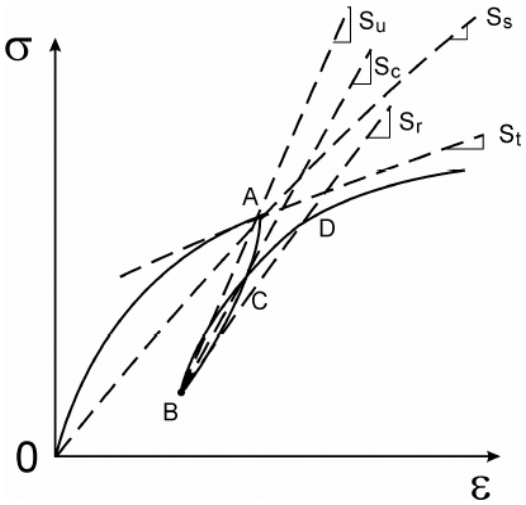

Figure 2.11 Definition of Soil Modulus (Briaud, 2001)

The reload modulus E_r is obtained from the slope between B and D. E_r is used to calculate the movement of the pavement under reloading by the same truck tire. Lastly, the cyclic modulus is obtained from the cyclic slope S_c in Figure 2.11. E_c is used for predicting the movement subjected to repeated wave loading (Briaud, 2001). Table 2.5 lists the typical value range for the soil modulus E.

Table 2.5 Value range for the static stress-strain modulus E_s (Bowles, 1997)

Soil		**E_s, MPa**	**Soil**		**E_s, MPa**
Clay	Very soft	2-15	Loess		15-60
	Soft	5-25	Sand	Silty	5-20
	Medium	15-50		Loose	10-25
	Hard	50-100		Dense	50-81
	Sandy	25-250	Sand and Gravel	Loose	50-150
Glacial till	Loose	10-150		Dense	100-200
	Dense	150-720	Shale		150-5,000
	Very dense	500-1,440	Silt		2-20

* Field values depend on stress history, water content, density, and age of deposit

Briaud (2001) stated that the soil modulus is influenced by many factors such as the soil state factor and loading factors. However, the use of the soil modulus is more accurate than that of the soil stiffness. The stiffness K, for instance, is defined as the ratio of the force divided by the displacement. It has units of force per unit length (kN/m). Accordingly, the relationship between the modulus and the stiffness is as follows:

$$E = f(K/B) \quad where, B = diameter \ \ (the\ case\ of\ a\ circular\ plate)$$

This relationship shows that if the loading areas are different, the stiffness measured with one test will be different from that measured with another test for the same elastic material. It is dependent on the area of the applied load. The modulus, however, would be the same.

Futhermore, there is a need to comprehend the relationship between the modulus and the water content for various types of soils. For example, if a very soft clay dries out, it can get a high modulus because the suction generates high compression stresses between the soil particles. This apparent stiffness, however, is destroyed as soon as the clay gets wet again. Besides, the water content, cementation, loading factor, and past stress history can affect the modulus (Briaud, 2001).

2.2.2. Bomag roller

Recently, the German-American Bomag group developed the VARIO CONTOL roller which contains two concentrically shafted out-of-balance masses (see Figure 2.12).

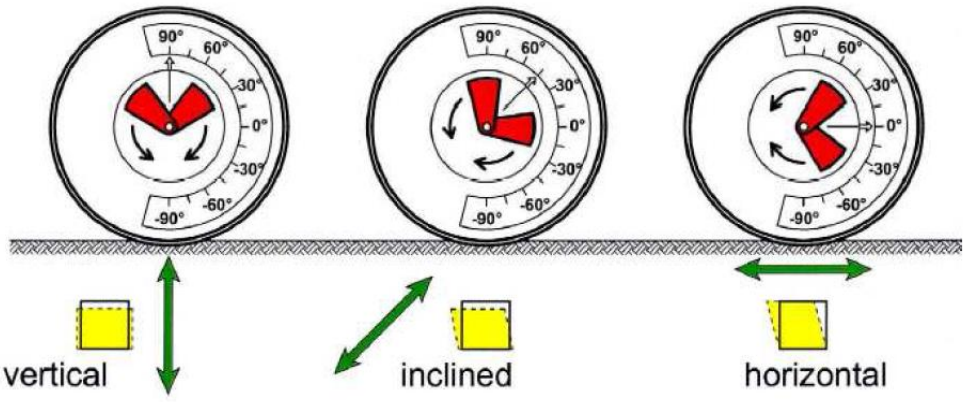

Figure 2.12 VARIO roller with different settings for direction of vibration (Bomag brochure)

This roller has the ability to automatically change the eccentric force to permit the continuous adjustment of the direction of excitation from vertical to horizontal and thus any reduction of the vertical portion of the excitation amplitude. In addition, VARIO CONTOL also has the continuous compaction measurement and monitoring system to record the generated material modulus by plotting the force settlement curve. The dynamic stiffness of the soil or other materials can be calculated as the slope of the curve on the loading portion (See Figure 2.13). These values can be converted into the dynamic modulus of the material being compacted.

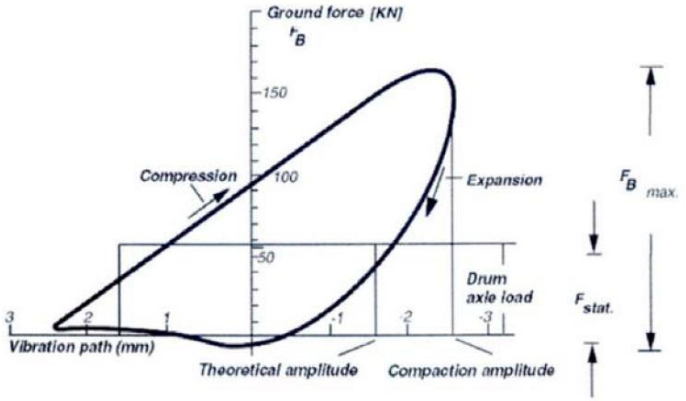

Figure 2.13 Force settlement curve of vibration roller drum (Bomag brochure)

The integrated control system collects all data to manage the IC rollers automatically according to two criteria: (1) If the roller is entering an undesirable double jump mode, the compaction amplitude is immediately reduced so that the drum goes back to the partial uplift mode; and (2) if the specified maximum compaction force/modulus is reached, the amplitude is immediately changed so that the applied force/modulus does not exceed the maximum force/modulus. These two criteria allow an optimized compaction process and consequently a highly uniform compaction. Figure

2.14 shows that if the compactive effort being applied to the soil increases, the slope of the loading position of the curve also increases. It means the soil stiffness and calculated E_{vib} value also increase, accordingly.

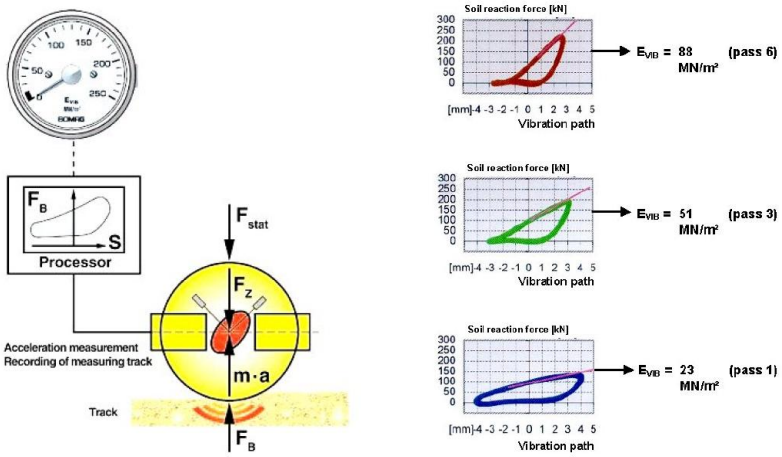

Figure 2.14 Principle of compaction quality measure E_{vib} (MN/m^2) (Bomag brochure)

As mentioned above, Bomag has the documentation system called BCM 05 as shown in Figure 2.15. This system can accept any GPS receiver to provide compaction data in a variety of ways to the roller operator and the project personnel.

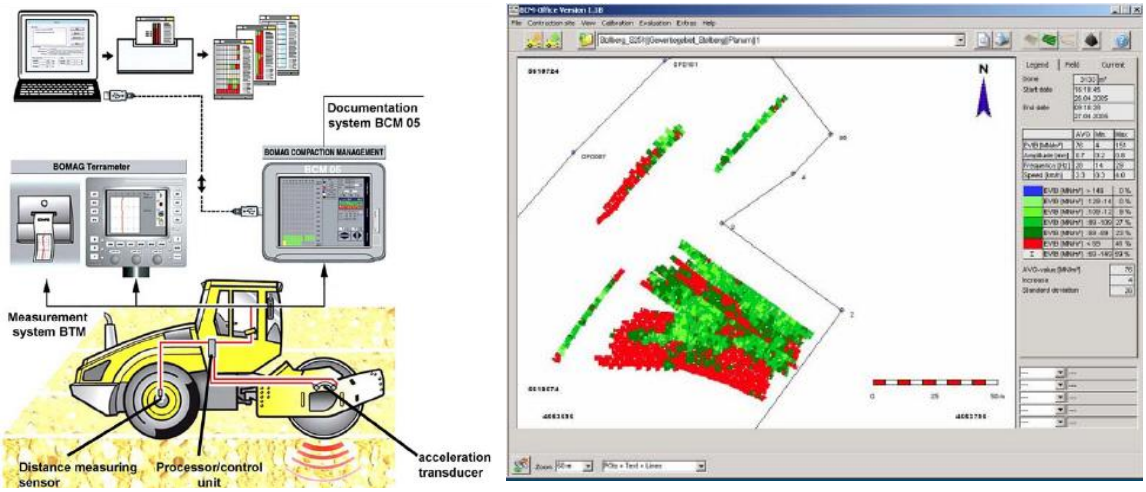

Figure 2.15 Bomag documentation system (Bomag brochure)

2.2.3. Ammann roller

The Ammann Compaction Expert (ACE) Plus calculates soil stiffness k_s once per cycle of vibration. The vibration roller compacts the ground until a required value of soil stiffness is reached. The Ammann k_s can be determined from the measured drum acceleration and lag (φ) between the eccentric mass position and displacement.

The Ammann ACE Plus eccentric assembly consist of two parts: inner mass and outer mass. The angle between the two masses is automatically controlled to provide the maximum eccentric force (angle = 0^o), zero eccentric force (angle = 180^o), and any eccentric force in between (0^o < angle < 180^o). The ACE Plus system performs closed loop feedback control of the drum and soil contact force Fs. It is possible to select three levels of F_s: (1) Low Force: $F_{s(max)}$ = 14 kN (3.1 kip), leading to measured z_d = 0.4 - 1.5mm (0.02 – 0.06 in);

(2) Medium Force: $F_{s(max)}$ = 20 kN (4.5 kip), leading to measured z_d = 1.0 - 2.0mm (0.04 - 0.08 in); and

(3) High Force: $F_{s(max)}$ = unlimited, leading to measured z_d = 2.0 - 3.0 mm (0.08 - 0.12 in).

To maintain the $F_{s(max)}$, the roller adjusts the eccentric mass moment with a selected force level. The excitation frequency is adjusted to maintain a phase lag φ between 140^o and 160^o. For high force levels, the frequency required to maintain the appropriate φ is 23 -25 Hz. Figure 2.16 shows the algorithms implemented in the control circuit of the AMMANN IC roller (ACE).

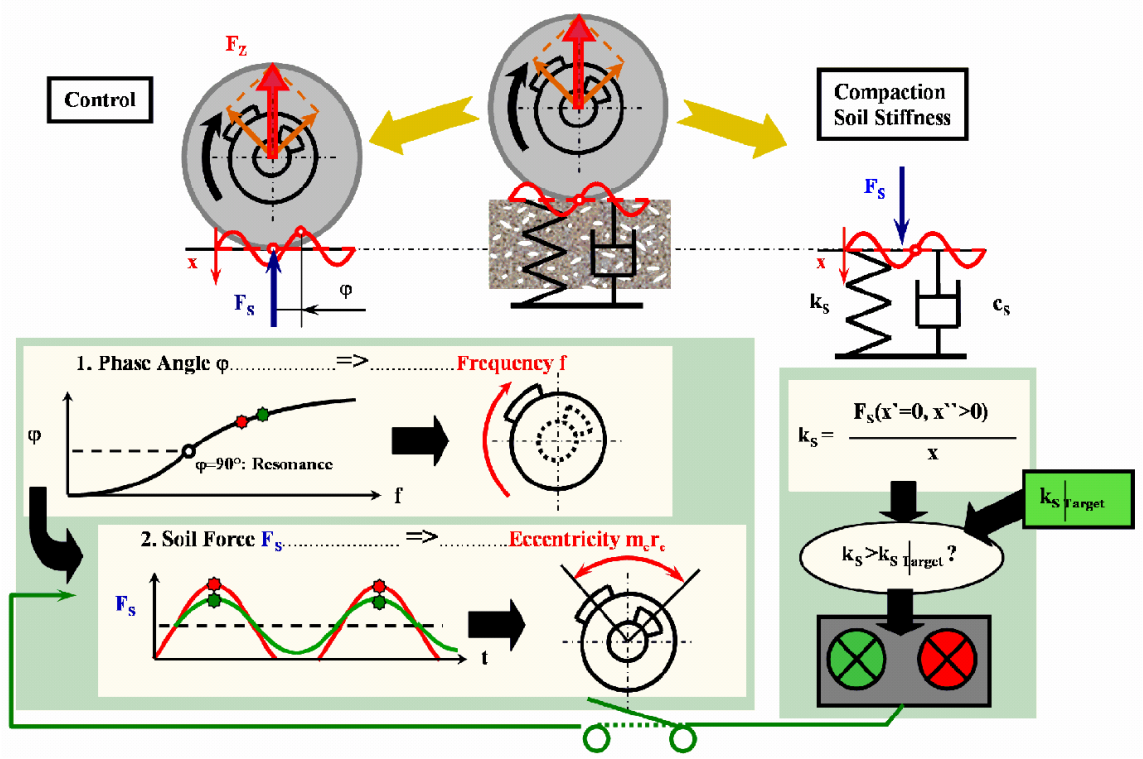

Figure 2.16 Principle of the automatic control of amplitude and frequency and the measurement of soil stiffness during the compaction process (Ammann brochure)

In addition, Figure 2.17 shows the effect of the automatic control in practice. On the first roller pass, the machine operates at the lowest frequencies and maximum amplitude to maximize the depth effect of the compaction work. On the following passes, the roller operates automatically at the increased value of frequency and the decreased value of amplitude to raise the bearing capacity of the surface. This means that the compaction power is increasingly transmitted into the layers near the surface. On the last roller pass, the machine operates at maximum frequency and low amplitude to compact the surface.

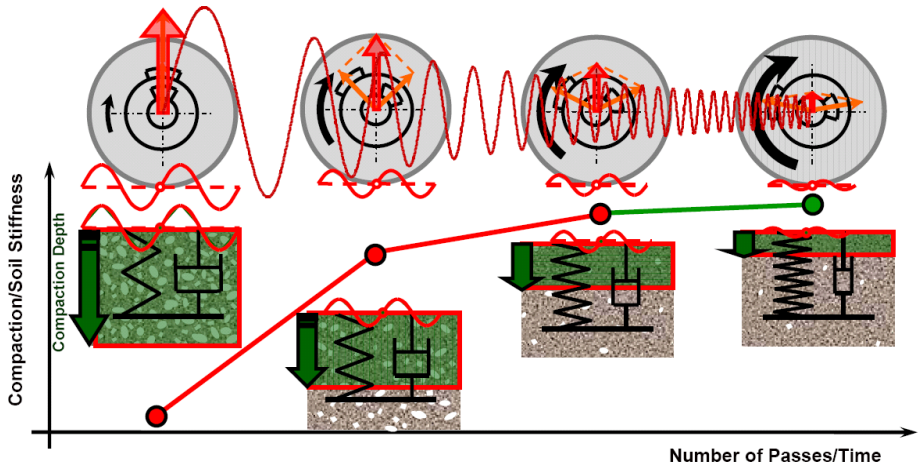

Figure 2.17 Ammann Compaction Expert ACE: automatic control of amplitude and frequency (Ammann brochure)

Like other IC rollers, the ACE Plus also has the documentation system. This system collects the data with x, y, and z coordinates by using differential GPS. Ammann indicated accuracies are ± 10 cm (3.9 in). During the compaction process, the values can be recorded and presented in a graphic visualized form. Figure 2.18 shows a compaction result comprising the soil stiffness attained and the number of roller passes.

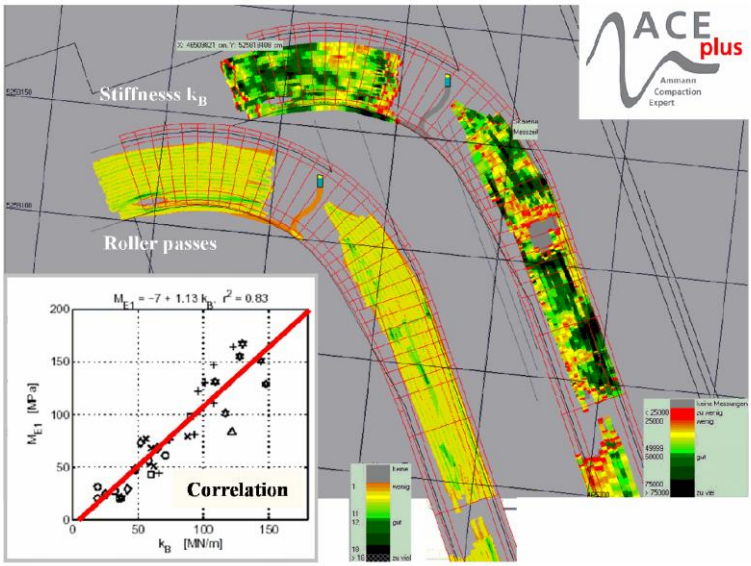

Figure 2.18 CCC using differential GPS technology (Ammann brochure)

2.2.4. Dynapac roller

The Dynapac Compaction Meter uses the Compaction Meter Value (CMV) developed by Geodynamik in the 1970s. The CMV indicates the stiffness of the compacted material: the higher the CMV, the stiffer the material. When the CMV stops increasing, the material is at maximum compaction. The CMV is defined as the ratio of the 2nd harmonic of the vertical drum acceleration amplitude $A_{2\Omega}$ (operating frequency Ω) divided by the 1st harmonic of the vertical drum acceleration amplitude A_{Ω}, multiplied by a constant c (typically value 300). The Dynapac roller performs feedback control of the eccentric excitation force. Figure 2.19 shows the effect of the automatic control in various ground conditions.

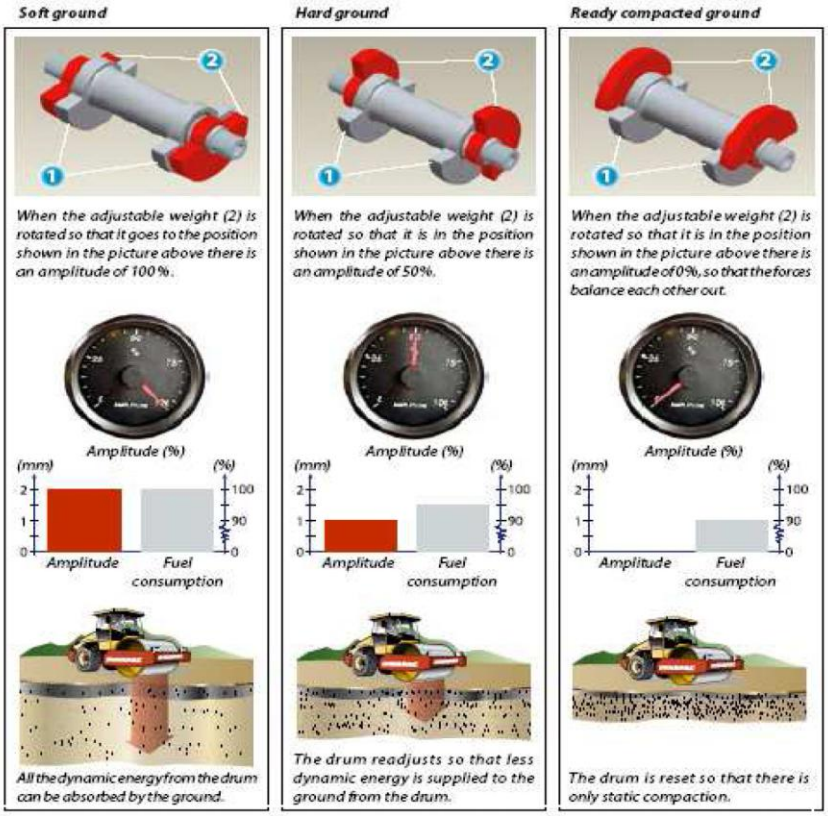

Figure 2.19 Dynapac's compaction optimizer (Dynapac brochure)

The Dynapac Compaction Analyzer (DCA) collects all roller data such as CMV, pass number, amplitude, and frequency, etc. It also presents the data in real-time graphic visualized form. The DCA is compatible with any GPS receiver as long as the correct National Marine Electronics Association messages are available. Figure 2.20 shows a Dynapac documentation system.

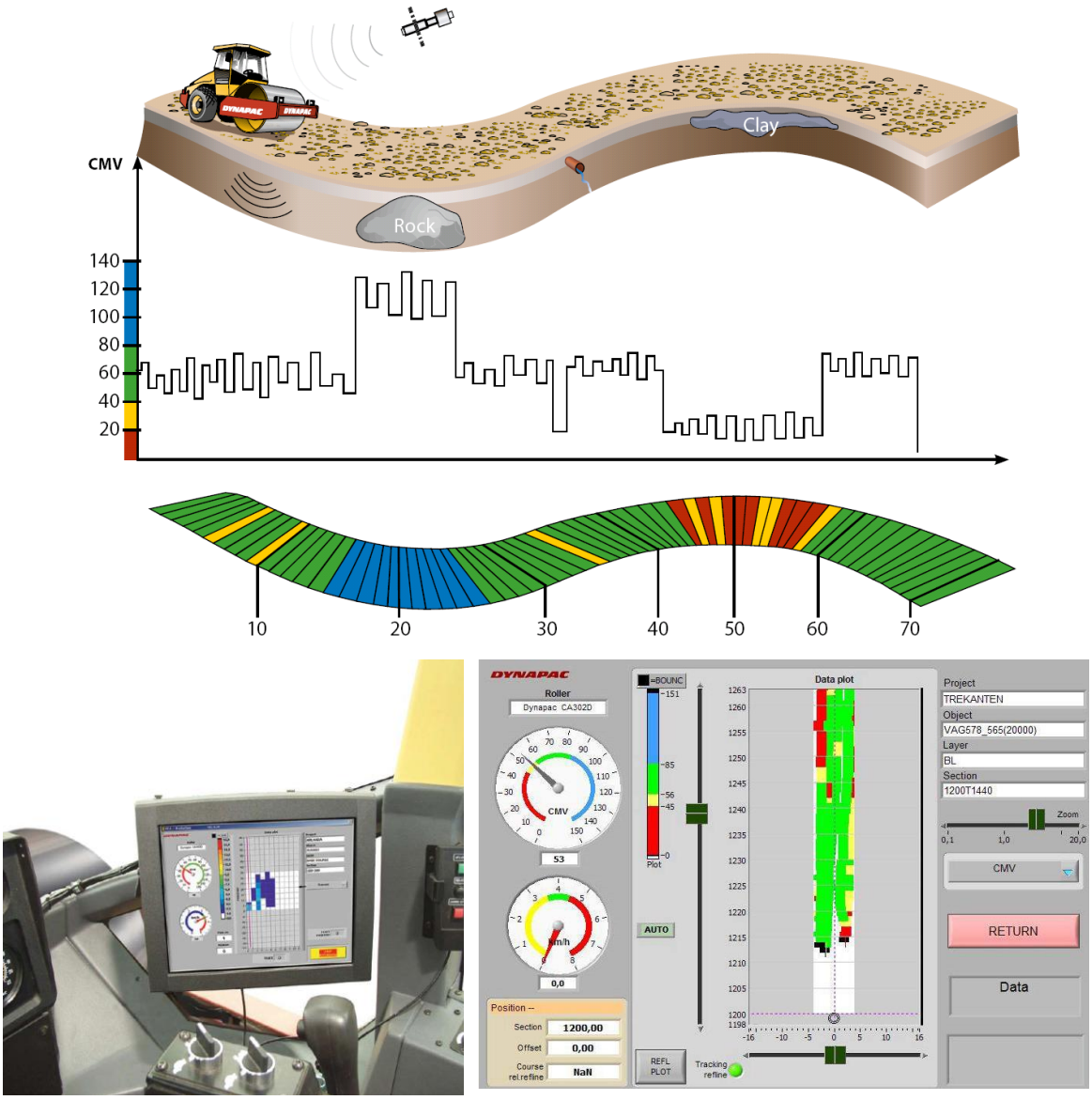

Figure 2.20 Dynapac mapping and documentation system (Dynapac brochure)

2.3. IMPACT ROLLERS

Traditionally, compaction machines for earthworks have considered the static weight, kneading action, or vibratory force to achieve the specific strength. However, when traditional rollers compact the sand subgrades in arid regions, some problems were found due to the inadequate energy output of traditional compaction rollers to compact the relatively dry sands in depth or to break the inter-particle bonds of collapsible sands. These problems have led to the development of impact compaction rollers.

Over the last 20 years, the use of impact compaction has grown for a wide range of earthworks projects around South Africa, Australia, and many other countries because roads have to withstand larger truck loads, airports carrying heavier aircraft, and many countries are reclaiming land from the sea. In particular, it was used for the construction of the Hong Kong Chep Lap Kok Airport runways, which was one of the largest construction projects in the 20^{th} century.

Impact compaction rollers consist of non-circular modules rotating due to the frictional force on the ground surface and falling to impact the ground dynamically. For instance, the LANDPAC has impact rollers with a 3-sided and a 5-sided module, and BOMAG has an 8-sided module towed at 10-12 km/h. In addition, the impact compaction rollers offer an alternative compaction solution that can prove cost-effective. The key feature of impact rollers is that they provide deeper layer compaction because they travel at a relatively high speed compared to conventional machines and impart substantial impact energy into the ground. Consequently, impact compaction rollers have a significantly greater influence depth than that of conventional rollers.

2.3.1. Landpac roller

The impact roller was invented by Aubery Berrangé who is a civil engineer in South Africa. In the early 1990s, the United Kingdom Landpac purchased the patent rights from many of Aubery Berrangé's designs and Landpac improved the models to develop the commercial machines. Now, Landpac's High-energy impact compaction (HEIC) has three-sided machine and five-sided machines shown in Figure 2.21.

<A 3-sided impact roller>

<A 5-sided impact roller>

Figure 2.21 Landpac impact compactor (Landpac web site)

The HEIC application is used to improve the engineering properties of soil and to compact the marginal materials in-situ without the need for removal both above and below the groundwater level. Basically, the HEIC consists of cam-shaped and pentagonal steel drums, which are from 10 to 14 tonnes in weight and from 150mm to 230mm in drop heights, and they provide repeated high energy impacts at the ground surface by rotating at speeds from 10-12 km/h.

The HEIC commonly records the influence depth from 2m to 4m measured by cone penetration tests, dynamic probes, and heavy zone load testing. It is related to the

HEIC drum weight and the rotational drop height. The influence depth is dependent on the efficiency or energy loss of the HEIC process on the soft surfaces of the soil, the contact area of the HEIC drum face, and the moisture content of the soil.

In addition, the HEIC also has continuous compaction measurement and monitoring system, Continuous Impact Response (CIR), to record real time soil response at the initial phase during and at the final phase of HEIC. Landpac's CIR system also uses GPS technology to continuously calculate and record the position of the roller. At the same time, the measurement system on the roller is continuously measuring the stiffness of the soil being compacted. Figure 2.22 shows an example of such a system from Landpac.

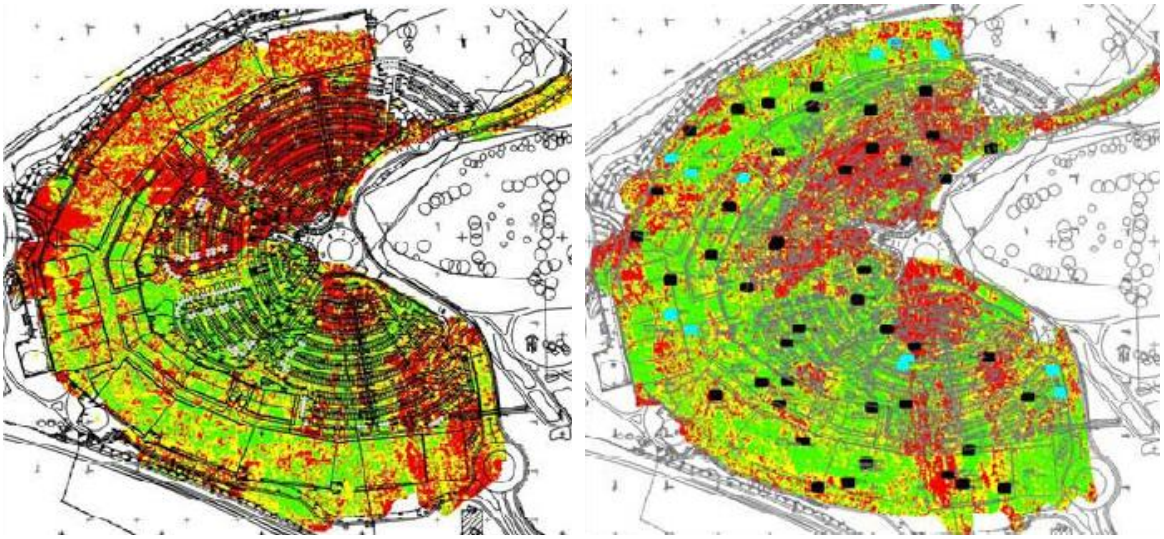

Figure 2.22 CIR system mapping (Landpac brochure)

2.3.2. Bomag roller

The German-American Bomag Group also developed the impact roller which was made up of three octagonal elements positioned axially next to each other and welded to the segment in a staggered arrangement. Unlike other impact rollers, Bomag has the lateral welded rings. These prevent the rollers from tipping when the middle octagonal element stands on edge for fast travel on soil. This polygonal impact roller is shown in Figure 2.23.

<Polygonal roller>

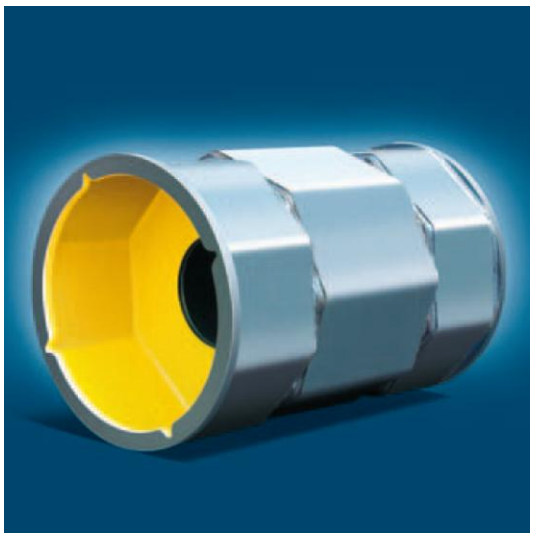

<the design of the polygonal drum>

Figure 2.23 Bomag polygonal roller (Bomag web site)

The advantage of the polygonal drum is the constantly changing direction of force resulting from the change between the plate segments and the wedge segments when the drum is rolling the soil surface. The plate segments compact the soil layer by applying concentrated vertical pressure. The wedge segments compact the soil layer by applying shearing force created by the high linear load. It produces a deformation effect by combining the rotation of the drum. This combination of the peak pressure and the

shearing forces result in kneading and detensioning of the soil which produce the high depth effect and compaction. Figure 2.24 shows the direction of the effective force with cylindrical and polygonal drums. On the other hand, this process produces a loose layer at the surface because trapped air in the soil layer can easily escape. Accordingly, the advantages of polygonal drums are primarily on thick lifts or for post-compacting subsoils.

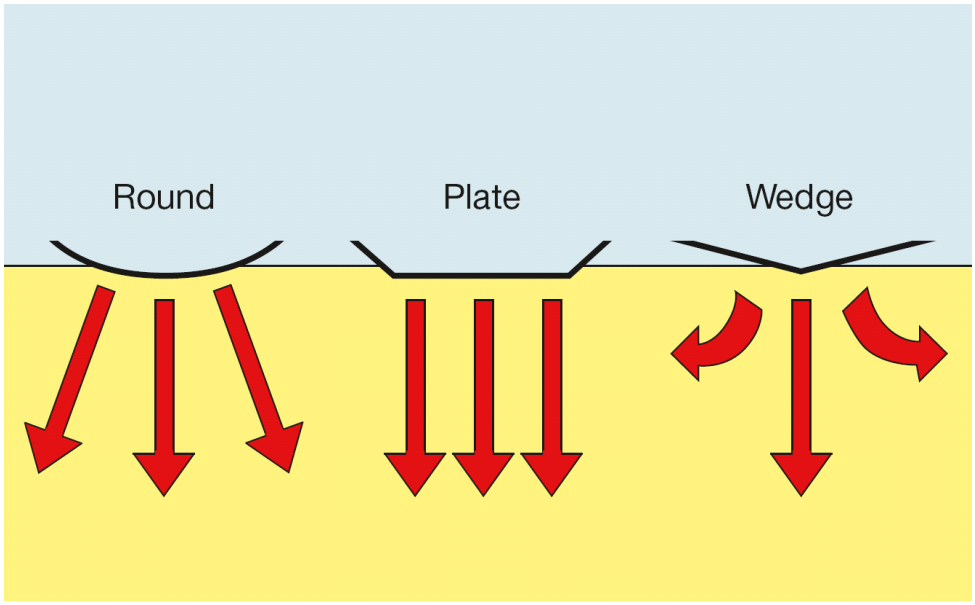

Figure 2.24 Effective directions of force with the cylindrical and polygonal drums (Bomag brochure)

2.3.3. Broons roller

The Australian Broons developed the square impact roller for earth working in the mid-1980s. This roller imparts a massive kinetic energy from 50kJ to 100kJ with every blow. It has been used by many industrial sectors in Australia such as civil engineering, property development, mining and road construction. In particular, in the mining industry, the demands are increasing because the impact rollers reduce the consumption of expensive tires or tire damage by crushing rocks which are used as the road material in the mining sector. Figure 2.25 shows Broons impact rollers and applications.

< Mining Project>

<Port Project>

Figure 2.25 Broons impact roller (Broons web site)

3. FINITE ELEMENT ANALYSIS

The system of an impact roller compacting a soil layer is fairly complex. These complex nonlinear interactions between the drum and the soil are difficult to capture through conventional analytical means. Therefore, explicit dynamic nonlinear finite element methodology will be used to evaluate the movement of the drum-ground interaction systems.

3.1. MODELING AND METHODOLOGY

The methodology to simulate the model of the drum-ground compaction follows these steps:

1. Construct a finite element model of the ground: soft soil (E=10MPa), medium soil (E=30MPa), and hard soil (E=50MPa).
2. Initialize the model of the ground to account for gravitational loading.
3. Simulate the impact rollers against the ground model.
4. Compare the results with field data conducted by the Bomag company with the polygonal drum (BW 225 DH-3).
5. Verify the model and discuss the conclusions.

   The details of these steps are presented in the following sections.

3.1.1. Geometry and Meshing

The total length of the soil model was 16 m (52.5 ft), while the total length of the planned compaction test was approximately 12.8 m (42 ft). Each test was modeled

separately with three different soil properties in order to figure out the compaction efficiency with different drum types: cylindrical, triangular, rounded triangular (Landpac's drum), pentagonal, and octagonal (Bomag's drum).

The soil was modeled using solid elements and the drums were modeled using shell elements with 100 mm (4 in.) thickness. The elements of soil located beneath the roller were meshed finely using the element characteristic size of about 100 mm (4 in.) to capture the soil deformation due to the compaction with more accuracy. The elements of the deeper soil are meshed more coarsely using the element characteristic size of about 200 mm (8 in.) to reduce the computational costs and time of the simulation since these soils are influenced less than the top soils. Hence, the model can have better representation of the load which is transferred from the drum during the compaction. Figure 3.1 shows the compaction model system.

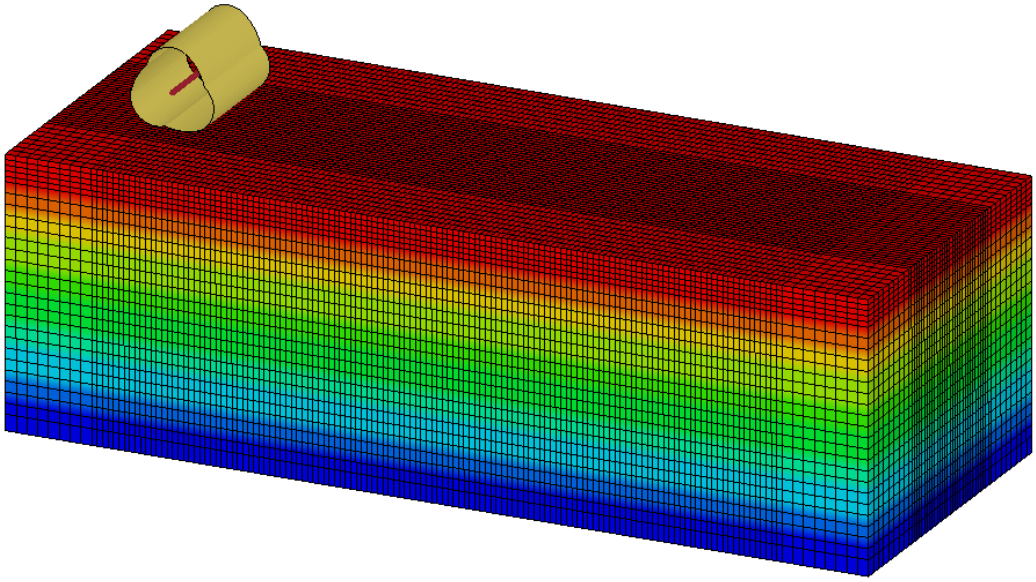

Figure 3.1 3D view of a drum and soil model

3.1.2. Contact

Although LS-DYNA features some of the most advanced contact algorithms available, modeling interaction between a moving drum and a soil is rather complex. To rotate the drum, an axis using a beam element is located in the middle of the drum mesh axially, and then it is drawn by constant velocity at 10km/h. These elements are coupled using the *CONSTRAINED_RIGID_BODIES features in LS-DYNA. The use of this coupling permits the drum mesh to be rotated by friction force between the drum mesh and the soil mesh.

Another coupling mechanism, *CONTACT_AUTOMATIC_SURFACE_TO_ SURFACE, was defined to account for the contact between the drum mesh and the soil mesh as shown in Figure 3.1. The soil is treated as a master material that is coupled with a slave material comprised of the drum and axis. The slave parts (i.e., drum and axis) can be placed anywhere on the master continuum part without any special mesh accommodation.

The contact friction between the drum and the soil was based on the estimated soil external friction angle. The soil friction angle ϕ was 30~35 degrees and then the contact friction was calculated to be 0.6~0.7 (tan ϕ).

3.1.3. Drum Model

For calculating the compaction efficiency of the impact compaction mechines, the interaction between the drum and the soil is very important and therefore has to be simplified in many respects and focused on the parameters that are the most important

for the problem at hand. For these reasons, the interaction between the drum and the soil has to be modeled in greater detail.

The FE models of the rollers consisted of simple representations of the mass which are 12tons (24,000lbs) with 1500mm diameter and 2200mm width. The simplified models of the drum being used are shown in Figure 3.2.

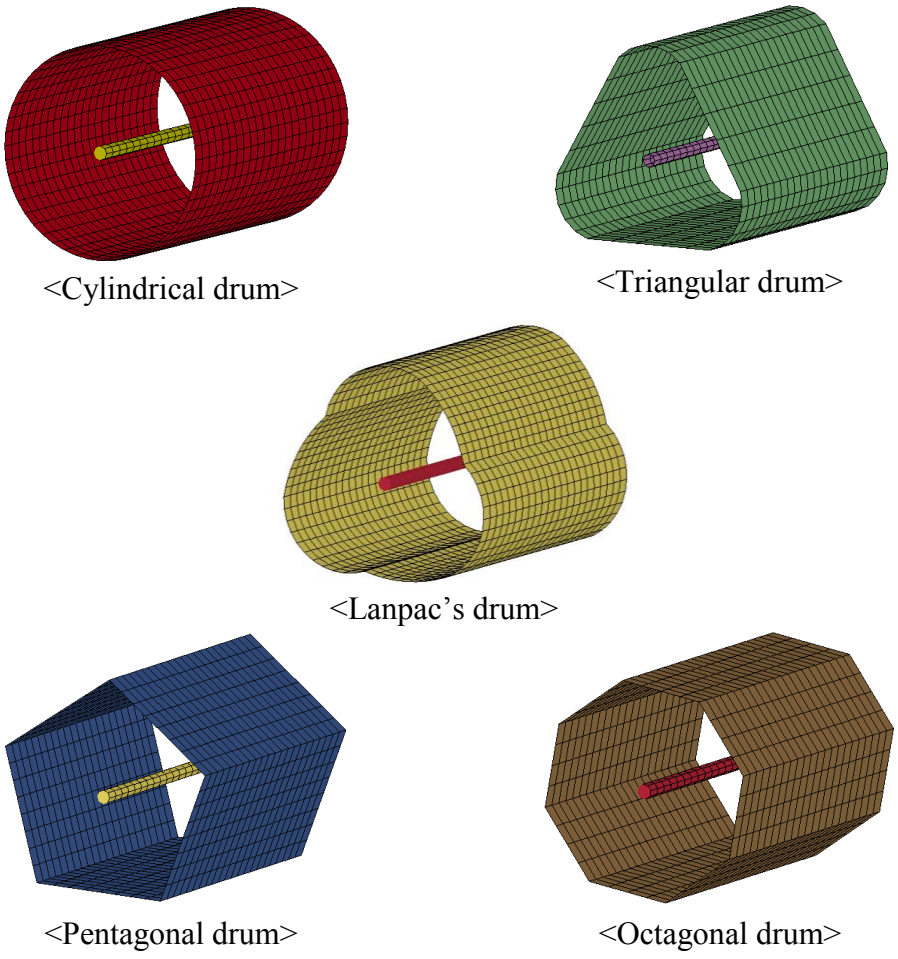

Figure 3.2 Drum models (12 tons)

3.1.4. Soil Material

There are several material options to be considered for modeling the soil in LS-DYNA. These material options range from the very simple elastic material to a nonlinear material model. In this study, the Druker-Prager model corresponding to the Mohr-Coulomb yield criterion is applied to present the behavior of the soil during compaction process. The Mohr-Coulomb criterion has clear physical meaning defined by shear strength parameters c and ϕ. However, it is difficult to implement in the finite element code for the reason that the Mohr-Coulomb criterion has six vertices in the π-plane. In order to obtain the criterion similar to the Mohr-Coulomb criterion, there are several ways to approximate the Mohr-Coulomb hexagonal surface as shown in Figure 3.3.

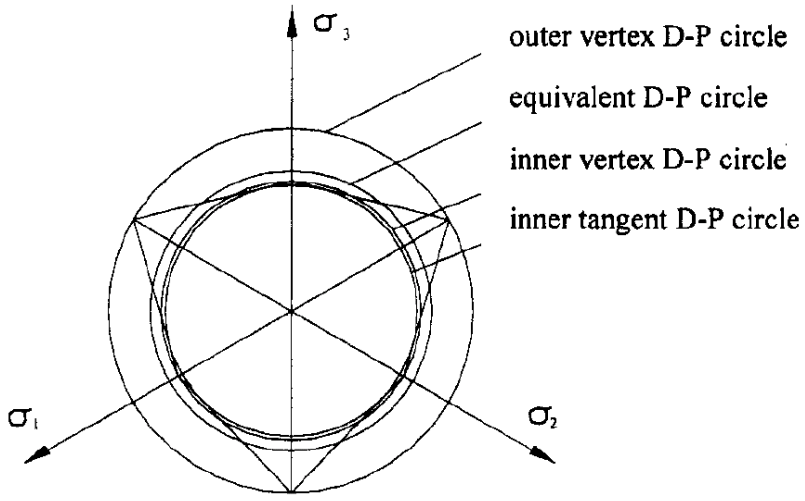

Figure 3.3 Different matching of the Mohr-Coulomb yield surface on the π-plane (Wang et al., 2006)

In order to match the two models in the outer vertex of the Mohr-Coulomb criterion in the π-plane (See Figure 3.3), the Mohr-Coulomb parameters (ϕ and c) can be converted to the Druker-Prager parameters (α and k) by using the following relations:

$$\alpha = \frac{2\sin\phi}{\sqrt{3}\,(3-\sin\phi)} \tag{3.1}$$

$$k = \frac{6c\cos\phi}{\sqrt{3}\,(3-\sin\phi)} \tag{3.2}$$

If the Druker-Prager parameters are determined by the equivalent of the Mohr-Coulomb criterion, α and k are written by

$$\alpha = \frac{2\sqrt{3}\sin\phi}{\sqrt{2}\,\sqrt{3}\,\pi\,(9-\sin^2\phi)} \tag{3.3}$$

$$k = \frac{6\sqrt{3}\,c\cos\phi}{\sqrt{2}\sqrt{3}\,\pi\,(9-\sin^2\phi)} \tag{3.4}$$

If the Druker-Prager parameter are defined by the inner vertex of the Mohr-Coulomb criterion in the π-plane, α and k are given as

$$\alpha = \frac{2\sin\phi}{\sqrt{3}\,(3+\sin\phi)} \tag{3.5}$$

$$k = \frac{6c\cos\phi}{\sqrt{3}\,(3+\sin\phi)} \tag{3.6}$$

If the Druker-Prager parameters are determined by matching the inner tangent of the Mohr-Coulomb criterion in the π-plane, α and k are defined as

$$\alpha = \frac{\sin\phi}{\sqrt{(9+3\sin^2\phi)}} \tag{3.7}$$

$$k = \frac{3c\cos\phi}{\sqrt{(9 + 3\sin^2\phi)}} \tag{3.8}$$

where ϕ and c are the angle of internal friction and cohesion, respectively.

In this study, the outer vertex Druker-Prager circle corresponding to the parameters in Eq. (3.1) and (3.2) are used.

The advantage of the Druker-Prager criterion is smoothness in the stress space which makes the criterion be easily implemented in the computer program. Furthermore, it is adequate for analyzing the mechanical properties of soil and rock masses and produces good results for geotechnical engineering problems (Wang et al, 2006).

1) Pre-Yield Behavior

The pre-yield behavior is modeled as linear elastic using the generalized Hook's Law. The stress-strain relationship of the linear elastic isotropic case is given by

$$\begin{Bmatrix} \varepsilon_{11} \\ \varepsilon_{22} \\ \varepsilon_{33} \\ \varepsilon_{12} \\ \varepsilon_{13} \\ \varepsilon_{23} \end{Bmatrix} = \begin{bmatrix} 1/E & -\nu/E & -\nu/E & 0 & 0 & 0 \\ -\nu/E & 1/E & -\nu/E & 0 & 0 & 0 \\ -\nu/E & -\nu/E & 1/E & 0 & 0 & 0 \\ 0 & 0 & 0 & 1/2G & 0 & 0 \\ 0 & 0 & 0 & 0 & 1/2G & 0 \\ 0 & 0 & 0 & 0 & 0 & 1/2G \end{bmatrix} \begin{Bmatrix} \sigma_{11} \\ \sigma_{22} \\ \sigma_{33} \\ \tau_{12} \\ \tau_{13} \\ \tau_{23} \end{Bmatrix} \tag{3.9}$$

In this equation, the shear modulus, G, can be written in terms of E and υ as G = E/2(1+υ). If the material is characterized by its elastic bulk modulus, K, and its elastic shear modulus, G, the elastic strain increment can be expressed as (Chen and Baladi, 1985)

$$d\varepsilon_{ij}^{e} = \frac{d\,I_1}{9K}\delta_{ij} + \frac{d\,s_{ij}}{2G} \tag{3.10}$$

where, $d\varepsilon_{ij}^{e}$ is the elastic strain increment;

$I_1 = \sigma_{11} + \sigma_{22} + \sigma_{33}$ is the first invariant of the stress tensor;

$s_{ij} = \sigma_{ij} - \frac{I_1}{3}\delta_{ij}$ is the deviatoric stress tensor;

$K = \frac{E}{3(1-2\upsilon)}$ is the bulk modulus;

and δ_{ij} is the kronecker delta.

It is convenient for soil modeling by assuming that the distortion of the soil is caused by the deviator stresses and that the soil volume change is caused by the hydrostatic stresses. The deviator stress matrix is given by

$$\begin{pmatrix} s_{11} & \tau_{12} & \tau_{13} \\ \tau_{21} & s_{22} & \tau_{23} \\ \tau_{31} & \tau_{32} & s_{33} \end{pmatrix} = \begin{pmatrix} \sigma_{11} & \tau_{12} & \tau_{13} \\ \tau_{21} & \sigma_{22} & \tau_{23} \\ \tau_{31} & \tau_{32} & \sigma_{33} \end{pmatrix} - \begin{pmatrix} p & 0 & 0 \\ 0 & p & 0 \\ 0 & 0 & p \end{pmatrix} \tag{3.11}$$

where $p = \frac{I_1}{3} = \frac{\sigma_{11} + \sigma_{22} + \sigma_{33}}{3}$ is the hydrostatic stress.

Using the deviator stresses, the first invariant of the deviator stress is

$$J_1 = s_{ij} = s_{11} + s_{22} + s_{33} = s_1 + s_2 + s_3 = 0 \tag{3.12}$$

The second invariant of the deviator stress is

$$J_2 = \frac{1}{2}s_{ij}s_{ij} = \frac{1}{6}\left[(\sigma_1 - \sigma_2)^2 + (\sigma_2 - \sigma_3)^2 + (\sigma_3 - \sigma_1)^2\right] = \frac{1}{3}\left(I_1^2 - 3I_2\right) \tag{3.13}$$

The third invariant of the deviator stress is

$$J_3 = \frac{1}{3} s_{ij} s_{jk} s_{ki} = \frac{1}{27}\left(2I_1^3 - 9I_1 I_2 + 27I_3\right) \tag{3.14}$$

Now, the advantage of using the stress deviator tensor is apparent. The first invariant J_1 of this tensor is always zero.

2) Initial yield surface

The Druker-Prager criterion in the case of a perfectly plastic material, originally proposed in 1952, is defined as

$$f(I_1, J_2) = \alpha I_1 + \sqrt{J_2} - k = 0 \tag{3.15}$$

where $I_1 = \sigma_{11} + \sigma_{22} + \sigma_{33} = \sigma_1 + \sigma_2 + \sigma_3$ is the first invariant of the stress tensor,

$J_2 = 1/2\, s_{ij} s_{ij}$ is the second invariant of the deviator stress, and

α and k are material constants.

The yield surface of this criterion in the principal stress space, the meridians and cross-section on the π-plane is shown in Figure 3.4 (Chen and Saleeb, 1982).

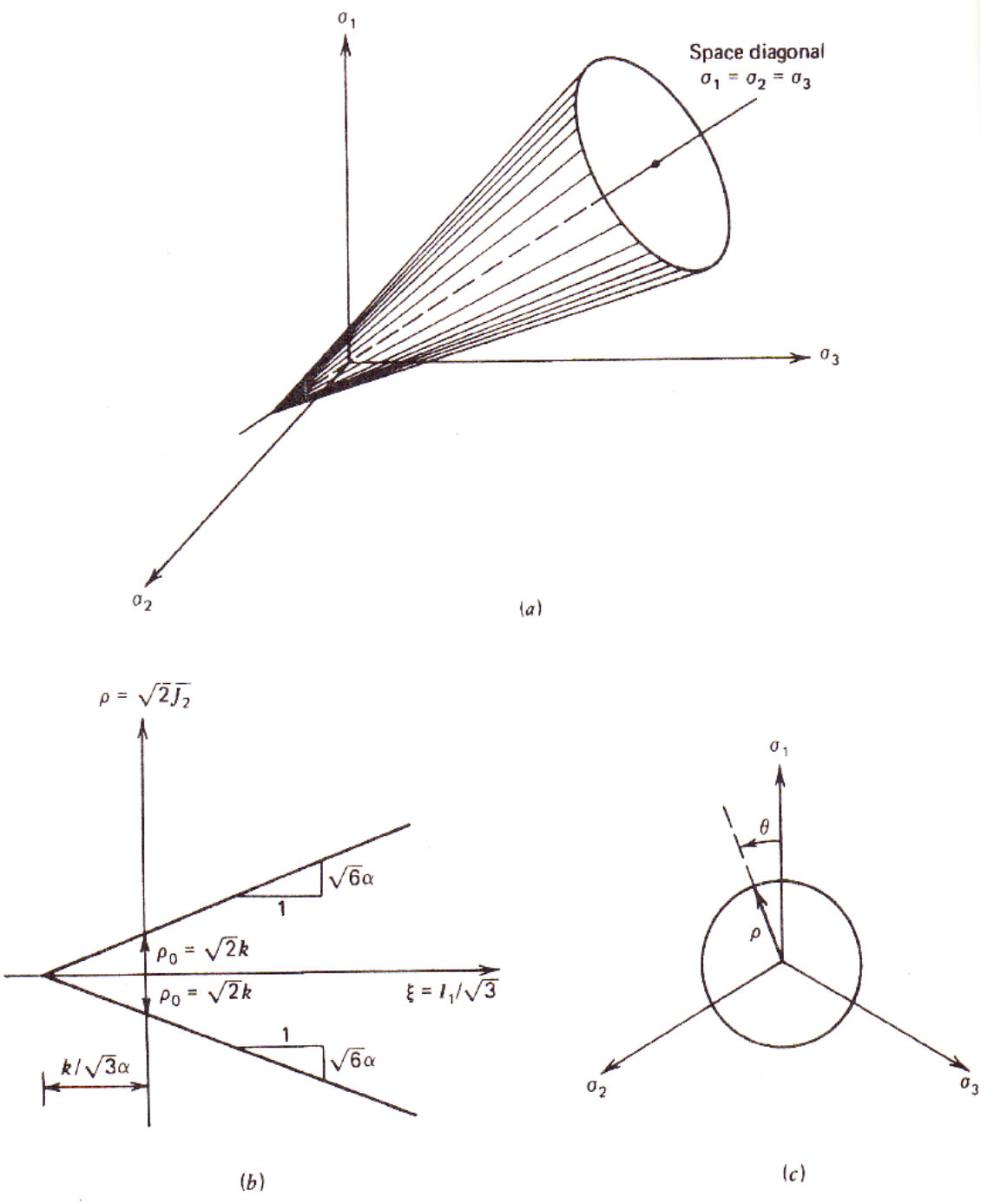

Figure 3.4 Druker-Prager yield surface (a) Principal stress space (b) Meridian plane (θ = constant) (c) Deviatoric plane (Chen and Saleeb, 1982)

As mentioned above, the Druker-Prager yield surface can be defined in terms of a Mohr-Coulombs failure surface and then converted internally with the expression of the measure of the deviatoric stress. This is because the measure of the deviatoric stress is very convenient so that it allows the matching of the different stress values in compression and tension in the deviatoric plane. With the expression of the measure of the deviatoric stress, the Druker-Prager yield surface is given by

$$f = t - p\tan\beta - d = 0 \tag{3.16}$$

where $t = \frac{q}{2}\left[1 + \frac{1}{K} - \left(1 - \frac{1}{K}\right)\left(\frac{r}{q}\right)^3\right]$ is a measure of the deviatoric stress

$$q = \sqrt{3J_2} = \sqrt{\frac{3}{2}s_{ij}s_{ji}} = \sqrt{\frac{1}{2}\left[(\sigma_1 - \sigma_2)^2 + (\sigma_2 - \sigma_3)^2 + (\sigma_3 - \sigma_1)^2\right]}$$

$$r = \left(\frac{27}{2}J_3\right)^{1/3} = \left(\frac{9}{2}s_{ij}s_{jk}s_{ki}\right)^{1/3} = \left(\frac{27}{2}J_3 - 9J_1J_2 + J_1^3\right)^{1/3}$$

$p = \frac{1}{3}trace(\sigma) = \frac{1}{3}(\sigma_{11} + \sigma_{22} + \sigma_{33})$ is the hydrostatic pressure stress,

K is the shape factor for yield surface (See Figure 3.5),

and β is the material friction angle and d is its cohesion in the p-t plane as indicated in Figure 3.6.

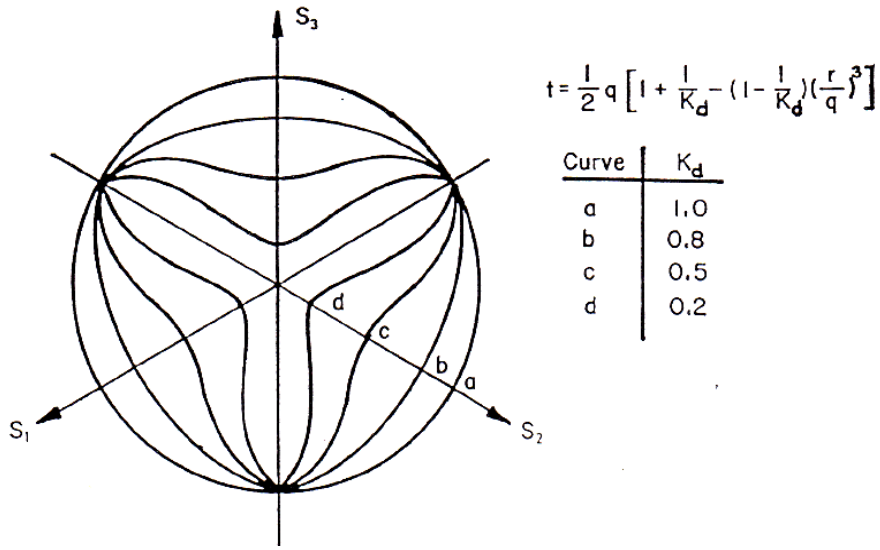

Figure 3.5 Projection of the Druker-Prager yield surface on the π-plane (LS-DYNA theory manual)

The effect of different values of K on the shape of the yield surface on the π-plane is described in Figure 3.5. To keep the convexity of the yield surface, the range of the K-value is $0.8 \le K \le 1.0$. In this study, the K-value is simply taken as 1.0.

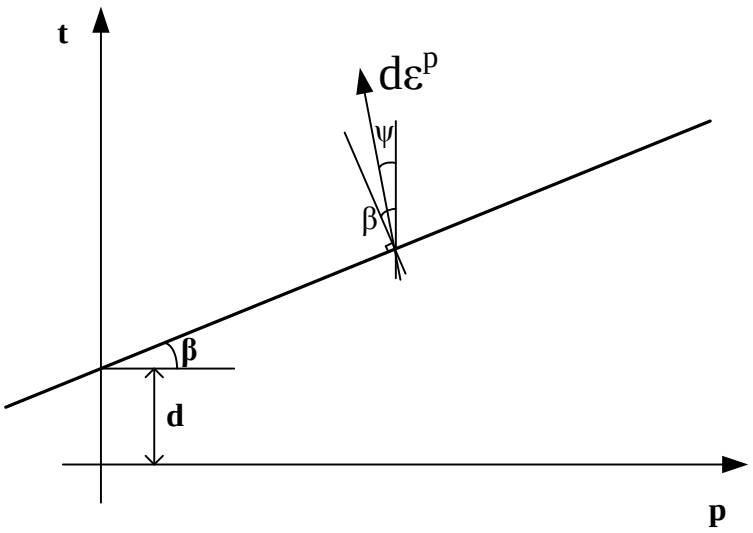

Figure 3.6 Yield surface of the Druker-Prager model on the p-t plane

To achieve correspondence between the original Druker-Prager model parameters (α and k) and the modified Druker-Prager model parameters (β and d), at least three triaxial compression tests are required to determine the parameters ϕ and c. The Mohr-Coulomb parameters (ϕ' *and* c') can be converted to modified Druker-Prager parameters by using the following equations:

$$\tan\beta = \frac{6\sin\phi}{3-\sin\phi} \tag{3.17}$$

$$d = \frac{6c\cos\phi}{3-\sin\phi} \tag{3.18}$$

In this study, the soil material parameters are defined in Table 3.1.

Table 3.1 Properties of the soil mesh

Material	C (kPa)	γ (kN/m$^{3)}$	E (MPa)	ν	φ (deg)	ψ (deg)
Poorly compacted soil	1	19	10	0.35	30	0
Med. compacted soil	1	20	30	0.35	35	0
Well compacted soil	1	21	50	0.35	40	0

3) Flow rule

Plastic strain will occur when the current stress state is outside the elastic region. If the plastic-strain increment, $d\varepsilon_{ij}^{p}$, is considered as a vector in the plastic-strain space superimposed on the stress space, $d\varepsilon_{ij}^{p}$ can be written as

$$d\varepsilon_{ij}^{p} = d\lambda \frac{\partial g}{\partial \sigma_{ij}} \tag{3.19}$$

where $d\lambda$ is a non-negative scalar

The direction of the plastic strain increment is determined by the gradient vector $\partial g / \partial \sigma_{ij}$ and $d\lambda$ defines the magnitude of the plastic strain increment.

In Eq. 19 above, when the plastic potential function g is equal to the yield function f, it is called the associated flow rule or normality condition. Another case is called the non-associated flow rule.

In most soil behavior, the dilation angle will never be constant. For small shearing strains, the dilation angle is non-linear. However, it converges to zero (default) at larger stains. Figure 3.7 shows the typical behavior of loose and dense granular soils.

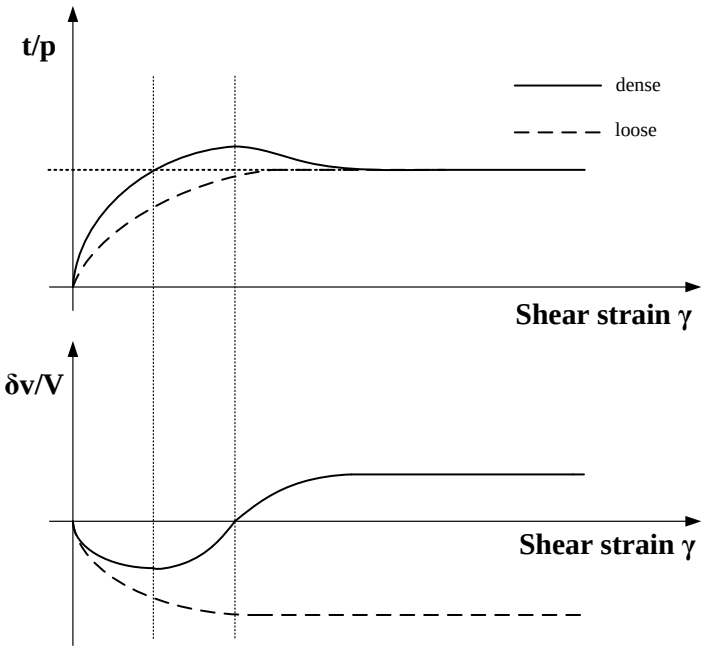

Figure 3.7 The typical behavior of loose and dense granular soils

In LS-DYNA, the dilation angle is approximately calculated by the following equation:

$$\psi = \left[\sin^{-1}\left(\frac{\delta V_p}{\delta \gamma_p}\right)\right], \ or \ \sin\psi = \left(\frac{t}{p} - m\right) \tag{3.20}$$

where δV_p is the increment of the volumetric strain;

$\delta \gamma_p$ is the increment of the shear strain; and

t is the deviatoric stress; p is the pressure; and m is the material constant.

In this model, the plastic potential function, g, is given as

$$g = t - p\tan\psi \tag{3.21}$$

The plastic deformation will occur in a direction normal to the plastic potential, thus, ψ = β (associated flow rule). In case of ψ = 0, the dilation will not occur.

The geometric interpretation of ψ is shown in Figure 3.6.

4) Hardening rule

A yield surface changes during the loading process because the stress state point always lies on it. However, there are an infinite number of evolutions of the yield surface that exist. It is one of the main problems in the plastic theory to determine how loading surface evolves. For this study, the Druker-Prager model implemented in LS-DYNA is elastic perfectly plastic material (i.e., only one surface exists which serves as the yield and failure surface). Thus, there is no hardening.

3.1.5. Initialization of the soil model for gravitational loading before compacting

The soil model was initialized to account for gravitational loading. Gravity loading builds up the initial stress in depths. The initialized soil stress condition by gravity force for the model was shown in Figure 3.8.

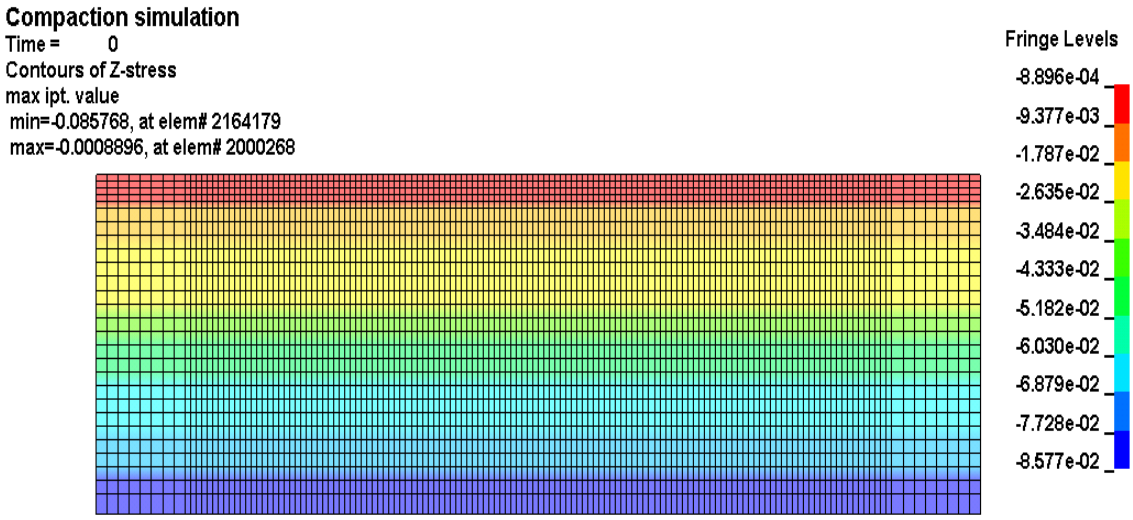

Figure 3.8 Established gravity force on the soil model by depth

3.2. CYLINDRICAL ROLLER: Soil E= 10MPa, 30MPa, and 50MPa

Numerical simulations were used as the primary modeling tool to study the behavior of the impact rollers since calculating and/or predicting the improvement in the ground after compaction are not easy. In this study, the aim of the modeling is to determine the approximate distribution of stress under an impact roller and the influence depth. It is commonly defined to the depth at which the vertical stress has decreased to one-tenth of the stress at the surface.

With this definition, the influence depth of the soil Modulus E=10MPa, 30MPa, and 50MPa are 1.25m, 0.95m, and 0.9m, respectively as shown in Figure 3.10. The model of the simulation with the cylindrical roller to determine the influence depth on the variable soil types is shown in Figure 3.9.

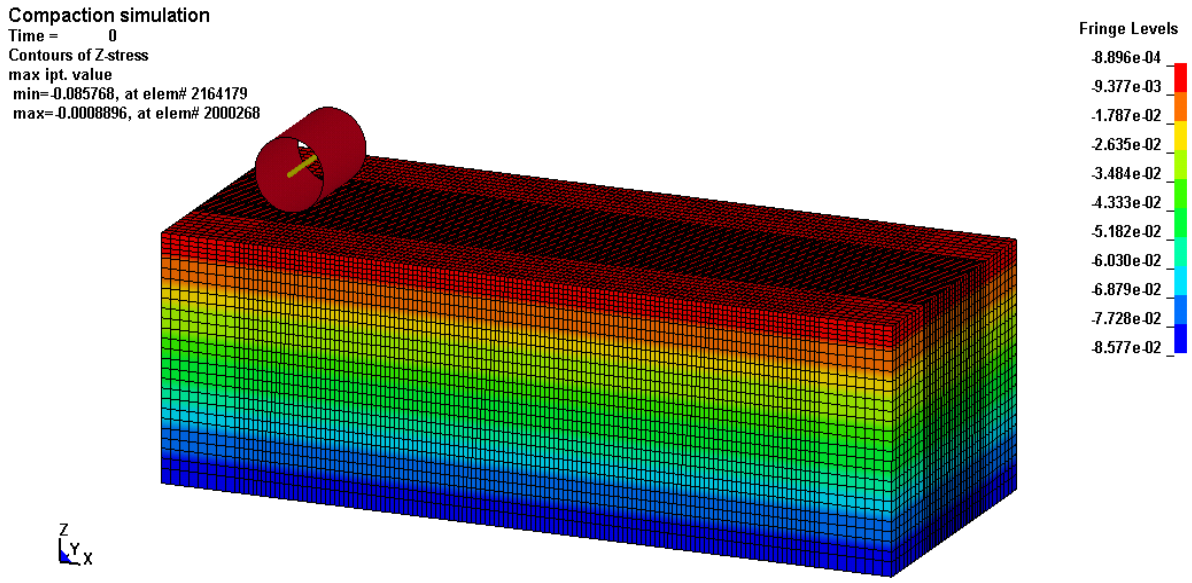

Figure 3.9 Ground-roller interaction model using the cylindrical drum

1) Influence depth

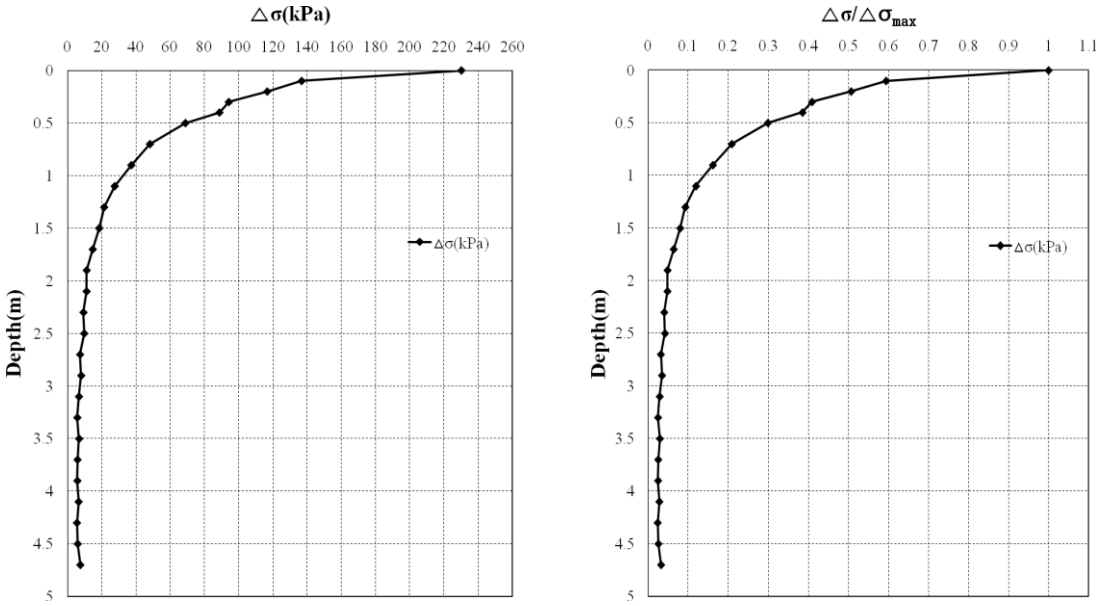

(a) Stress distribution under the drum in soil (E=10MPa, γ=19kN/m^3, φ=30°)

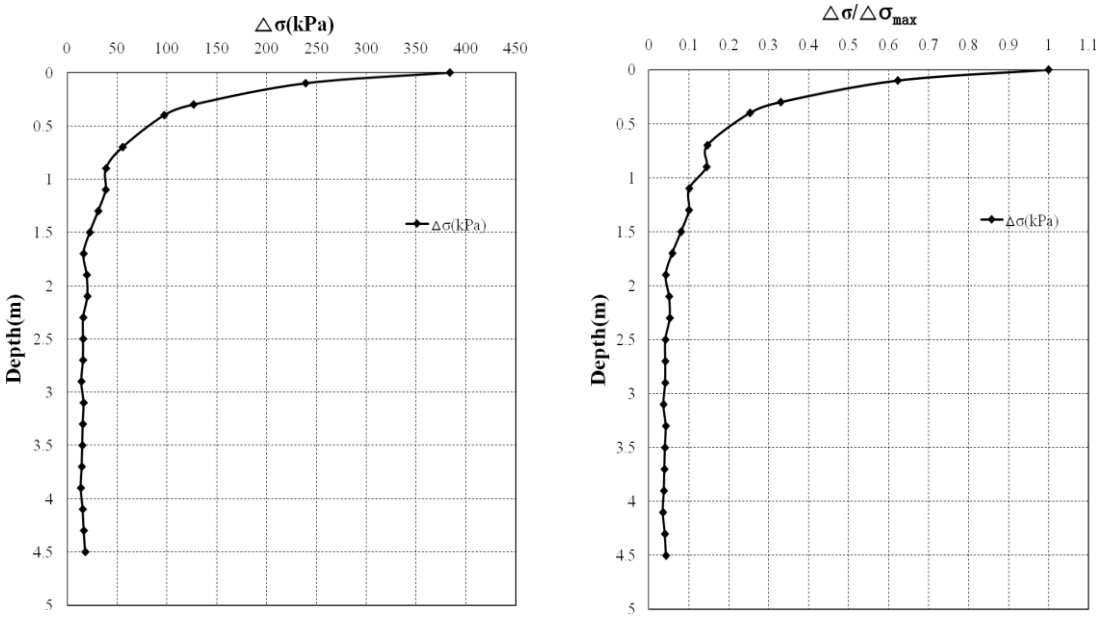

(b) Stress distribution under the drum in soil (E=30MPa, γ=20kN/m^3, φ=35°)

Figure 3.10 Vertical stresses distribution under the cylindrical drum for different soil types: (a) Soil properties: E=10MPa, γ=19kN/m^3, φ=30°, (b) Soil properties: E=30MPa, γ=20kN/m^3, φ=35°, and (c) Soil properties: E=50MPa, γ=21kN/m^3, φ=40°

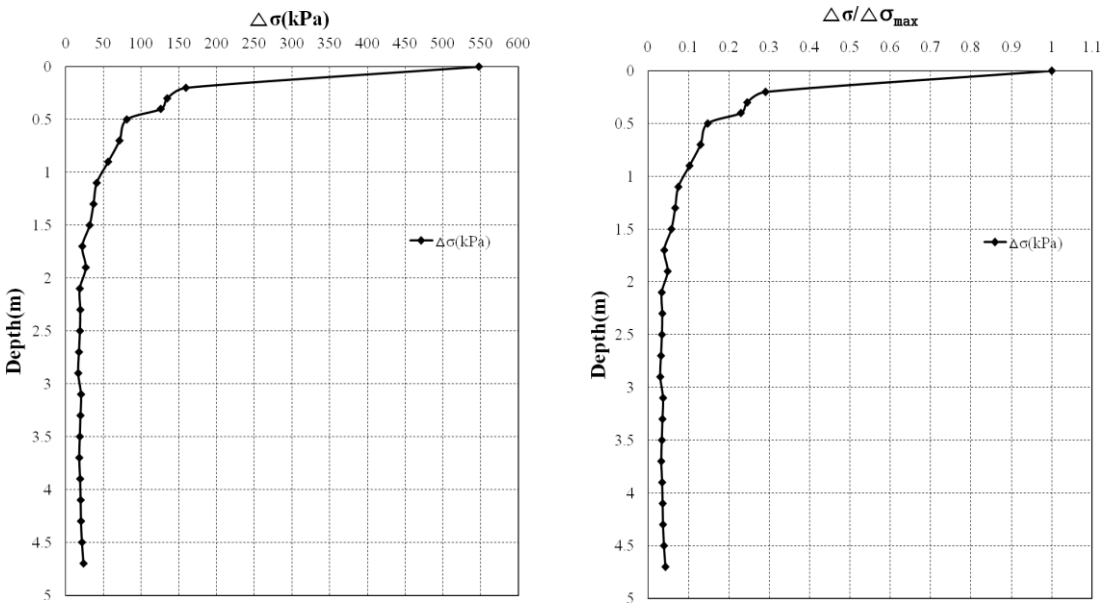

(c) Stress distribution under the drum in soil (E=50MPa, γ=21kN/m^3, φ=40°)

Figure 3.10 continued

In order to compare the depth of influence in the different soil types, the vertical stresses are divided by the maximum stress at the surface to normalize the stress distribution curves. As a result, the depth of influence is deeper in poorly compacted soil (i.e., loose soil) while the maximum stress is higher in well-compacted soil (i.e., dense soil). It is clear evidence that the larger contact areas are better for deep compaction. Figure 3.11 shows the depth of influence in the ground as a reaction to the different types of soil properties.

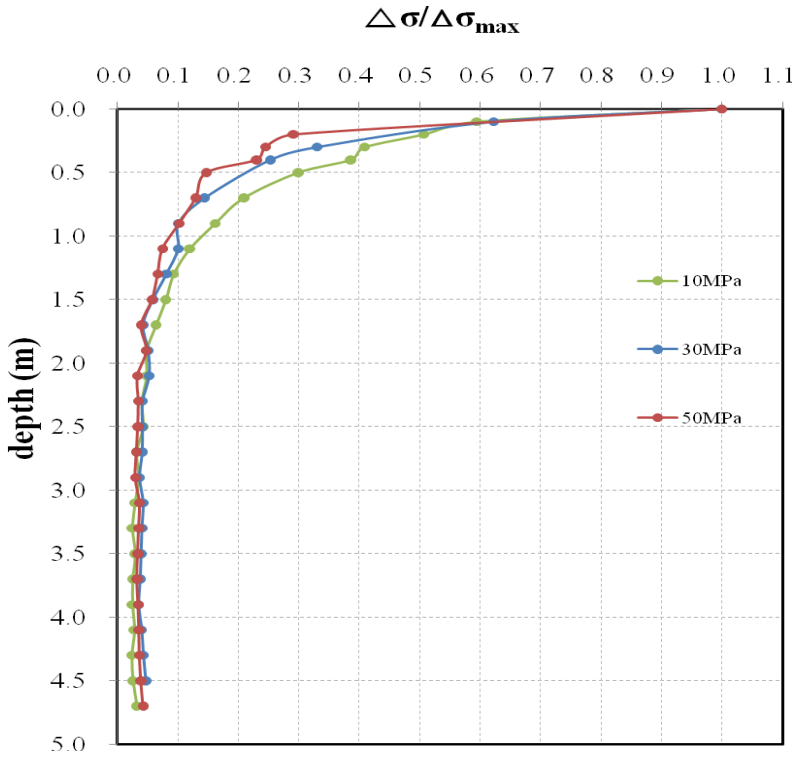

Figure 3.11 Comparison of the stress distribution using the cylindrical drum for different soil types

2) Displacement

A typical pattern of the displacement measured is also plotted in Figure 3.12. As the roller approached, the soil recorded a slight uplift and then noticeable permanent displacement. The surface deformations for soil Modulus E=10Mpa, 30Mpa, and 50Mpa are 15.75 mm, 4.46 mm, and 2.05 mm, respectively.

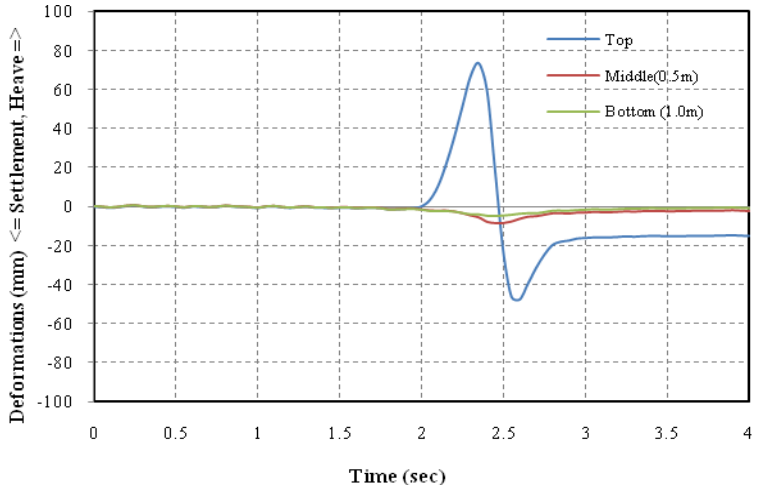

(a) Displacement of a given point as the roller passes (E=10MPa, γ=19kN/m^3, φ=30°)

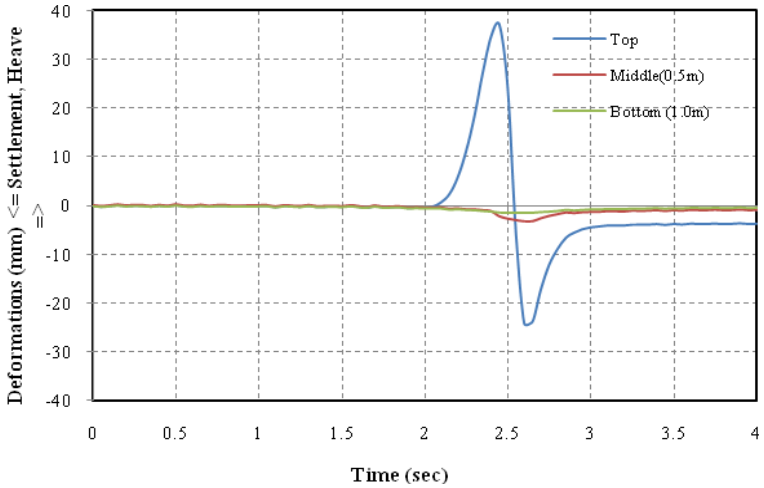

(b) Displacement of a given point as the roller passes (E=30MPa, γ=20kN/m^3, φ=35°)

Figure 3.12 Displacements relative to the beginning of the measurements under the cylindrical drum

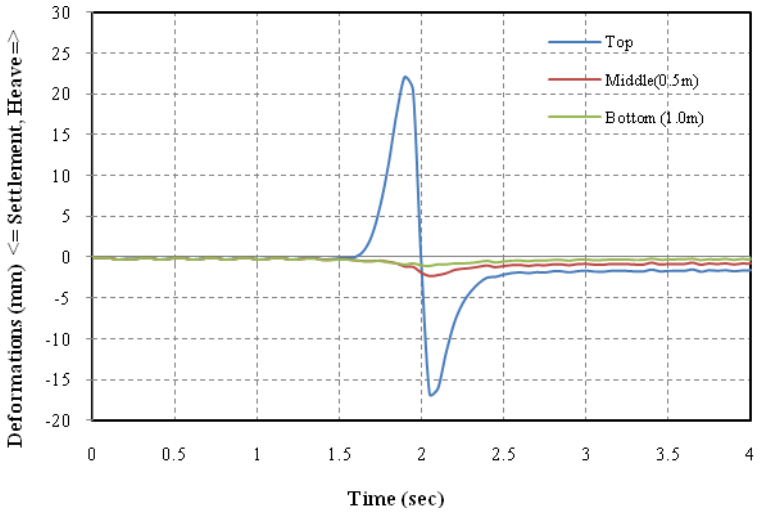

(c) Displacement of a given point as the roller passes (E=50MPa, γ=21kN/m^3, φ=40°)

Figure 3.12 continued

Figure 3.13 shows the visualized stress distribution during the simulation process in using the cylindrical drum. It shows that the stress distribution is constant during the whole compaction process. This can explain the fact that the cylindrical rollers achieve the smooth and even surface when finished. In addition, the vertical stress generated by the cylindrical drum is higher in dense soil because dense soil allows less settlement than loose soil. The result is that the contact area in dense soils is smaller than in loose soils; therefore, the contact pressure in dense soils is much higher. Whereas, the depth of influence is not deep enough to compact thick layers (See Figure 3.10). It means that the cylindrical drum machines are suitable for compacting thin layers and finishing with an even surface.

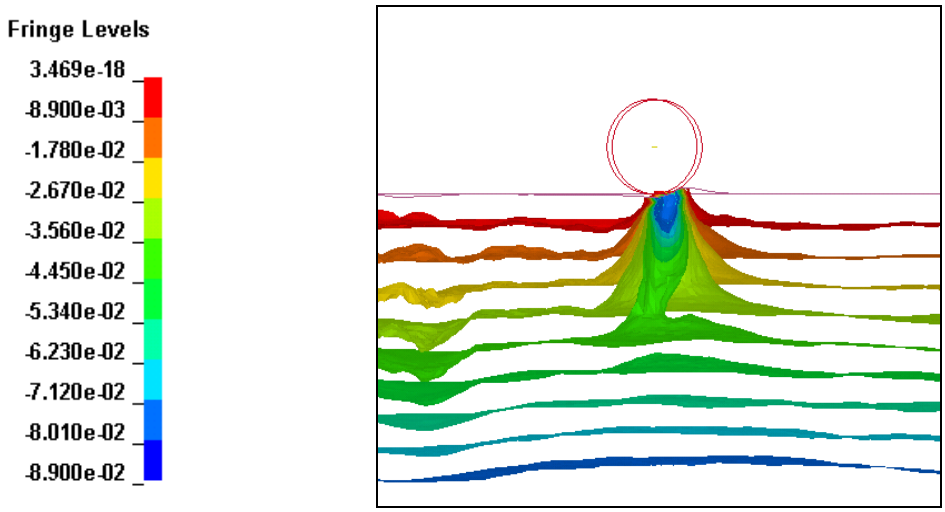

(a) Soil (E=10MPa, γ=19kN/m^3, φ=30°)

(b) Soil (E=30MPa, γ=20kN/m^3, φ=35°)

(c) Soil (E=50MPa, γ=21kN/m^3, φ=40°)

Figure 3.13 Vertical stress distribution under the cylindrical drum for different soil properties

3.3. TRIANGULAR ROLLER: Soil E= 10MPa, 30MPa, and 50MPa

The ground-roller interaction model using triangular drum is shown in Figure 3.14. In this case, the influence depth of the soil Modulus E=10MPa, 30MPa and 50MPa are 2.3m, 1.9m, and 1.5m, respectively. The results of the simulation to determine the depth of influence on the variable soil types are shown in Figure 3.15.

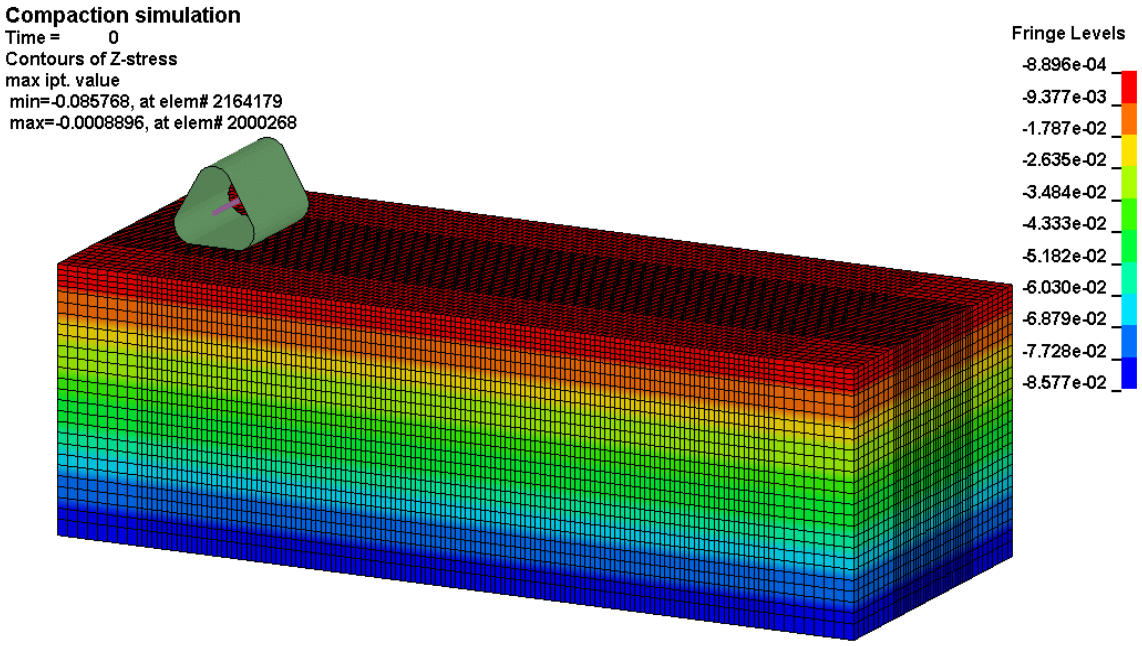

Figure 3.14 Ground-roller interaction model using the triangular drum

1) Influence depth

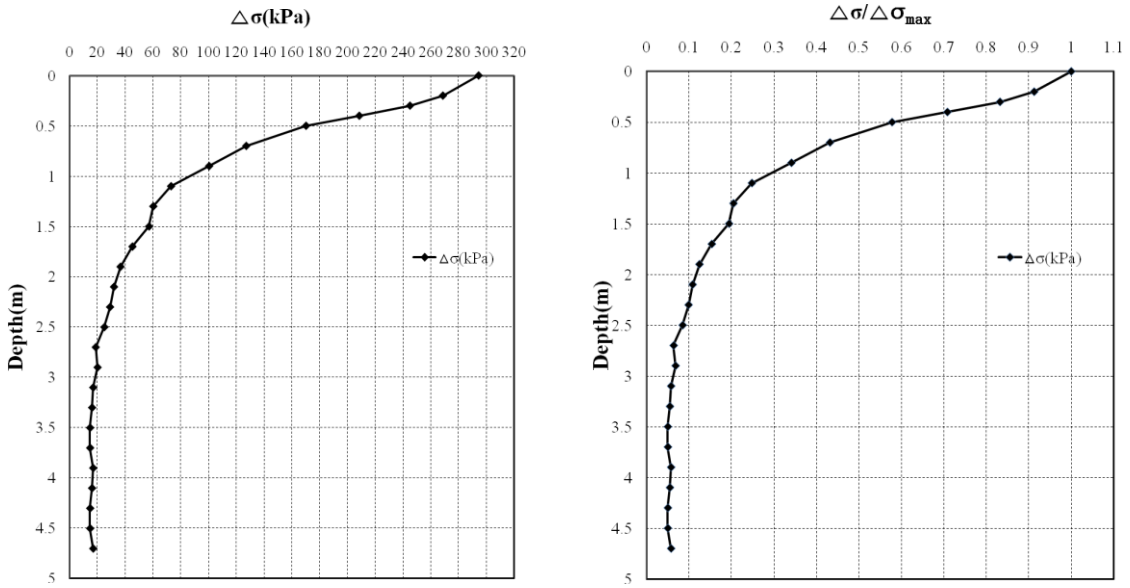

(a) Stress distribution under the drum in soil (E=10MPa, γ=19kN/m^3, φ=30°)

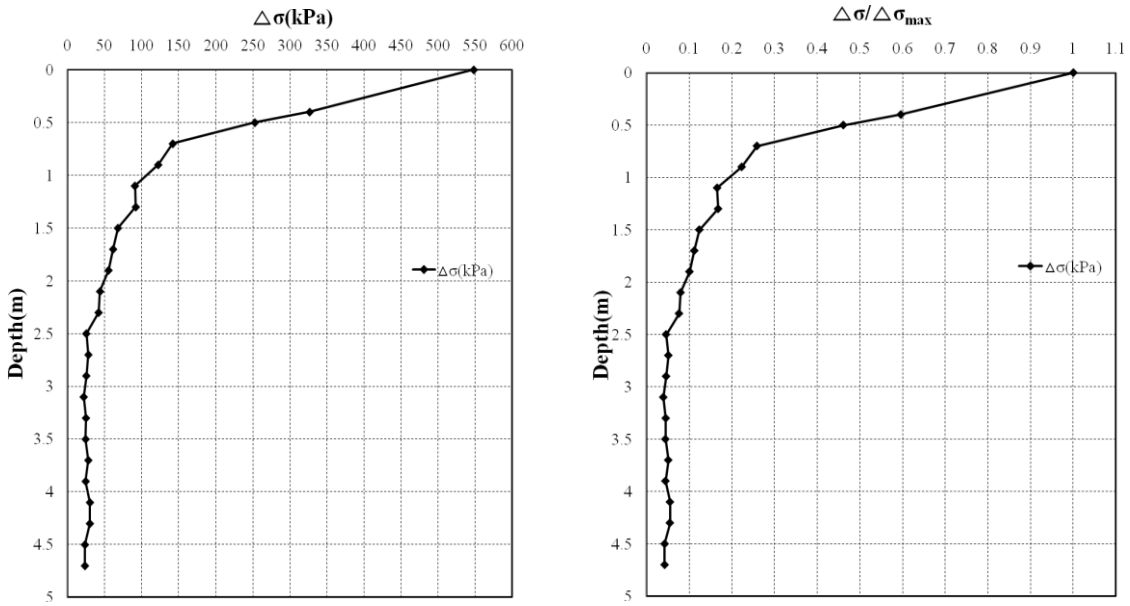

(b) Stress distribution under the drum in soil (E=30MPa, γ=20kN/m^3, φ=35°)

Figure 3.15 Vertical stresses distribution under the triangular drum for different soil types in using triangular drum: (a) Soil properties: E=10MPa, γ=19kN/m^3, φ=30°, (b) Soil properties: E=30MPa, γ=20kN/m^3, φ=35°, and (c) Soil properties: E=50MPa, γ=21kN/m^3, φ=40°

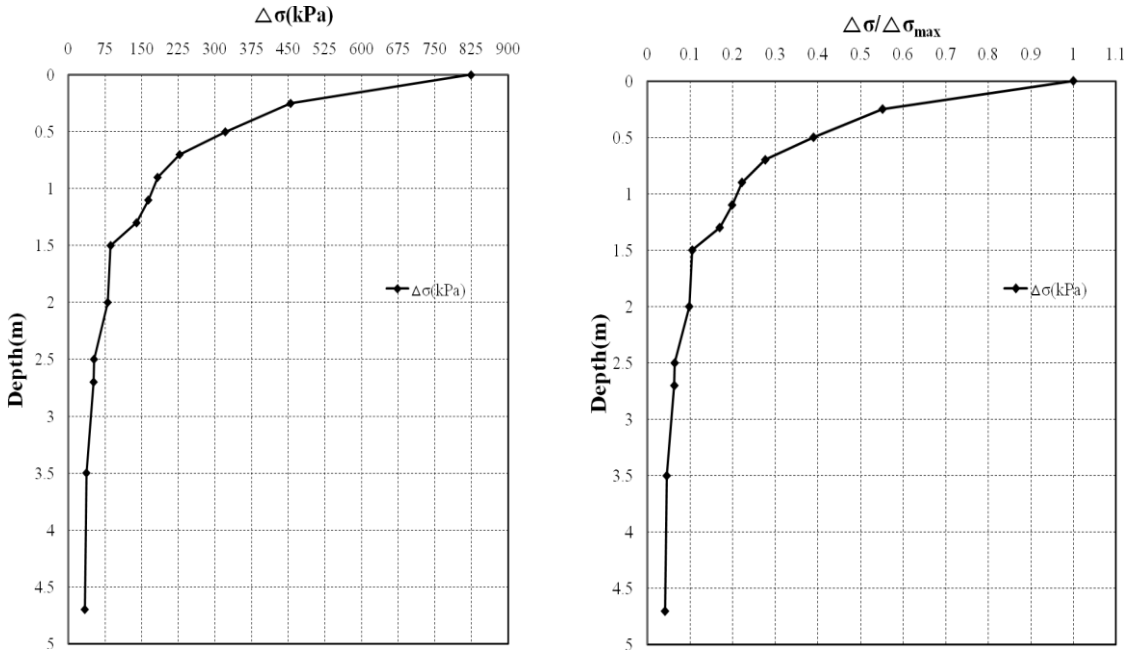

(c) Stress distribution under the drum in soil (E=50MPa, γ=21kN/m^3, φ=40°)

Figure 3.15 continued

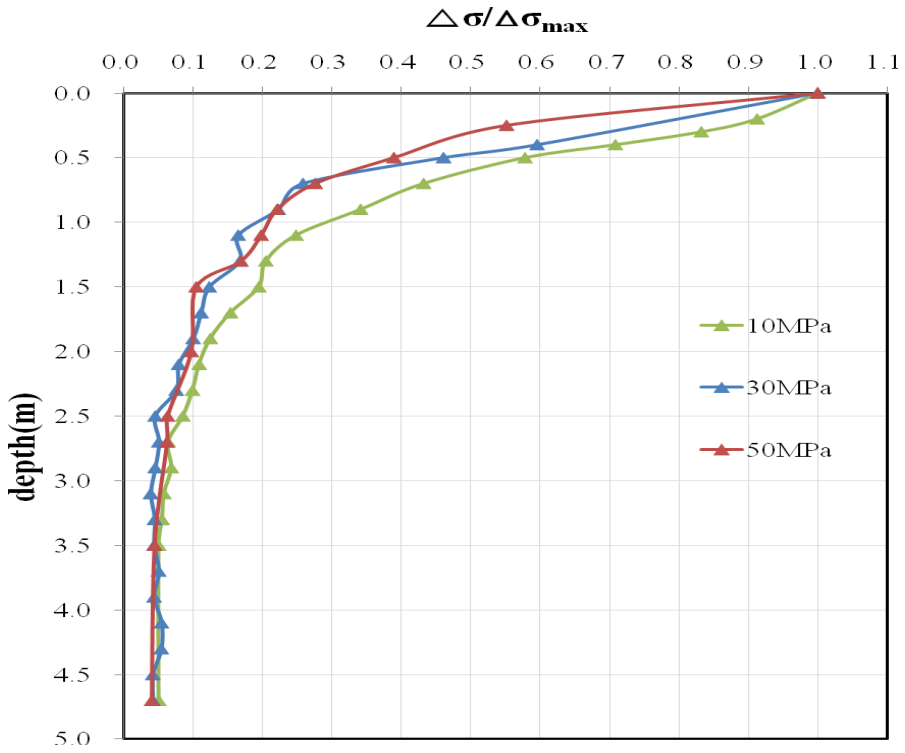

Figure 3.16 Comparison of the stress distribution using the triangular drum for different soil types

In addition, Figure 3.16 shows the comparison of the stress distribution for different soil types. The above results were obtained by selecting the maximum stress point to a depth of 5m. However, simply comparing the results using the maximum stress distribution does not represent the impact compaction phenomenon because the impact compaction rollers are comprised of the plate segments and the wedge segments. The plate segment takes over the concentrated compaction in the depth, whereas the wedge with its high linear load creates tensile splitting forces. These horizontal shearing forces shift the soil locally and remove the bracing of the soil particle structure which inhibits compaction.

2) Displacement

A typical pattern of the displacement measured is also plotted in Figure 3.17. As the roller approached, the soil recorded a slight uplift and then a noticeable permanent displacement. The surface deformations for the soil Modulus E=10MPa, 30MPa, and 50MPa are 32.89 mm, 22.82 mm, and 10.91 mm, respectively.

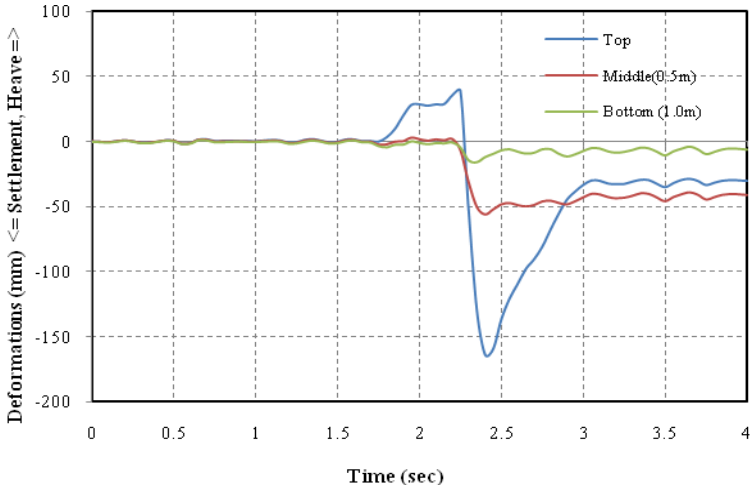

(a) Displacement of a given point as the roller passes (E=10MPa, γ=19kN/m^3, φ=30°)

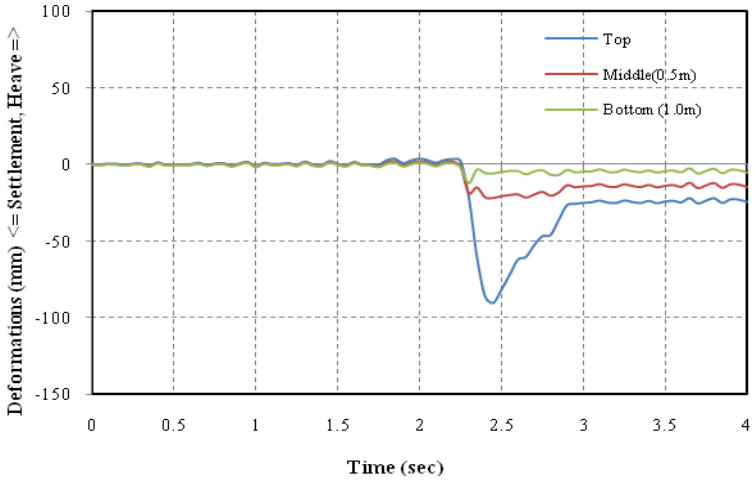

(b) Displacement of a given point as the roller passes (E=30MPa, γ=20kN/m^3, φ=35°)

Figure 3.17 Displacements relative to the beginning of the measurements under the triangular drum

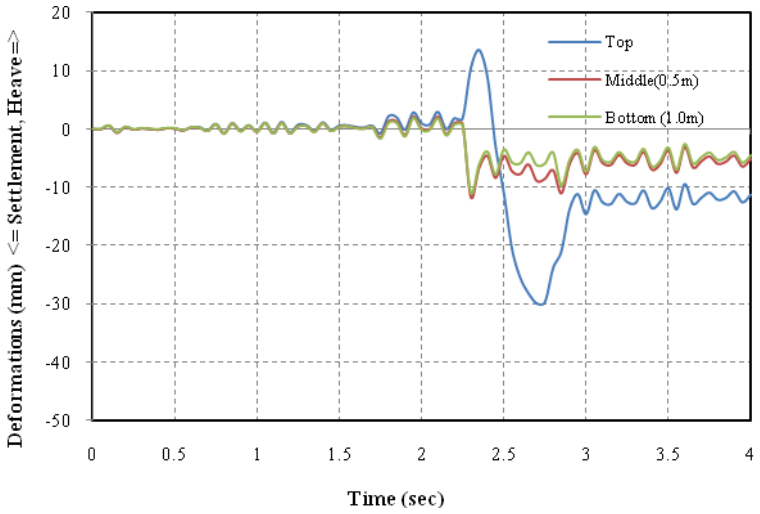

(c) Displacement of a given point as the roller passes (E=50MPa, γ=21kN/m^3, φ=40°)

Figure 3.17 continued

As mentioned before, the impact roller compaction is characterized by the plate and the wedge effect visualized by means of the representation of this pressure distribution in the dynamic simulation as shown in Figure 3.18.

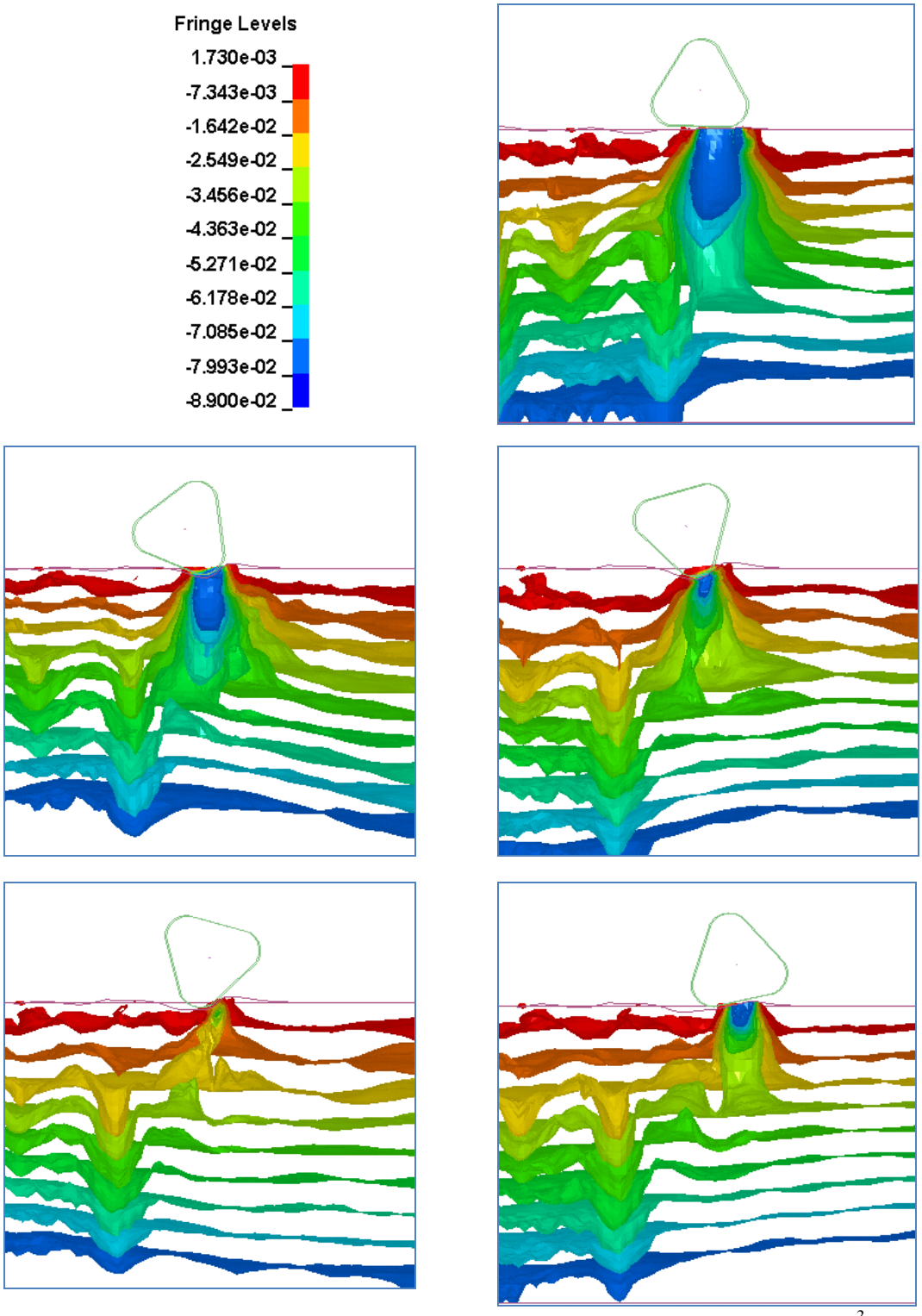

(a) Vertical Stress distribution under the drum in soil (E=10MPa, γ=19kN/m^3, φ=30°)

Figure 3.18 Compaction mechanism under the triangular drum

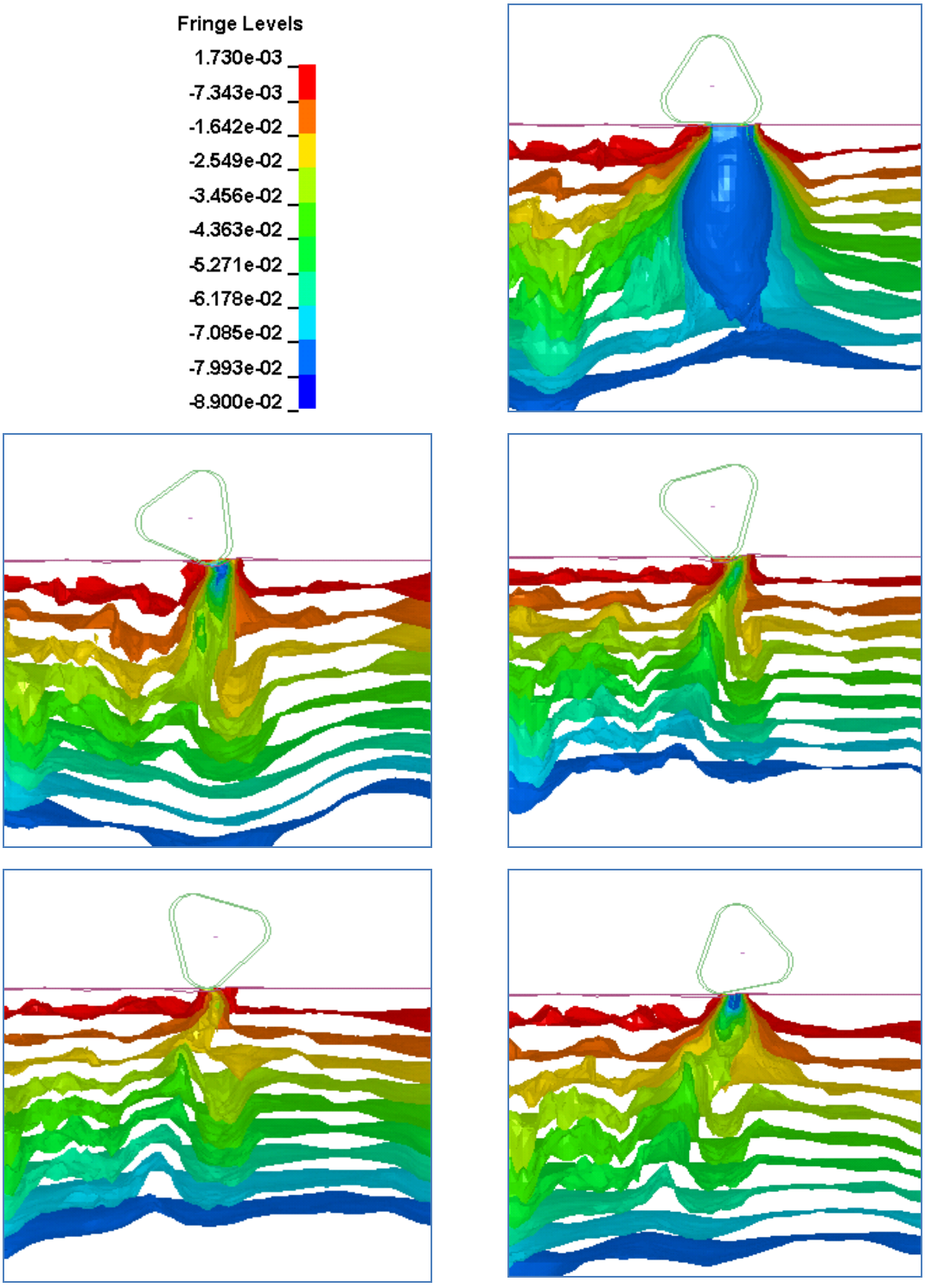

(b) Vertical stress distribution under the drum in soil (E=30MPa, γ=20kN/m^3, φ=35°)

Figure 3.18 continued

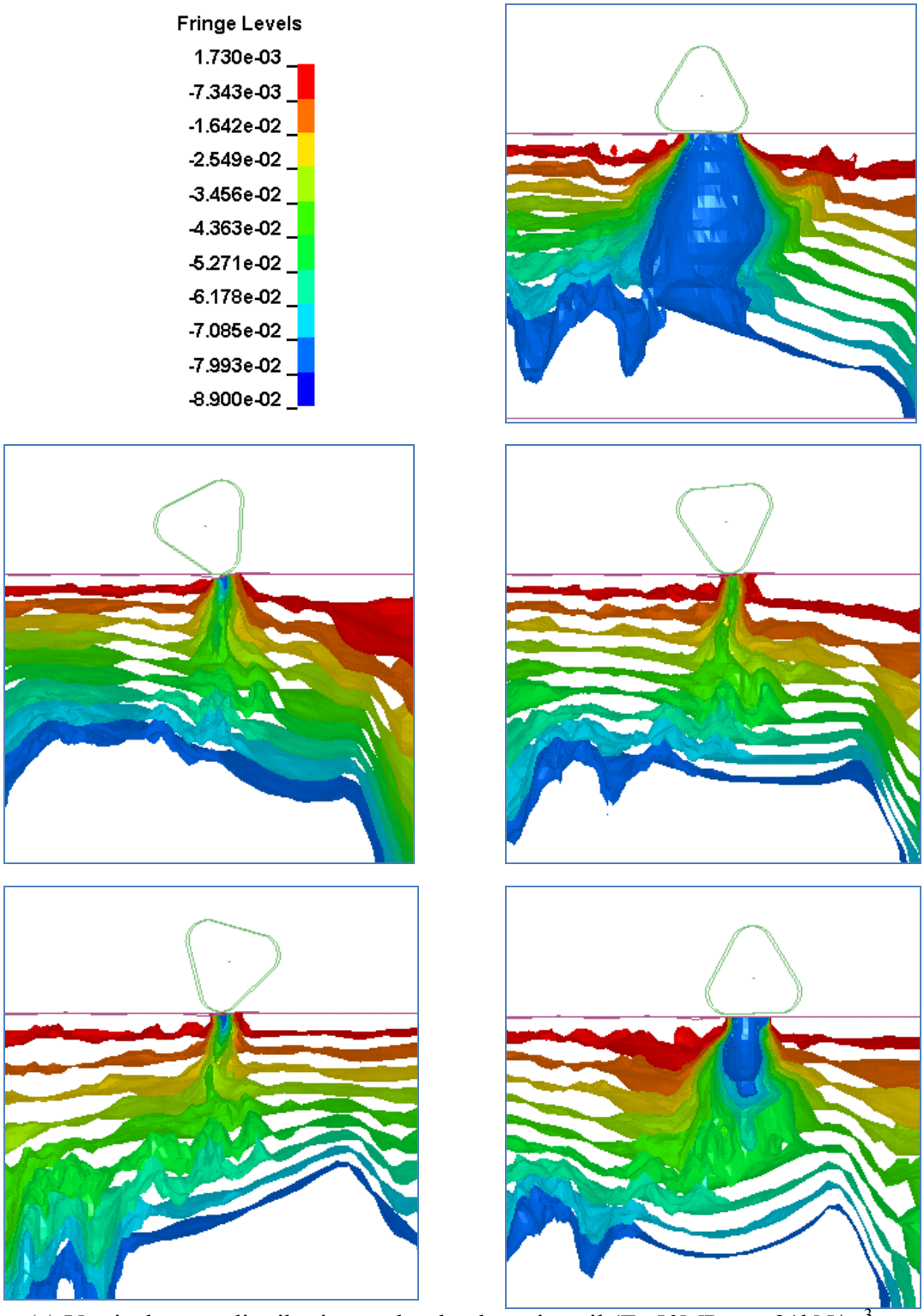

(c) Vertical stress distribution under the drum in soil (E=50MPa, γ=21kN/m^3, φ=40°)

Figure 3.18 continued

3.4. LANDPAC ROLLER: Soil E= 10MPa, 30MPa, and 50MPa

The ground-roller interaction model using the Landpac drum is shown in Figure 3.19. In this case, the depth of influence of the soil Modulus E=10MPa, 30MPa, and 50MPa are 1.9m, 1.6m, and 1.2m, respectively. The results of the simulation to determine the depth of influence on the variable soil types are shown in Figures 3.20 and 3.21.

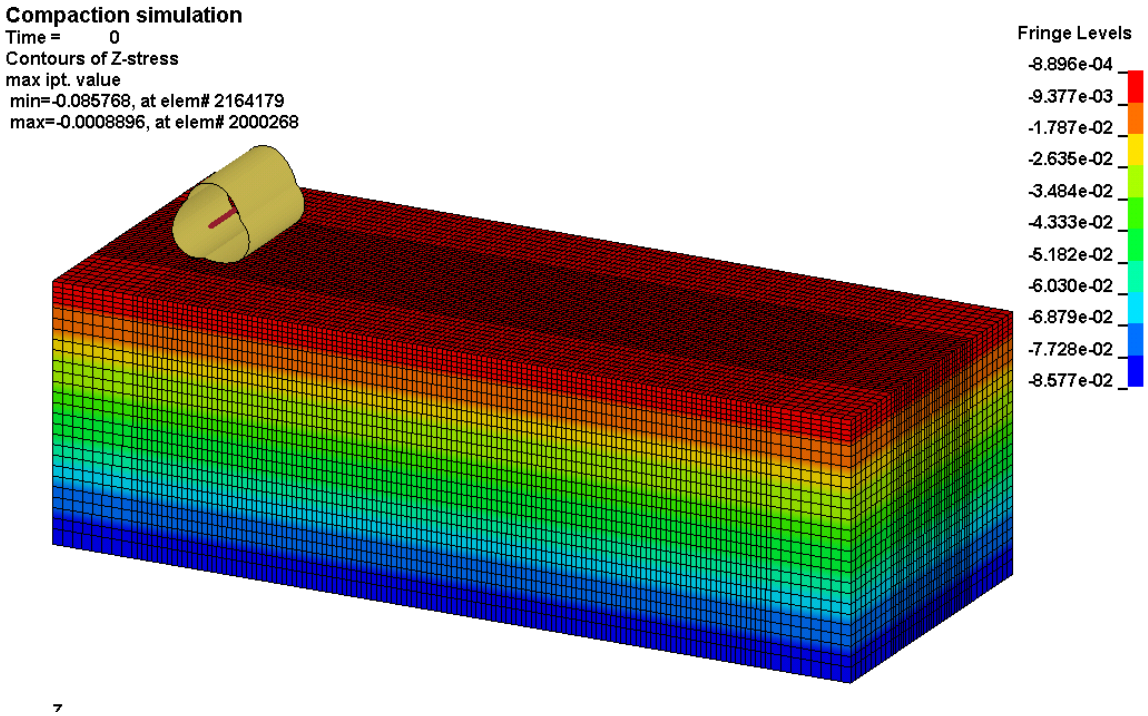

Figure 3.19 Ground-roller interaction model using the Landpac drum

1) Influence depth

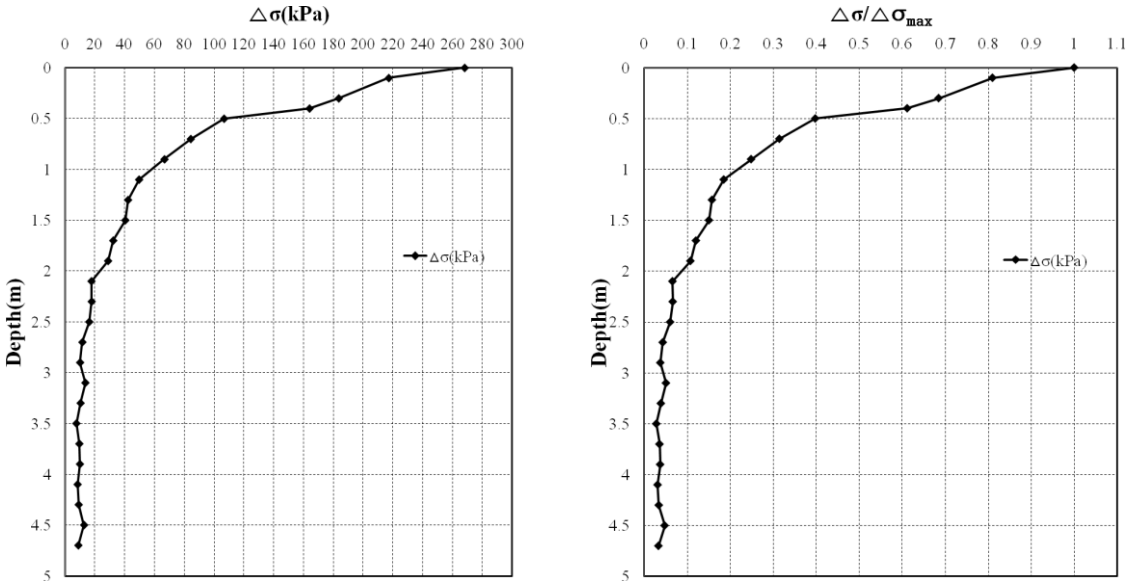

(a) Stress distribution under the drum in soil (E=10MPa, γ=19kN/m^3, φ=30°)

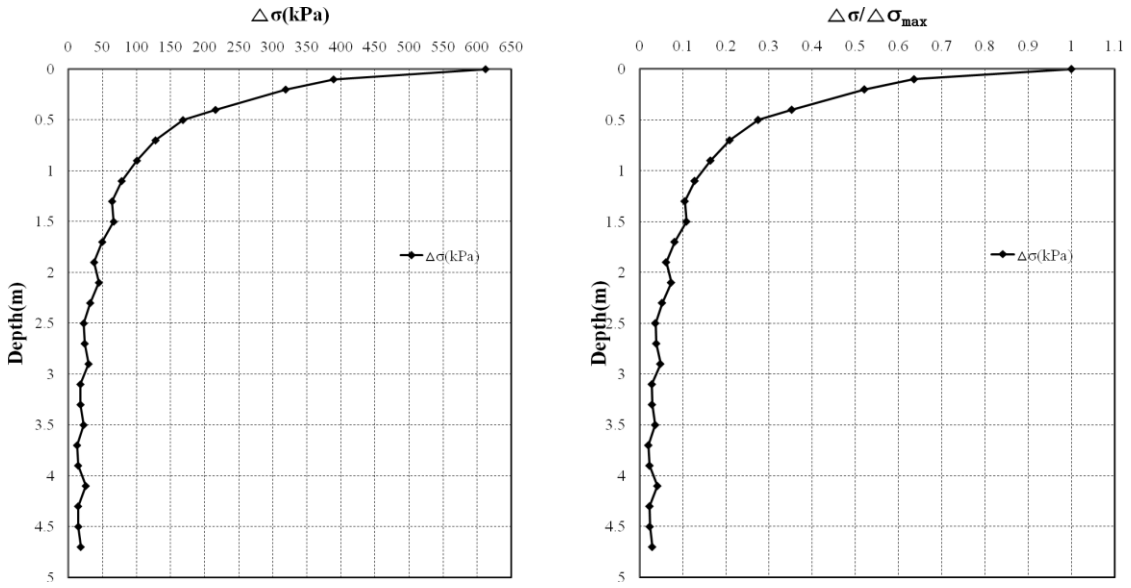

(b) Stress distribution under the drum in soil (E=30MPa, γ=20kN/m^3, φ=35°)

Figure 3.20 Vertical stresses distribution under the Lanpac drum for different soil types: (a) Soil properties: E=10MPa, γ=19kN/m^3, φ=30°, (b) Soil properties: E=30MPa, γ=20kN/m^3, φ=35°, and (c) Soil properties: E=50MPa, γ=21kN/m^3, φ=40°

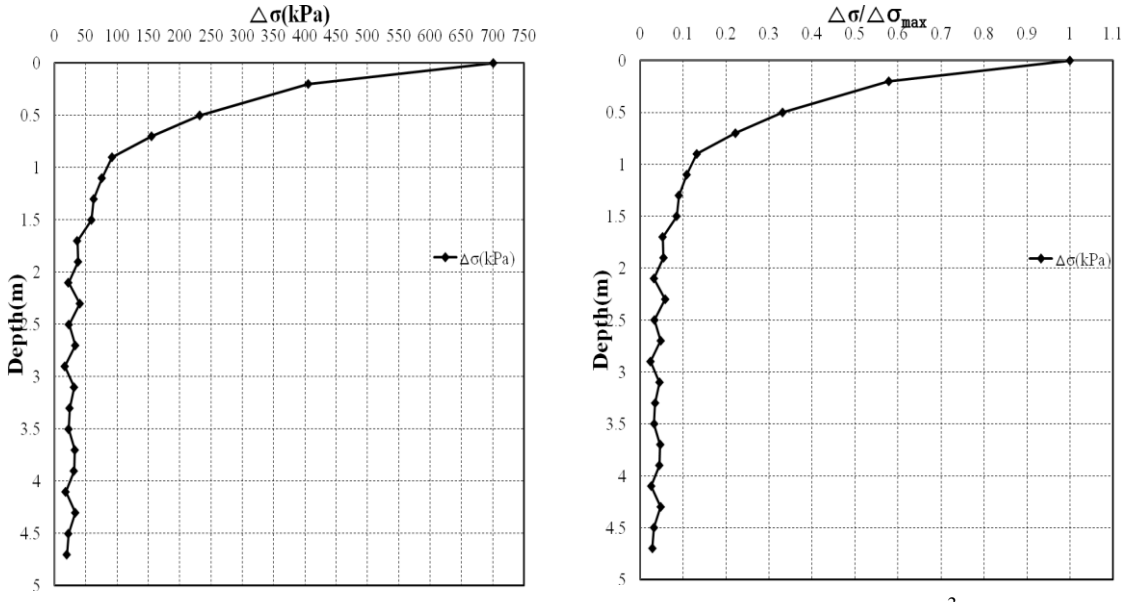

(c) Stress distribution under the drum in soil (E=50MPa, γ=21kN/m^3, φ=40°)

Figure 3.20 continued

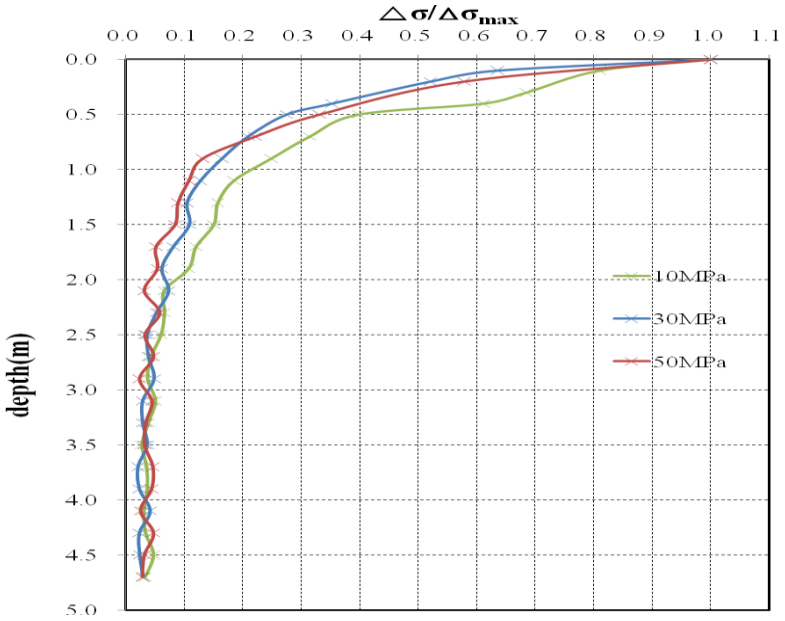

Figure 3.21 Comparison of the stress distribution using the Landpac drum for different soil types

2) Displacement

The surface displacement for the soil Modulus E=10MPa, 30MPa, and 50MPa are 26.02 mm, 17.28 mm, and 8.42 mm, respectively as shown in Figure 3.22

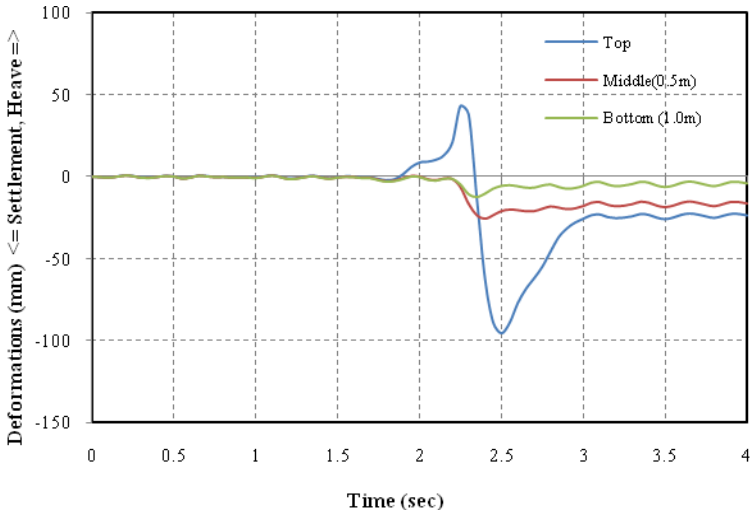

(a) Displacement of a given point as the roller passes (E=10MPa, γ=19kN/m^3, φ=30°)

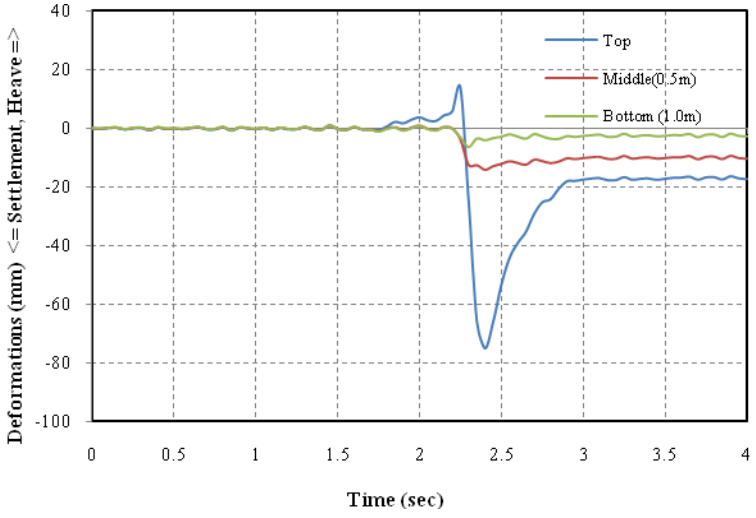

(b) Displacement of a given point as the roller passes (E=30MPa, γ=20kN/m^3, φ=35°)

Figure 3.22 Displacements relative to the beginning of the measurements under the Landpac drum

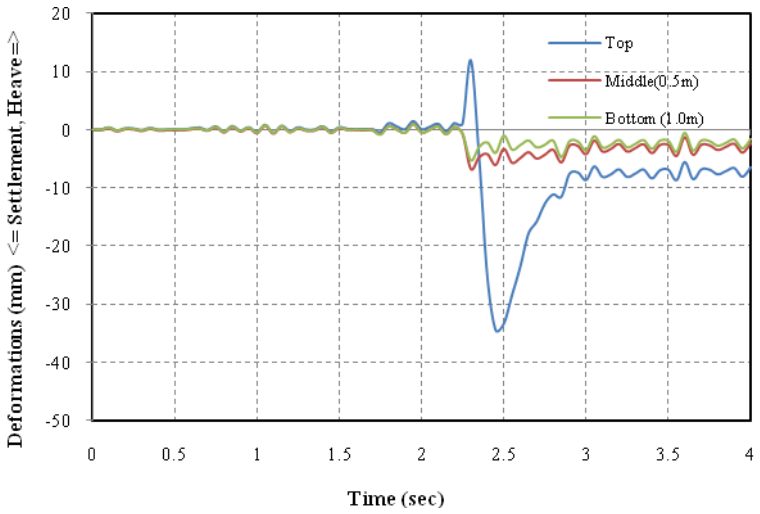

(c) Displacement of a given point as the roller passes (E=50MPa, γ=21kN/m^3, φ=40°)

Figure 3.22 continued

In addition, Figure 3.23 shows the visualized compaction mechanism under the Landpac roller.

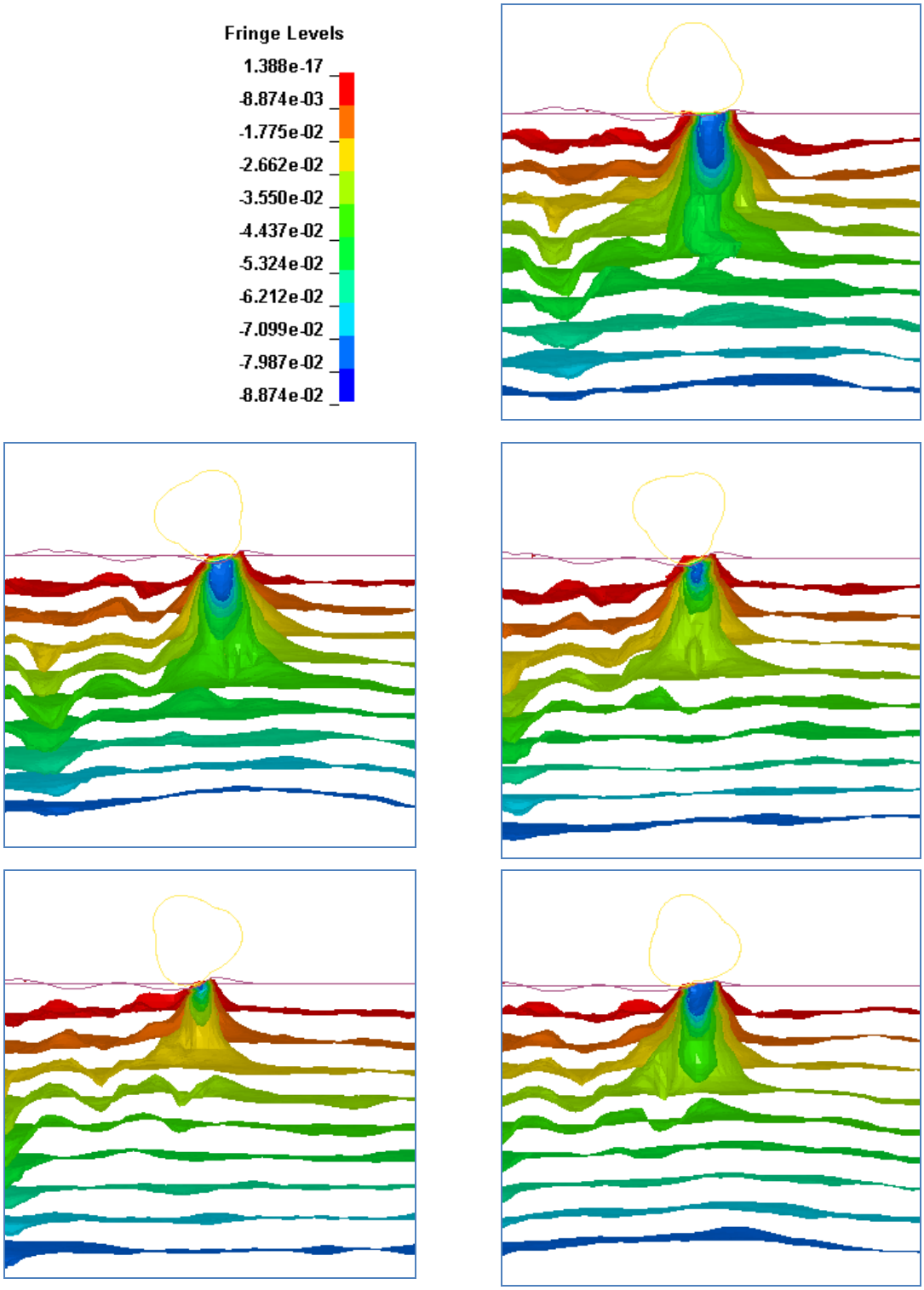

(a) Vertical stress distribution under the drum in soil (E=10MPa, γ=19kN/m^3, φ=30°)

Figure 3.23 Compaction mechanism under the Landpac drum

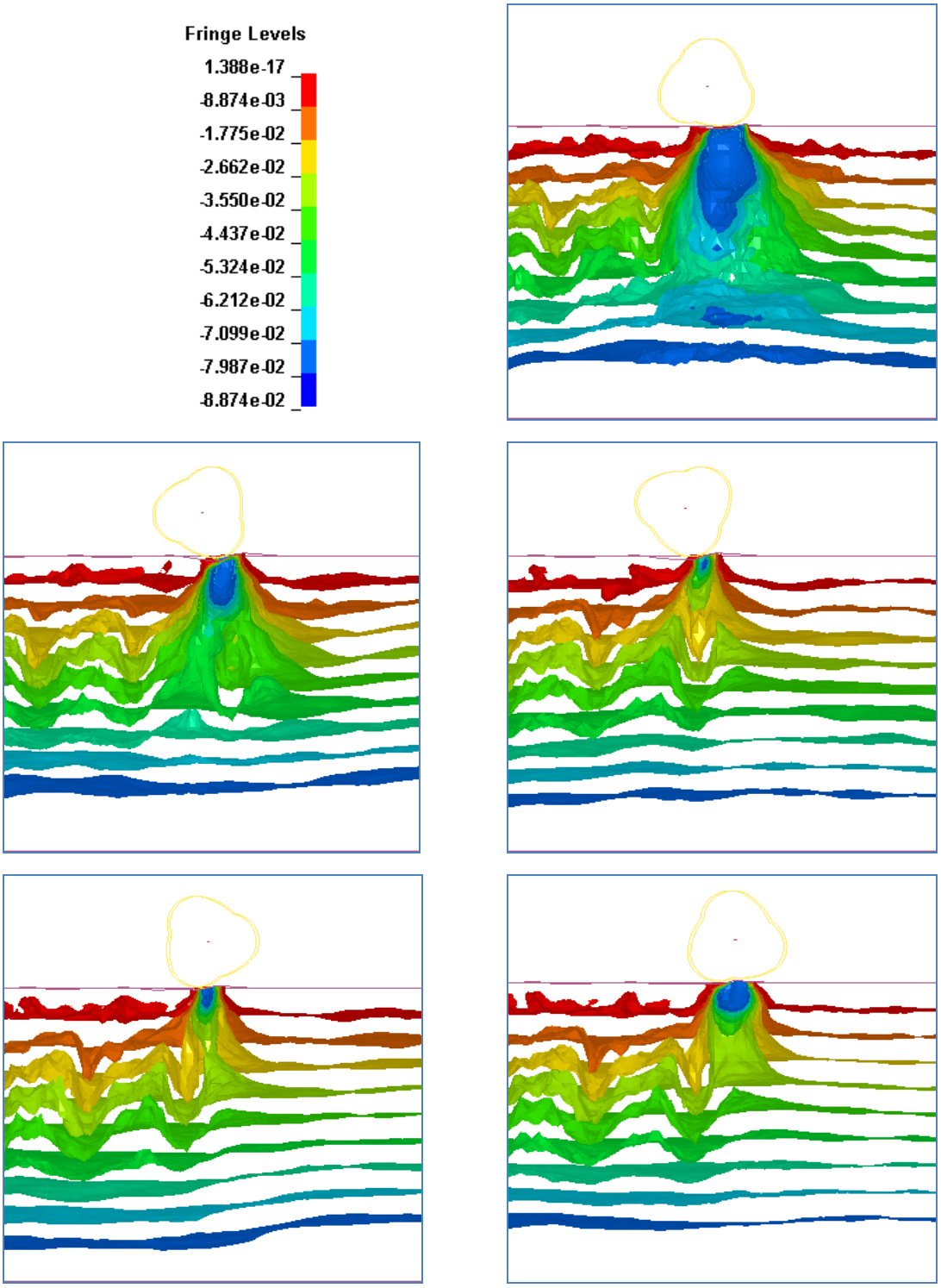

(b) Vertical stress distribution under the drum in soil (E=30MPa, γ=20kN/m^3, φ=35°)

Figure 3.23 continued

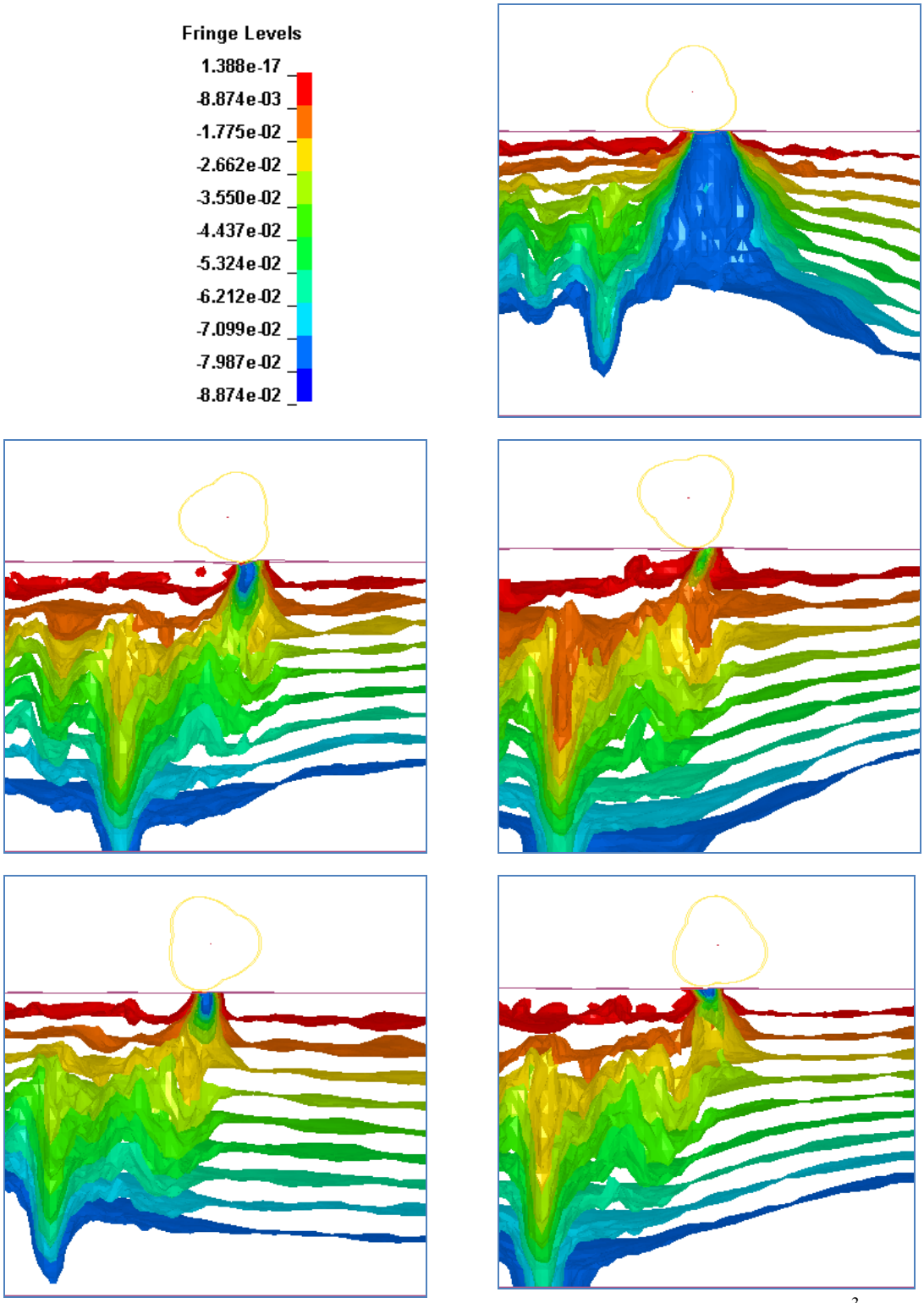

(c) Vertical stress distribution under the drum in soil (E=50MPa, γ=21kN/m^3, φ=40°)

Figure 3.23 continued

3.5. PENTAGONAL ROLLER: Soil E= 10MPa, 30MPa, and 50MPa

The ground-roller interaction model using the pentagonal drum (Landpac 5-sided roller) is shown in Figure 3.24. In this case, the depth of influence of the soil Modulus E=10MPa, 30MPa, and 50MPa are 1.6m, 1.4m, and 1.2m, respectively. The results of the simulation to determine the depth of influence on the variable soil types are shown in Figures 3.25 and 3.26.

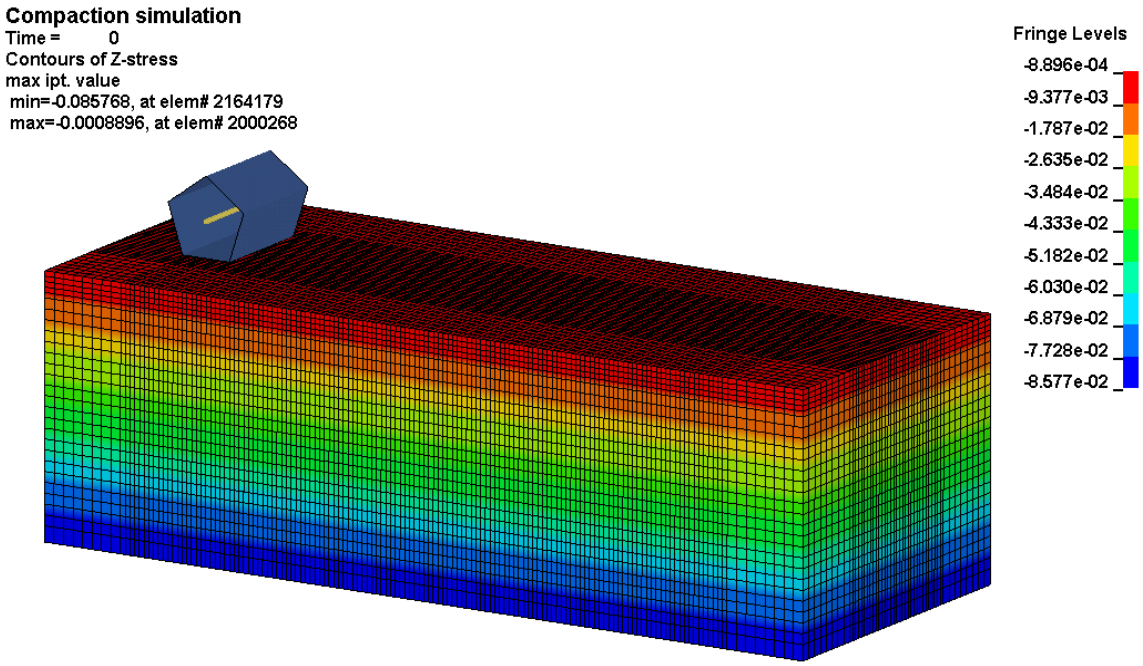

Figure 3.24 Ground-roller interaction model using the pentagonal drum

1) Influence depth

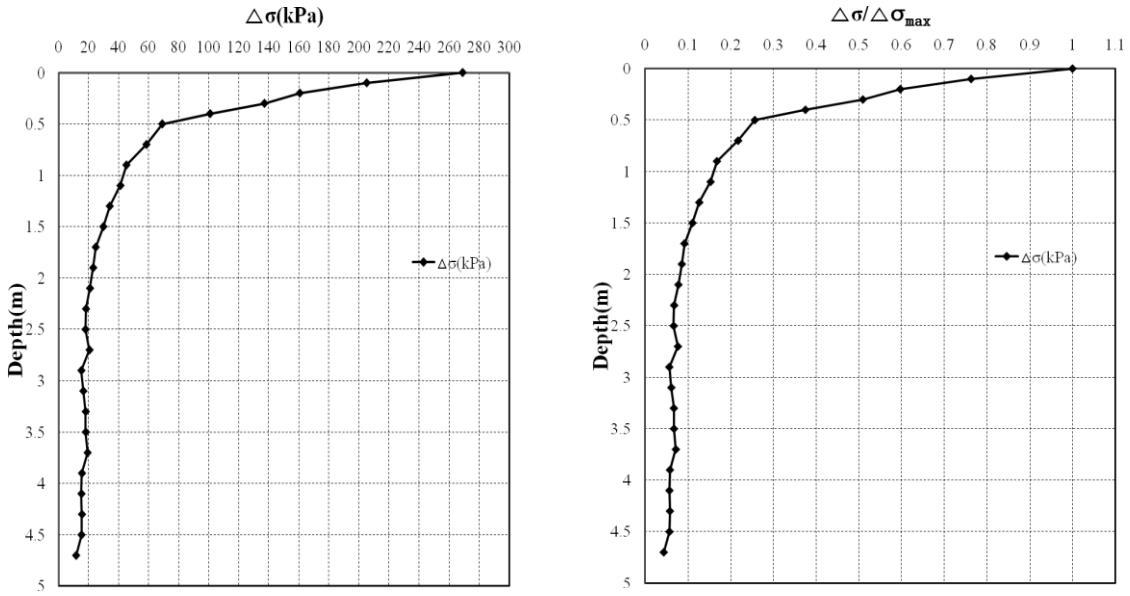

(a) Stress distribution under the drum in soil (E=10MPa, γ=19kN/m^3, φ=30°)

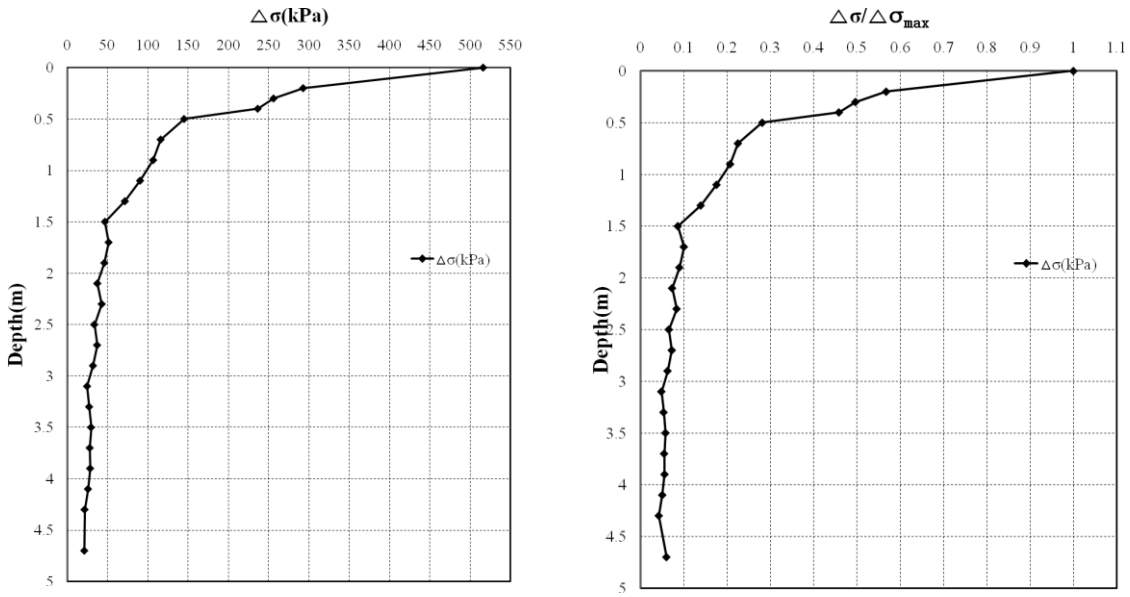

(b) Stress distribution under the drum in soil (E=30MPa, γ=20kN/m^3, φ=35°)

Figure 3.25 Vertical stresses distribution under the pentagonal drum for different soil types: (a) Soil properties: E=10MPa, γ=19kN/m^3, φ=30°, (b) Soil properties: E=30MPa, γ=20kN/m^3, φ=35°, and (c) Soil properties: E=50MPa, γ=21kN/m^3, φ=40°

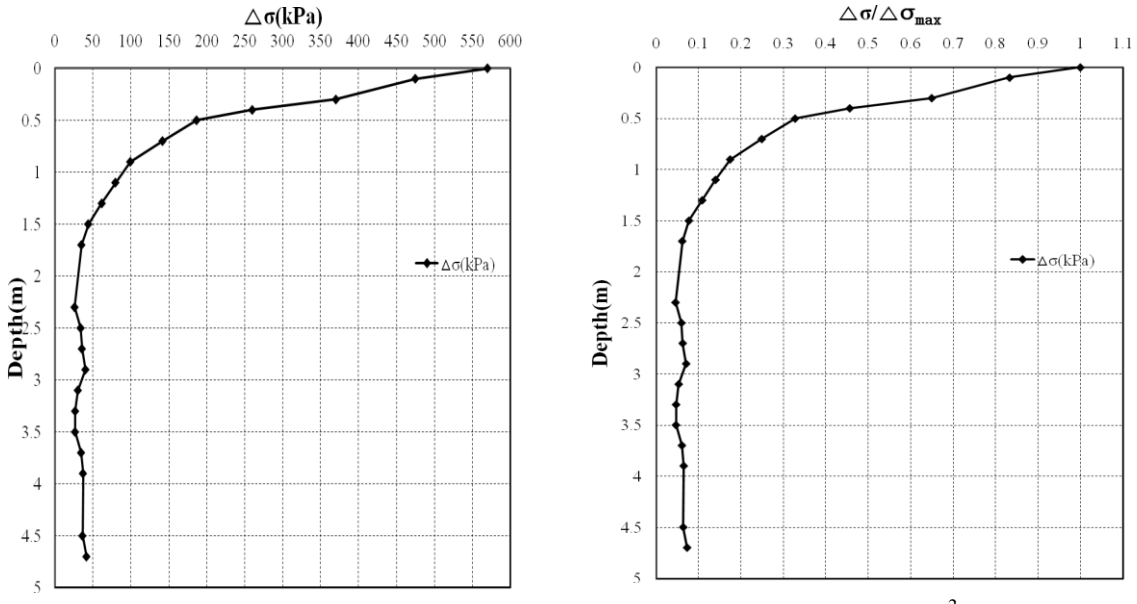

(c) Stress distribution under the drum in soil (E=50MPa, γ=21kN/m^3, φ=40°)

Figure 3. 25 continued

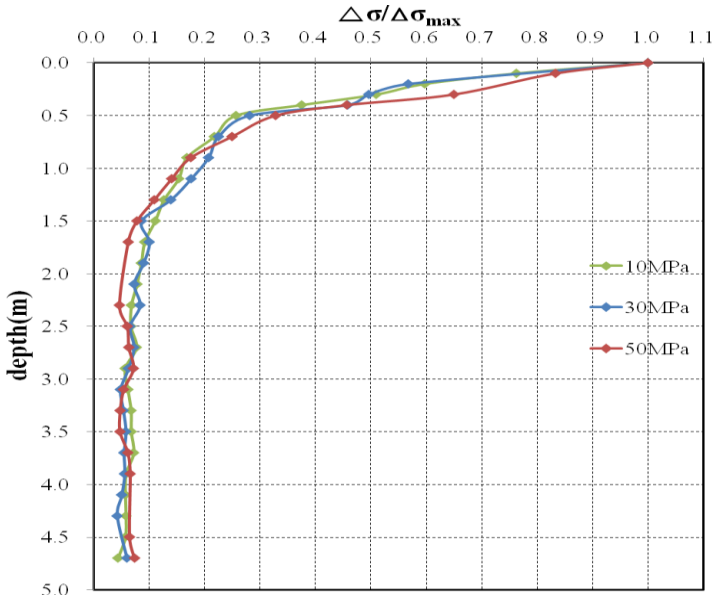

Figure 3.26 Comparison of the stress distribution using the pentagonal drum for different soil types

2) Displacement

The surface displacement for the soil Modulus E=10MPa, 30MPa, and 50MPa are 22.25 mm, 11.42 mm, and 5.49 mm, respectively as shown in Figure 3.27.

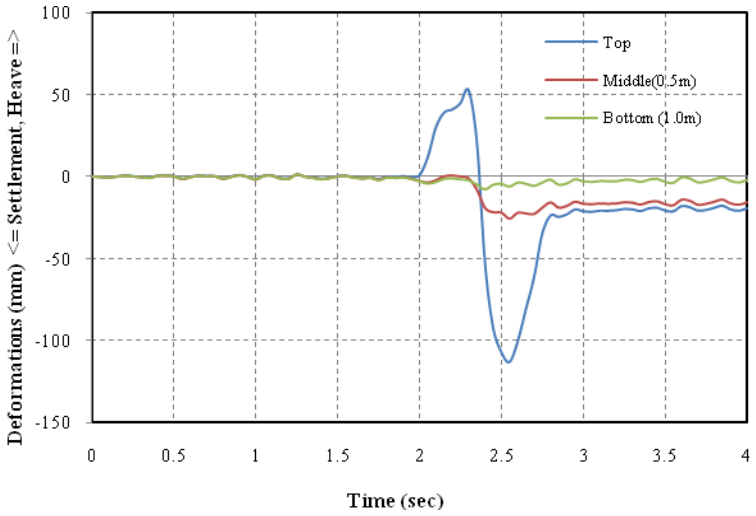

(a) Displacement of a given point as the roller passes (E=10MPa, γ=19kN/m^3, φ=30°)

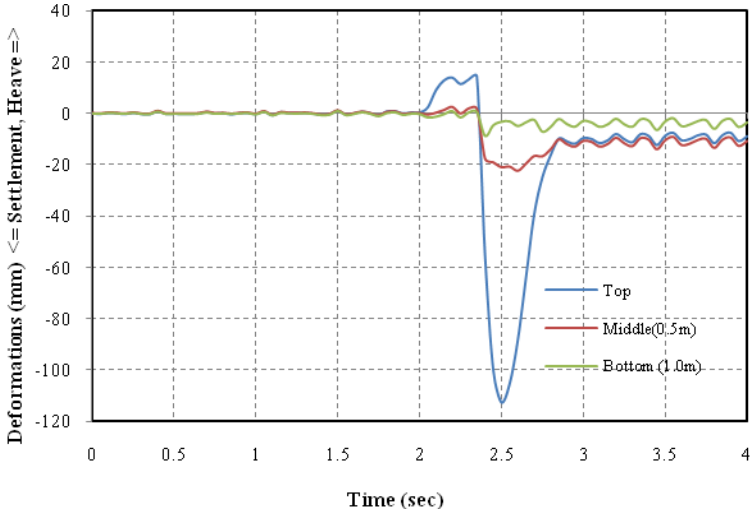

(b) Displacement of a given point as the roller passes (E=30MPa, γ=20kN/m^3, φ=35°)

Figure 3. 27 Displacements relative to the beginning of the measurements under the pentagonal drum

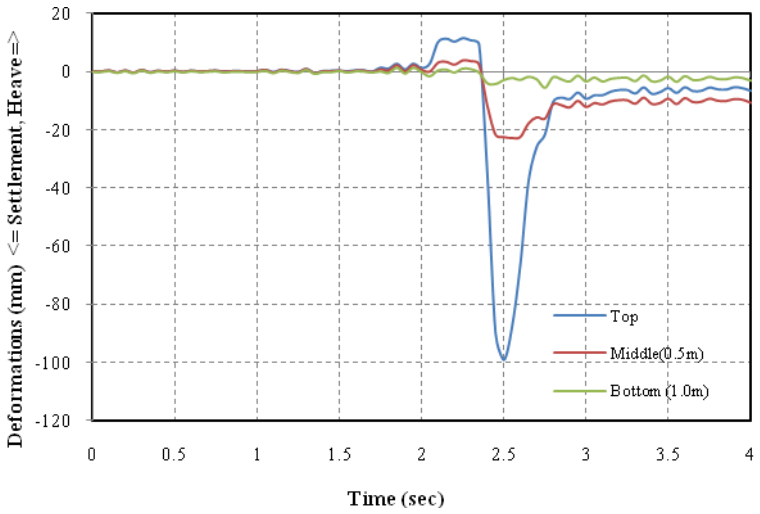

(c) Displacement of a given point as the roller passes (E=50MPa, γ=21kN/m^3, φ=40°)

Figure 3. 27 continued

In addition, Figure 3.28 shows the visualized compaction mechanism under the pentagonal roller.

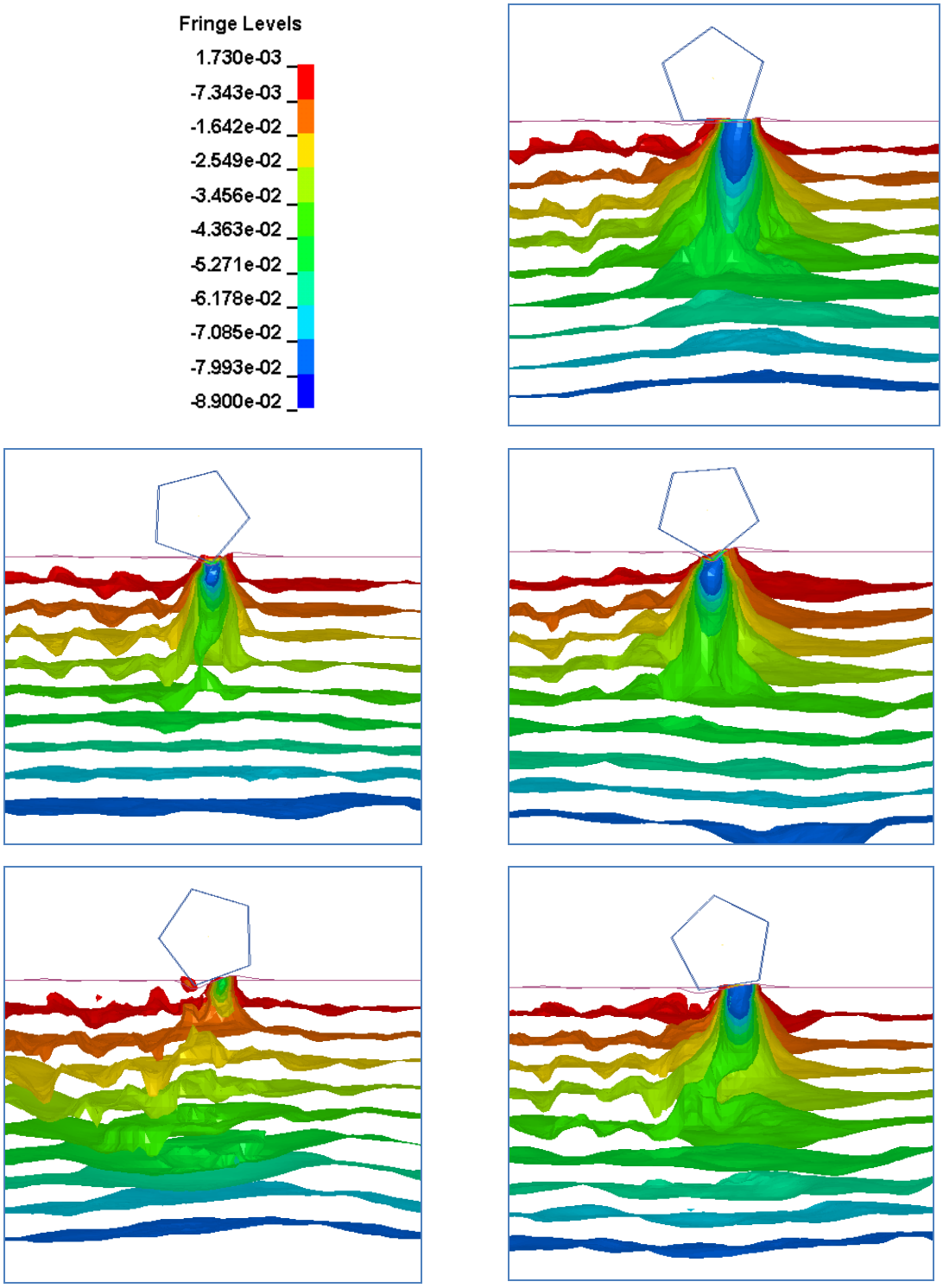

(a) Vertical stress distribution under the drum in soil (E=10MPa, γ=19kN/m^3, φ=30°)

Figure 3.28 Compaction mechanism under the pentagonal drum

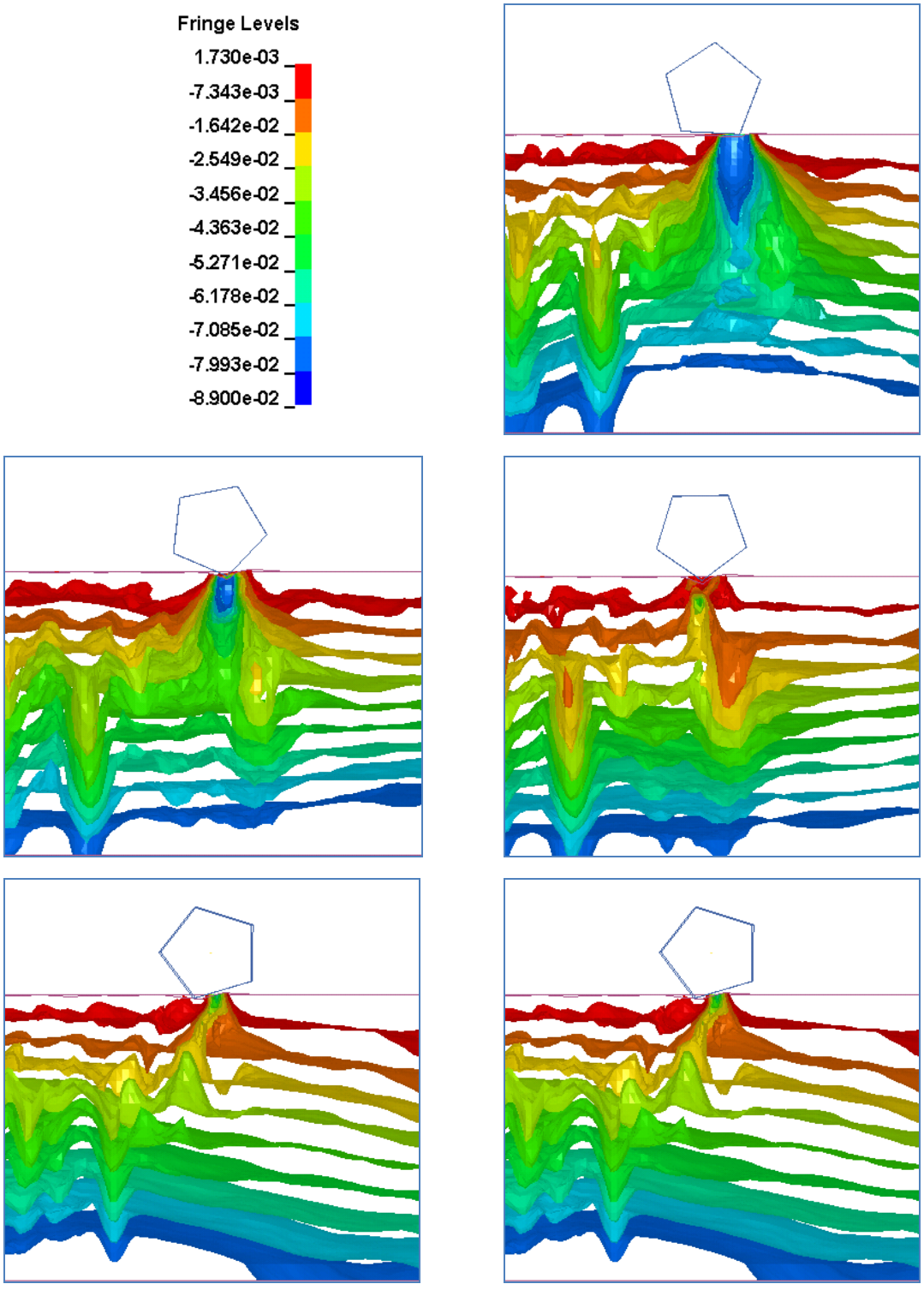

(b) Vertical stress distribution under the drum in soil (E=30MPa, γ=20kN/m^3, φ=35°)

Figure 3.28 continued

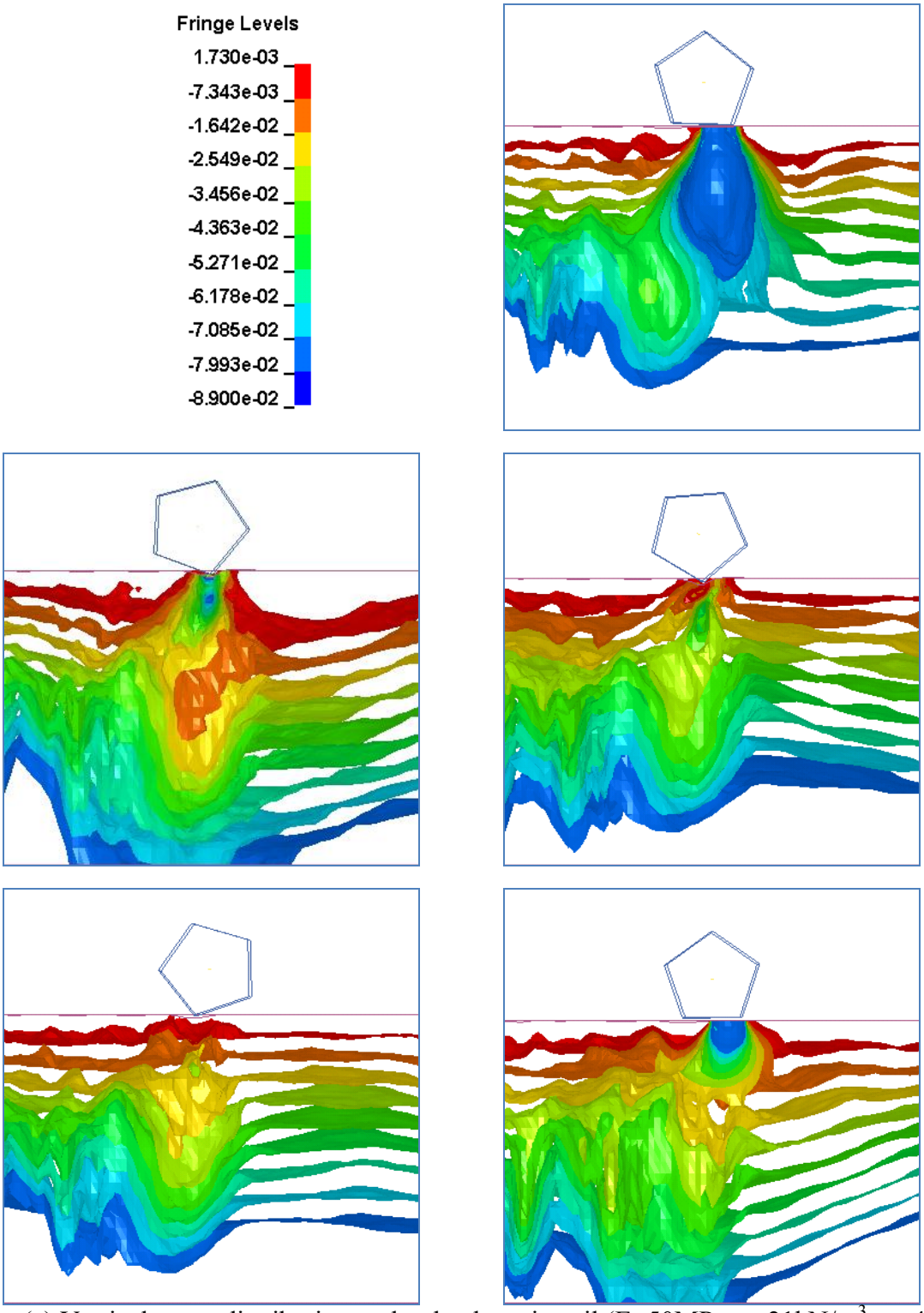

(c) Vertical stress distribution under the drum in soil (E=50MPa, γ=21kN/m^3, φ=40°)

Figure 3.28 continued

3.6. OCTAGONAL ROLLER: Soil E= 10MPa, 30MPa, and 50MPa

The ground-roller interaction model using the octagonal drum (Bomag roller) is shown in Figure 3.29. In this case, the depth of influence of the soil modulus E=10MPa, 30MPa, and 50MPa are 1.4m, 1.05m, and 0.93m, respectively. The results of the simulation to determine the depth of influence on the variable soil types are shown in Figure 3.30 and 3.31.

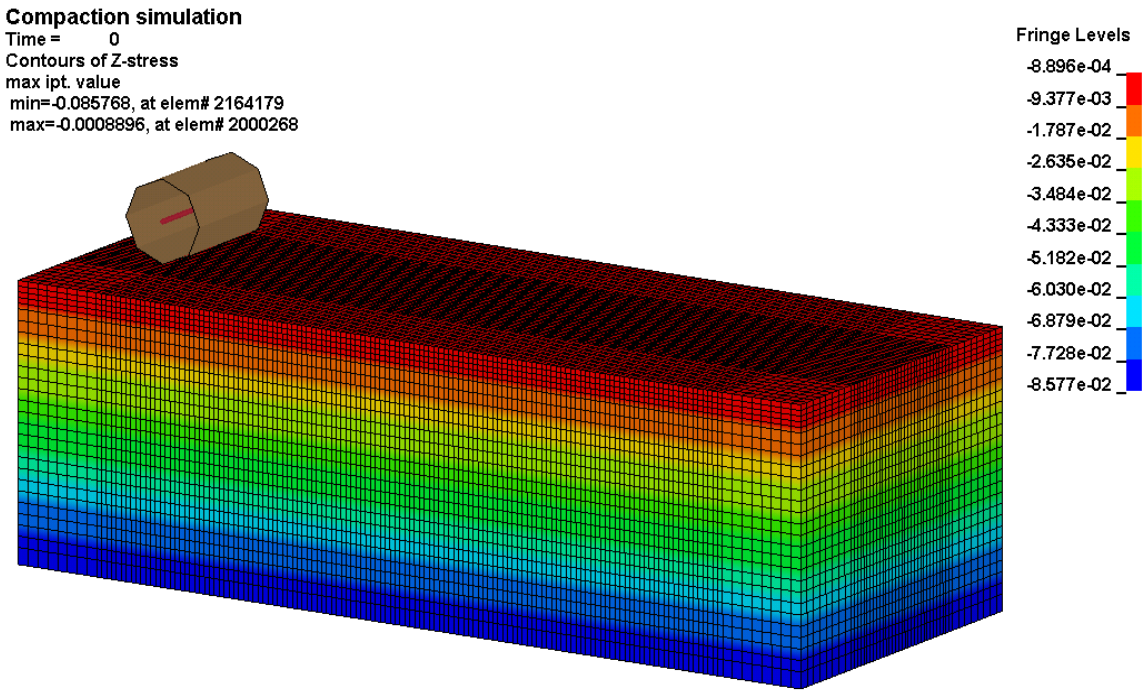

Figure 3.29 Ground-roller interaction model using the octagonal drum

1) Influence depth

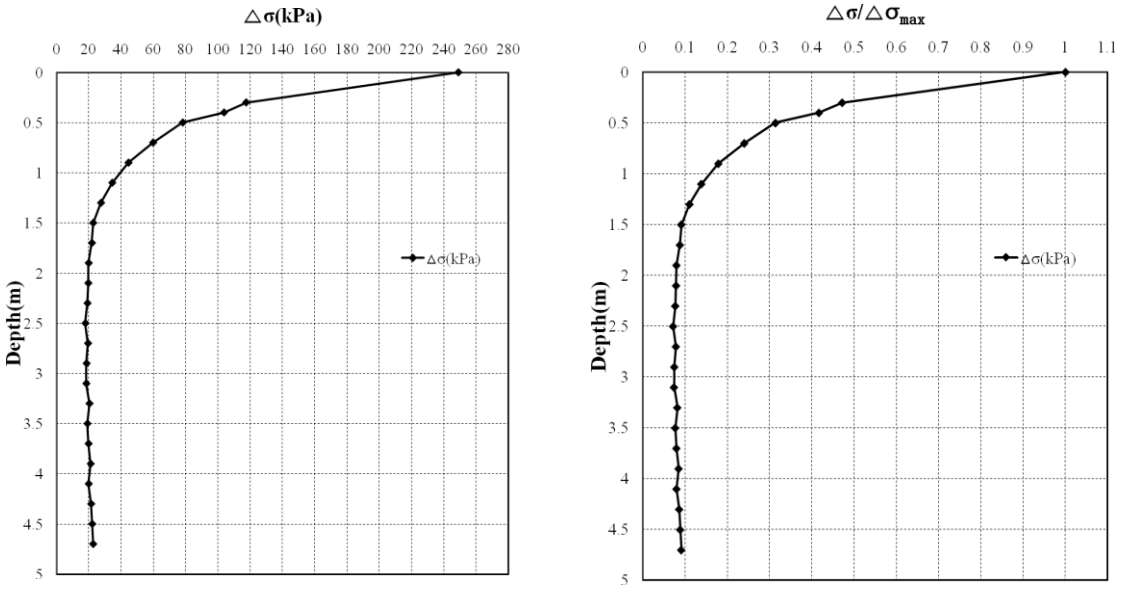

(a) Stress distribution under the drum in soil (E=10MPa, γ=19kN/m^3, φ=30°)

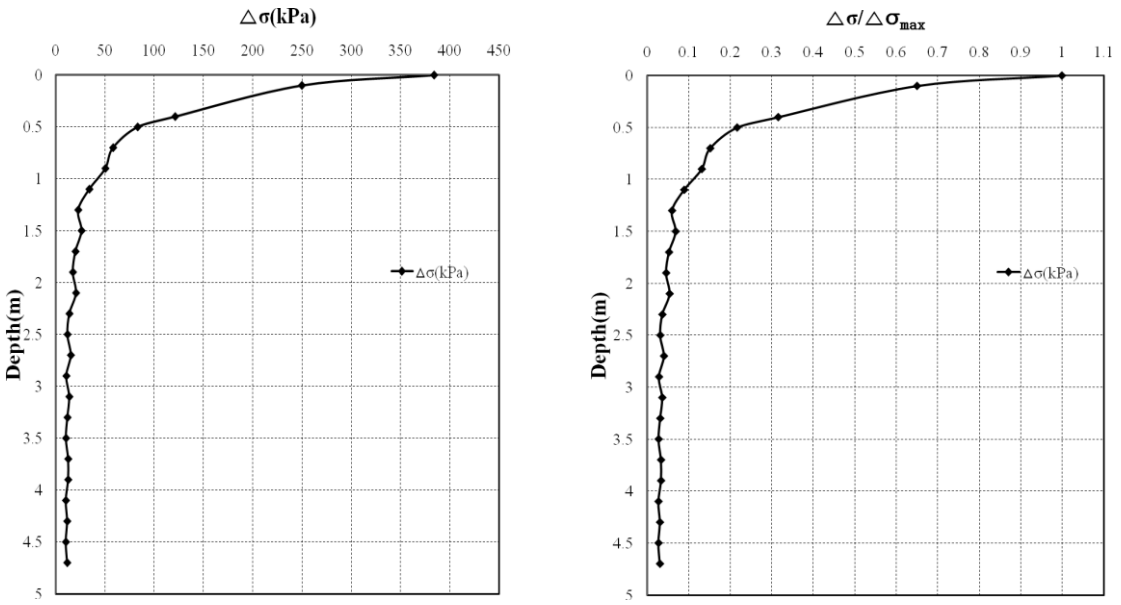

(b) Stress distribution under the drum in soil (E=30MPa, γ=20kN/m^3, φ=35°)

Figure 3.30 Vertical stresses distribution under the octagonal drum for different soil types: (a) Soil properties: E=10MPa, γ=19kN/m^3, φ=30°, (b) Soil properties: E=30MPa, γ=20kN/m^3, φ=35°, and (c) Soil properties: E=50MPa, γ=21kN/m^3, φ=40°

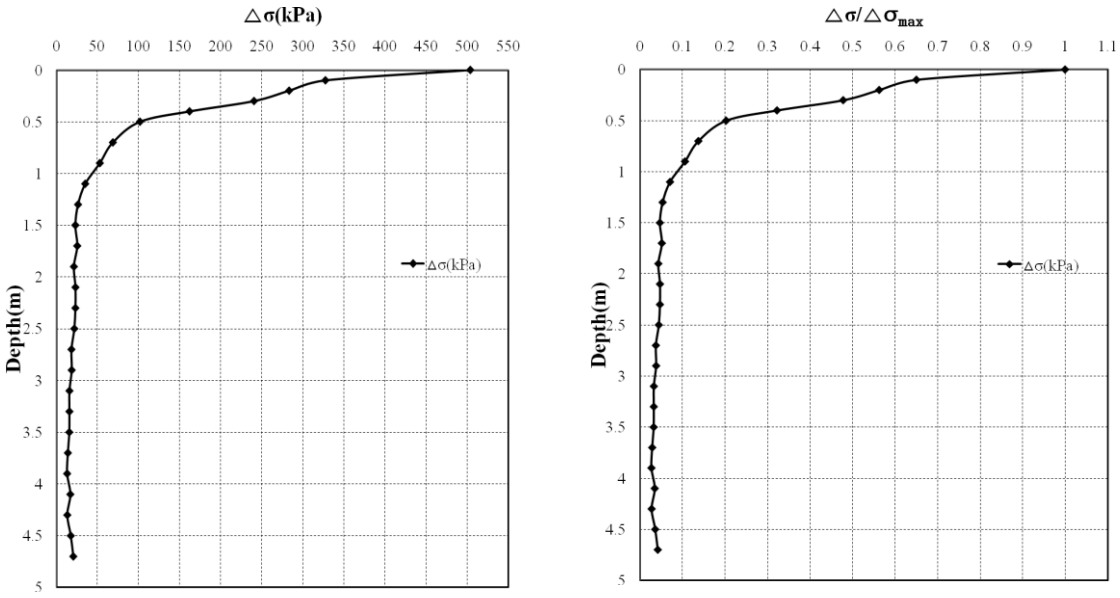

(c) Stress distribution under the drum in soil (E=50MPa, γ=21kN/m^3, φ=40°)

Figure 3.30 continued

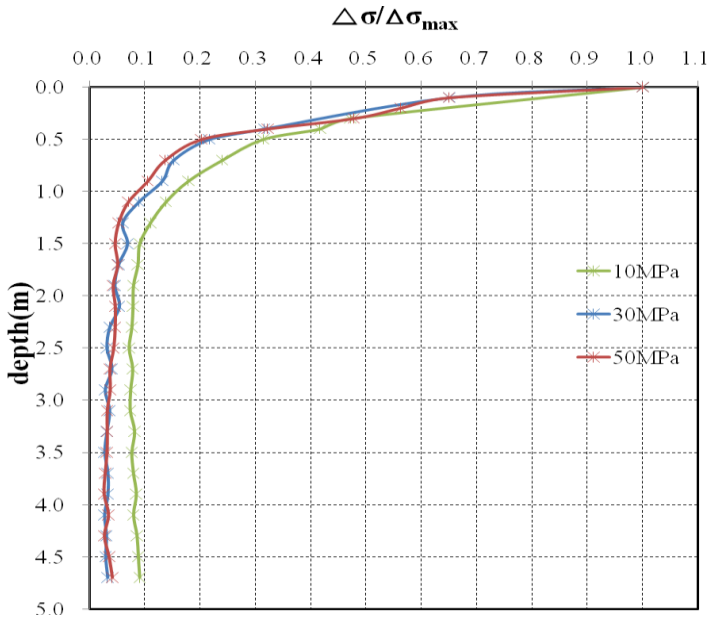

Figure 3.31 Comparison of the stress distribution using the octagonal drum for different soil types

2) Displacement

The surface displacement for the soil modulus E=10MPa, 30MPa, and 50MPa are 20.13 mm, 5.21 mm, and 2.26 mm, respectively as shown in Figure 3.32.

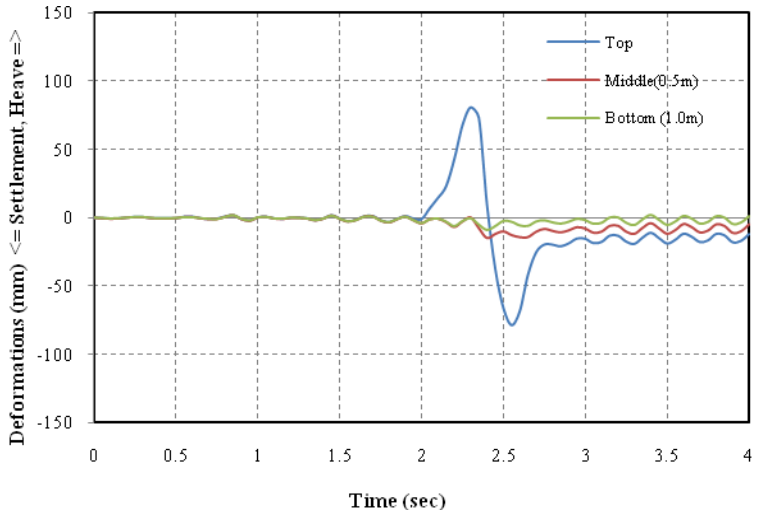

(a) Displacement of a given point as the roller passes (E=10MPa, γ=19kN/m^3, φ=30°)

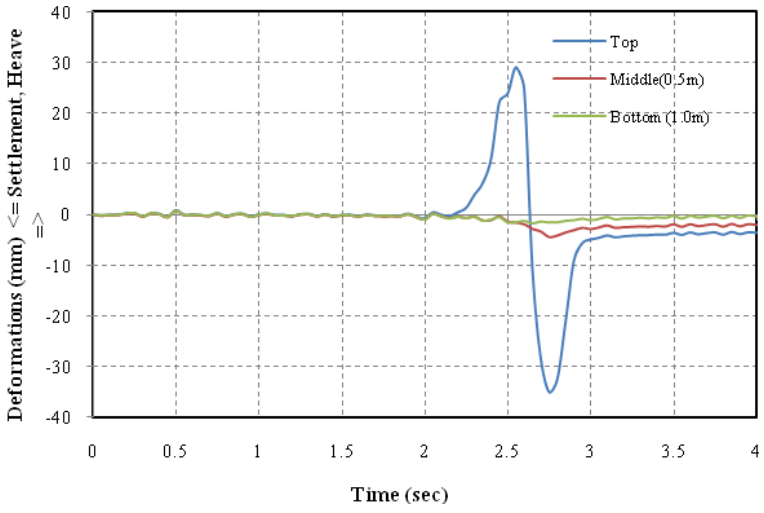

(b) Displacement of a given point as the roller passes (E=30MPa, γ=20kN/m^3, φ=35°)

Figure 3.32 Displacements relative to the beginning of the measurements under the octagonal drum

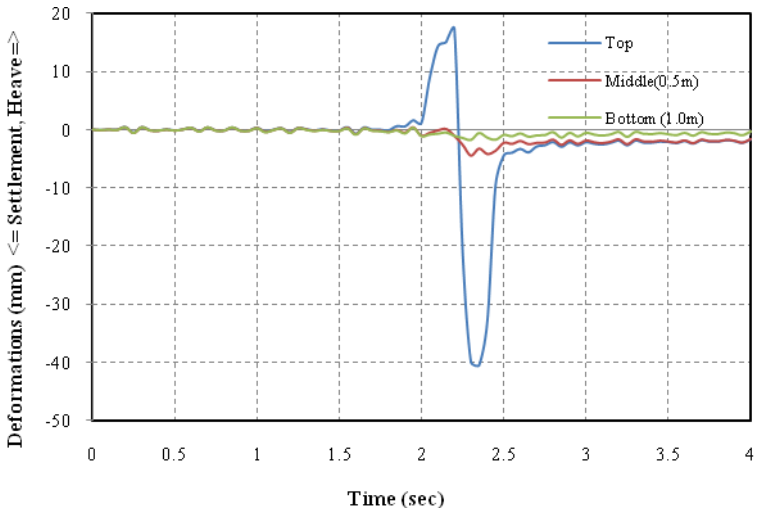

(c) Displacement of a given point as the roller passes (E=50MPa, γ=21kN/m^3, φ=40°)

Figure 3.32 continued

In addition, Figure 3.33 shows the visualized compaction mechanism under the pentagonal roller.

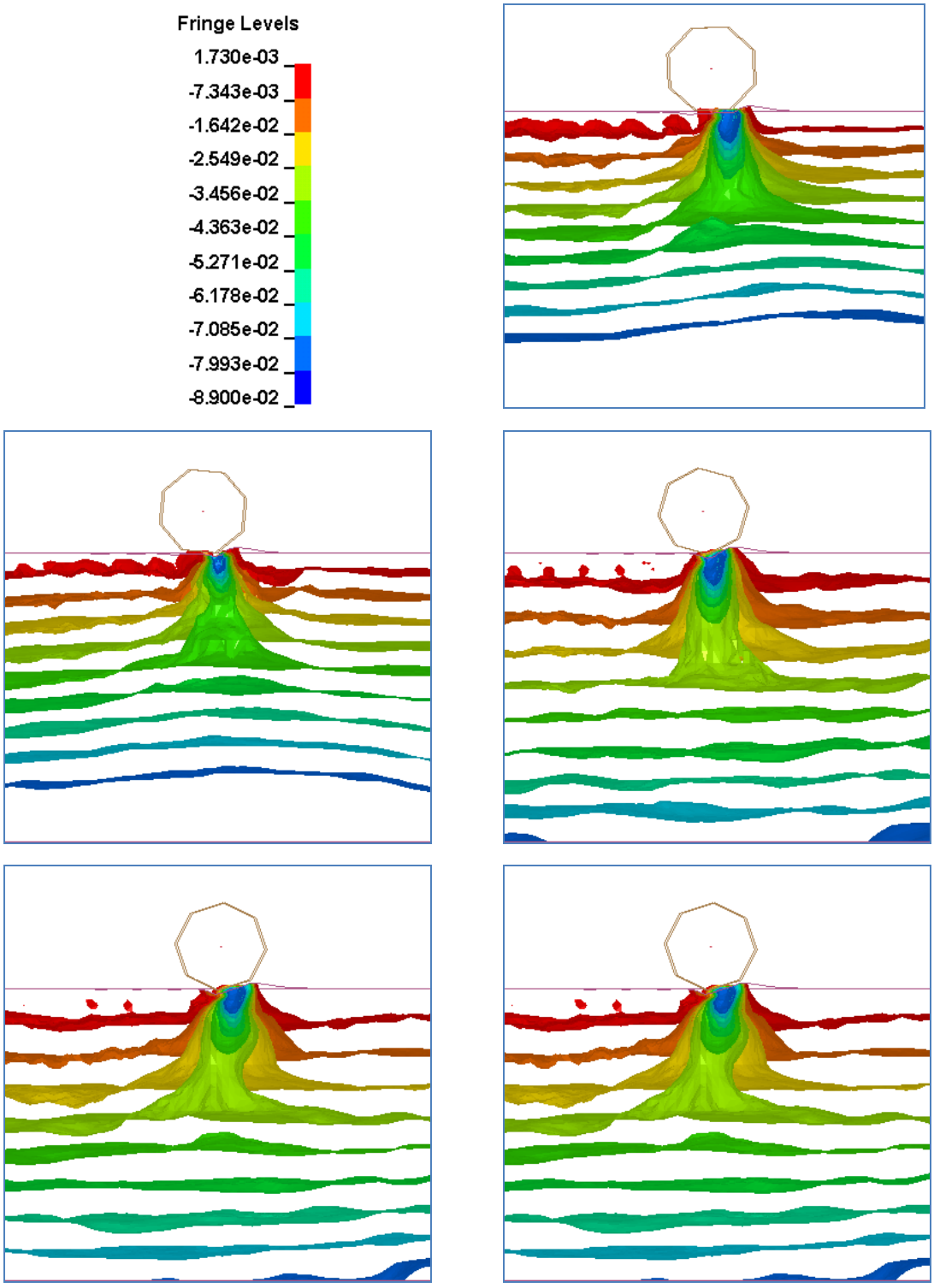

(a) Vertical stress distribution under the drum in soil (E=10MPa, γ=19kN/m^3, φ=30°)

Figure 3.33 Compaction mechanism under the octagonal drum

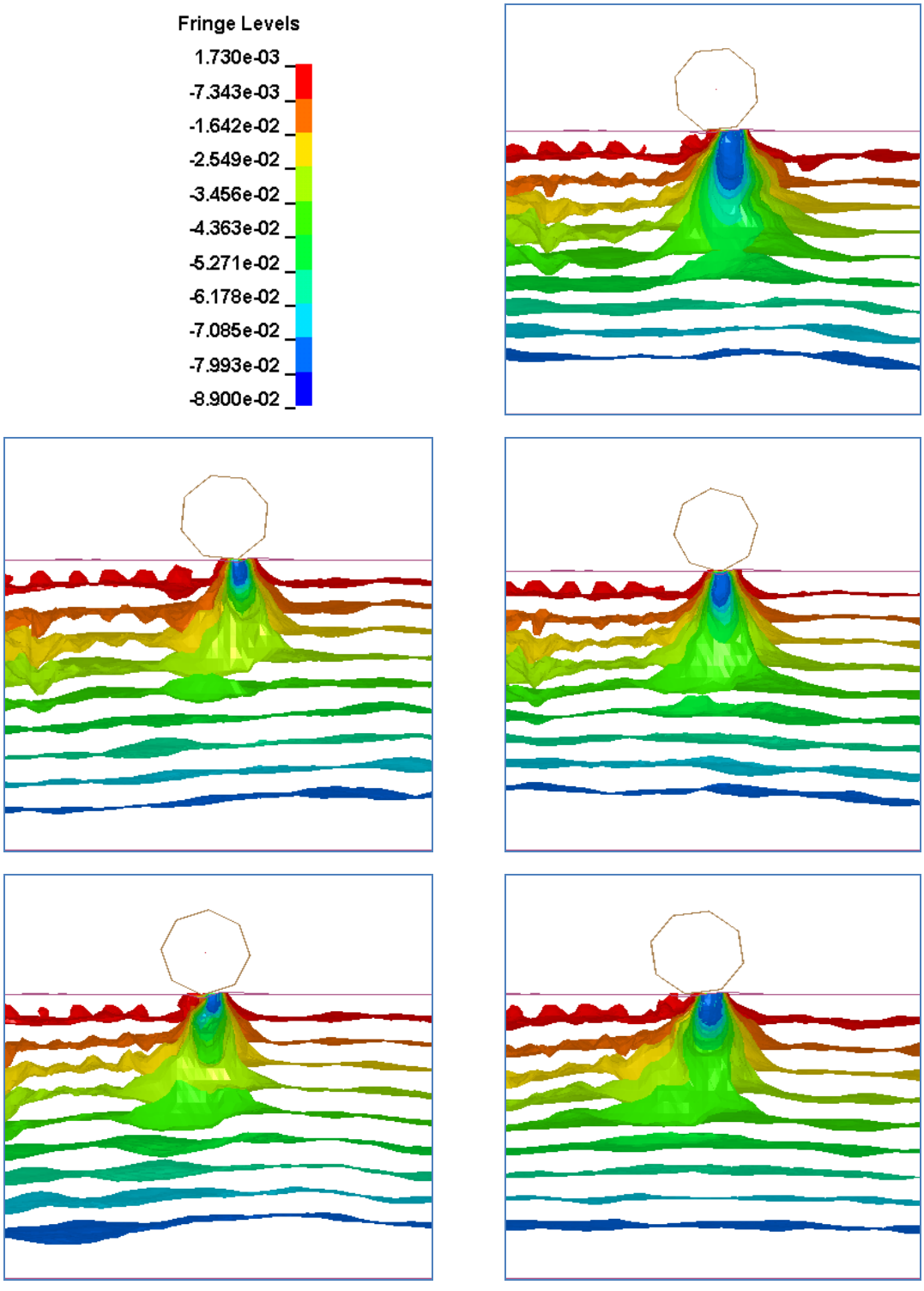

(b) Vertical stress distribution under the drum in soil (E=30MPa, γ=20kN/m^3, φ=35°)

Figure 3.33 continued

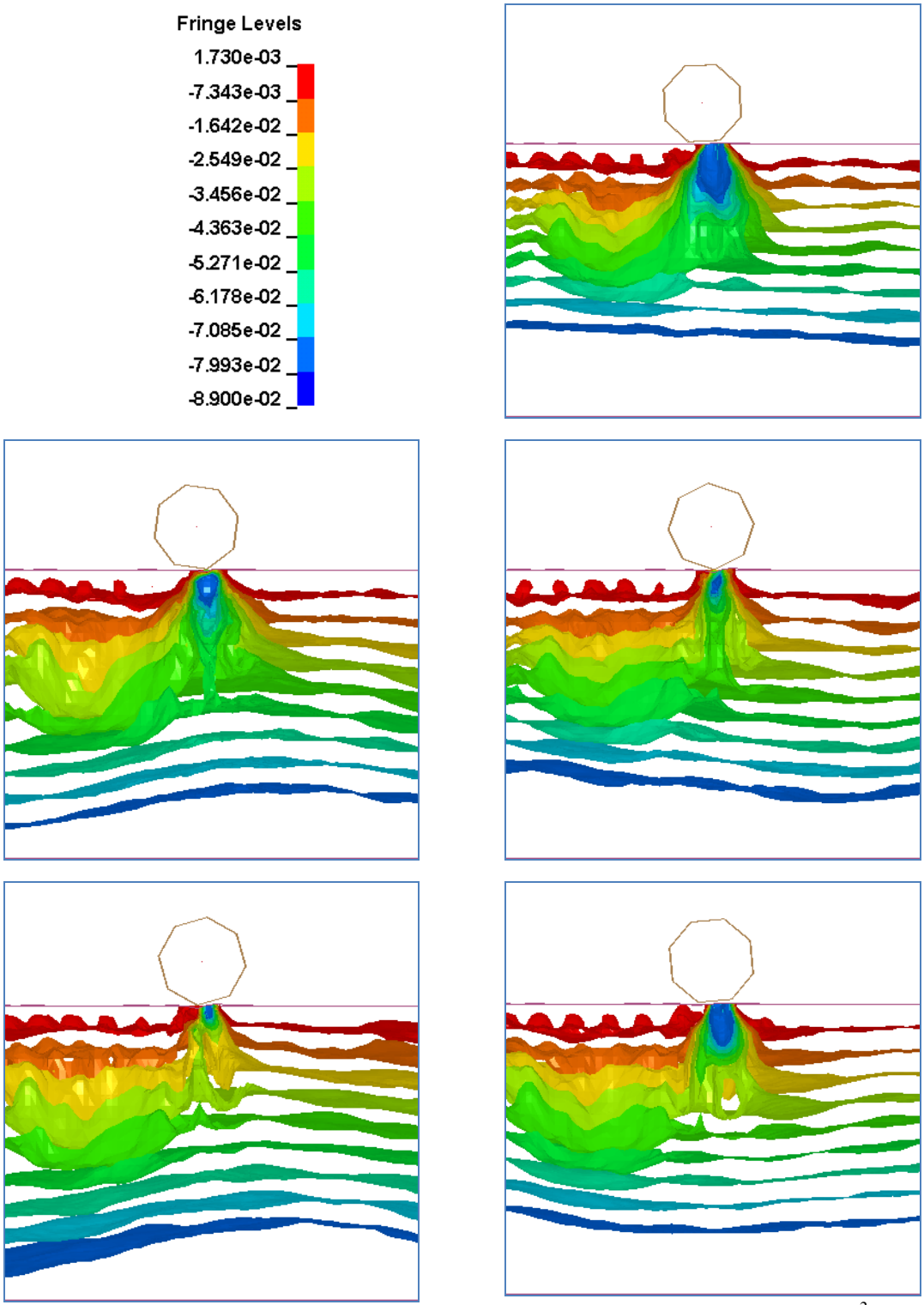

(c) Vertical stress distribution under the drum in soil (E=50MPa, γ=21kN/m^3, φ=40°)

Figure 3.33 continued

3.7. DISCUSSION OF SIMULATION RESULTS

In order to compare the depth of influence of the compaction process using the different types of impact rollers and to make the direct comparison between the impact roller shapes and the depth of influence, the vertical stress profiles are normalized by the ratio of the vertical stresses at each depth to the maximum stress at the surface. As a result, the influence depth is deeper when the roller has the larger contact area. Figure 3.34 shows the depth of influence in the ground as a reaction to the different types of roller shapes.

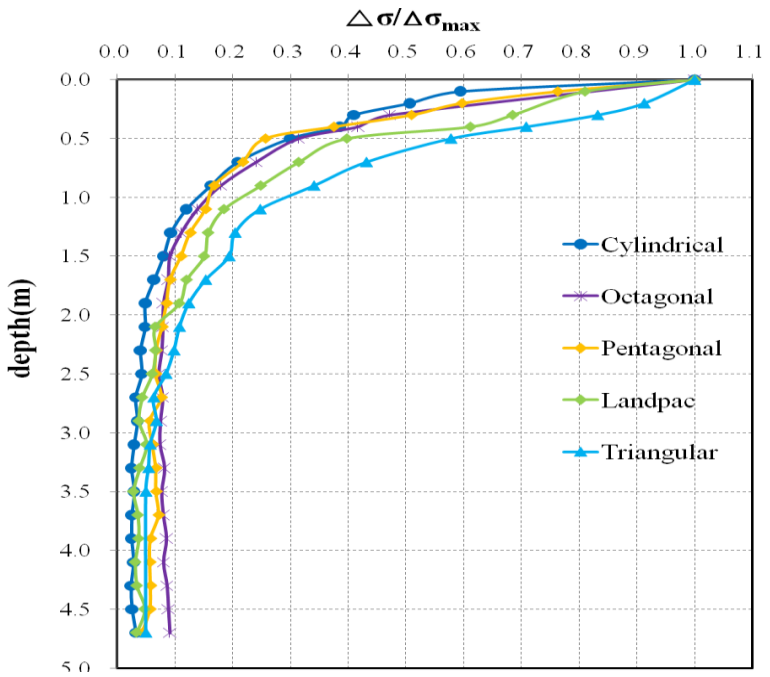

(a) Soil modulus = 10MPa

Figure 3.34 Comparison of the depth of influence in different soil types

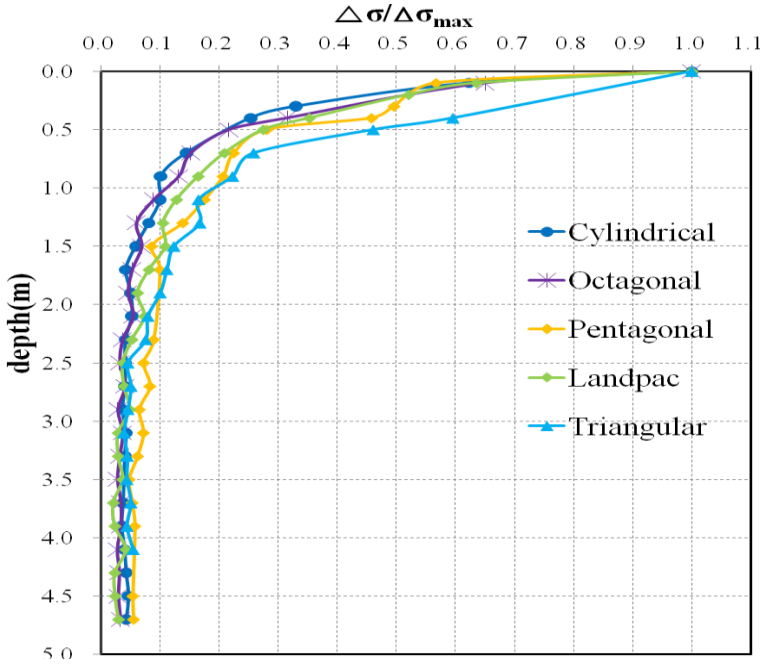

(b) Soil modulus = 30MPa

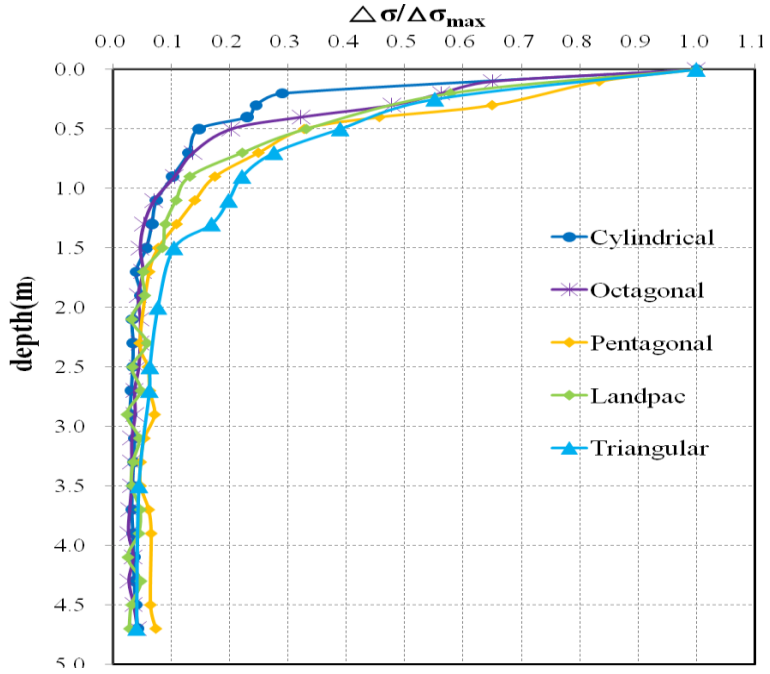

(c) Soil modulus = 50MPa

Figure 3.34 continued

Since the 1980s, theoretical and experimental research has been conducted to study the motion characteristics of impact roller compaction. Paige-Green (1998) conducted a detailed study of the impact compaction and stated that “larger loads and larger contact areas are better for deep compaction”. This numerical study theoretically proved that the contact area is the main factor for deep compaction even though the same load is applied. Figure 3.35 shows the depth of influence in different soil types and drum shapes. Using this graph, field engineers can make a decision how much thickness can be compacted for one layer in highways, embankments, airports, and/or many other projects.

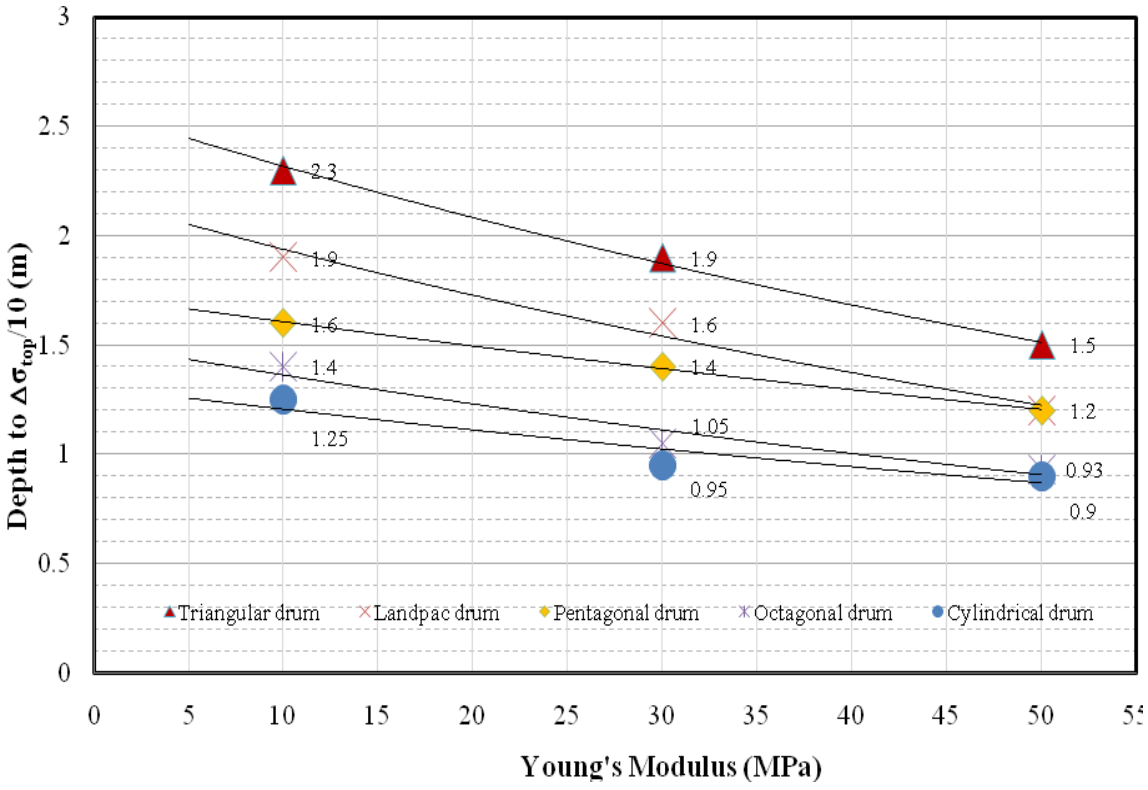

Figure 3.35 The depth of influence with different roller shapes

The contact area is one of the main limiting factors of cylindrical smooth rollers in deep compaction because the contact width of the applied line load is difficult to enlarge. In addition, an impact roller imparts generated momentum due to the rotational effect of the roller mass to the ground. It allows deeper compaction.

Paige-Green (1998) also stated that "Impact compaction…results in compaction at depth, with disturbance of the upper portion of the layer." As previously mentioned, this can be explained by the wedge effect that creates tensile splitting. These horizontal shearing forces shift the soil locally and remove the bracing of the soil particle structure which inhibits compaction. As a result, the area down to about 0.5 m remained looser.

The imparted force basically increases with the speed at which the rollers are towed since an impact roller generates high momentum at fast operation velocity. However, all impact rollers operate at a similar travel speed in the range of 8 to 11 km/h depending on the ground conditions because field engineers observed a "Skip mode", a drum trends to act with less impact, in excess of the recommended speed. In this study, a "Skip mode" is also observed in hard soil even though all rollers operate at a same travel speed of 10 km/h. It indicates that an operation speed should be decreased on hard material to avoid the "Skip mode". A typical pattern of the vertical stress in the octagonal drum and soil model is plotted in Figure 3.36. These show that the drum does not compact sufficiently soil getting harder.

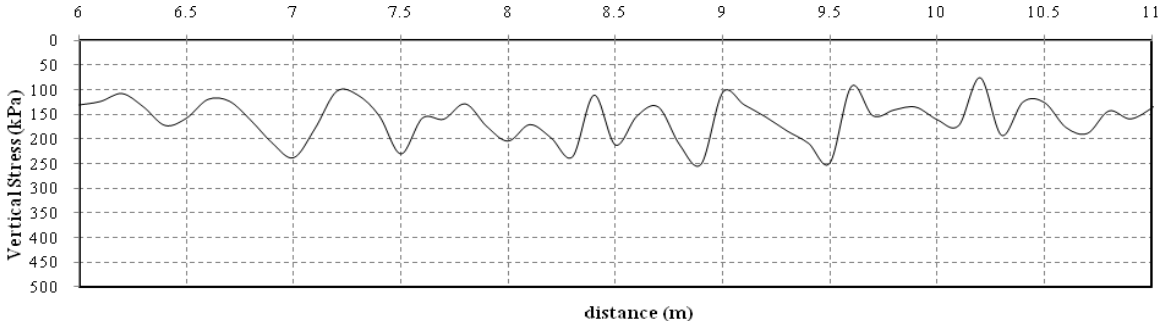

(a) Vertical stress in soil (E=10MPa, γ=19kN/m^3, φ=30°)

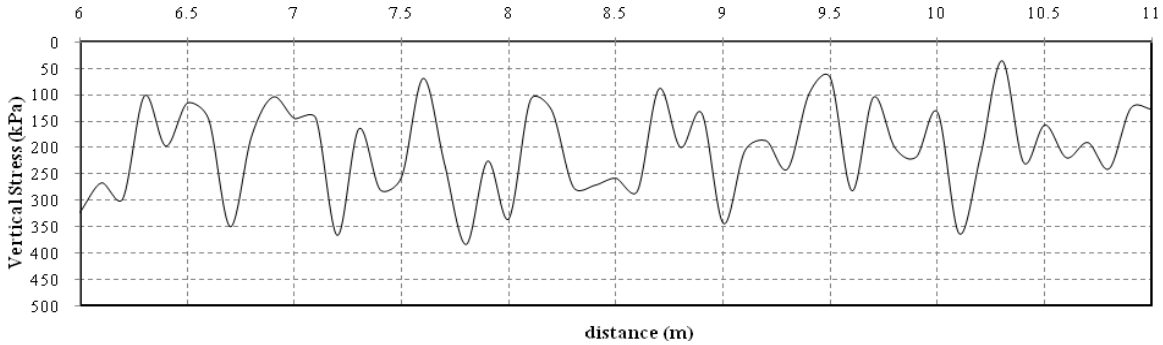

(b) Vertical stress in soil (E=30MPa, γ=20kN/m^3, φ=35°)

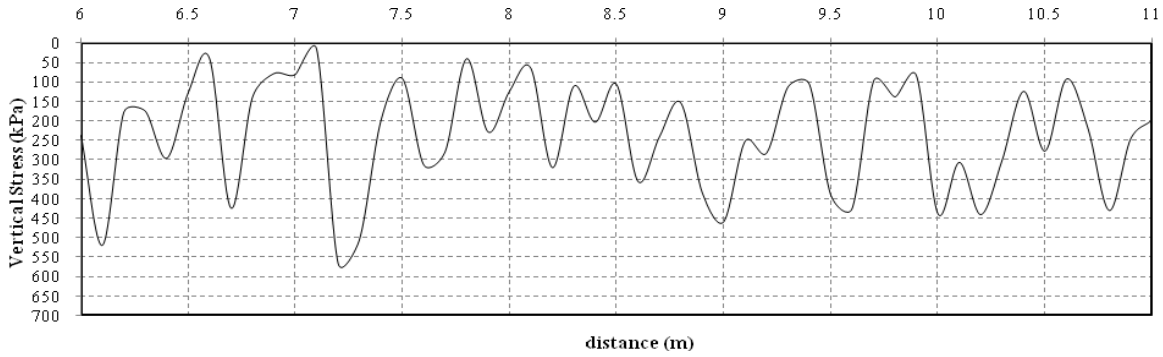

(c) Vertical stress in soil (E=50MPa, γ=21kN/m^3, φ=40°)

Figure 3. 36 Vertical stresses under the drum at surface in octagonal model

4. COMPARISON OF MEASURED AND PREDICTED RESULTS

In the previous section, the simulation model's results for predicting the influence depth and deformation in the ground were described. The aim of this section is to verify the proposed model and discuss some of the shortfalls. In order to verify the model results, the previous field data (e.g., Bomag (Wallrath, W., 2004) and Broons field experiment data) and the observational features of the ground improvement patterns are used. The reasonable agreement between the simulation results and measured values was found in the ground improvement patterns. These are stiffness, density, SPT, and vertical strain profiles. The numerical model was also checked against the analytical results of the vertical stress under the drum and a good correlation was found.

4.1. AN OVERVIEW OF THE GROUND IMPROVEMENT PATTERNS IN SITU

Little information was found in the literature about the impact compaction that could help to understand the compaction phenomenon under the impact rollers. Before the development of any mathematical prediction tools, Lukas (1986) conducted the in situ experiment to develop the typical patterns of behavior based on the field test results. As a result, he found that the average improvement will be less than the maximum amount that generally occurs at a depth of 1/3 to 1/2 of the maximum depth of improvement, and the improved pattern seems to show that the surface is loosened and compaction takes place deeper down. Finally, he suggested the ground improvement pattern as shown in Figure 4.1. In this improvement pattern, where the surface is

loosened and compaction takes place deeper down, is useful information to understand the impact compaction.

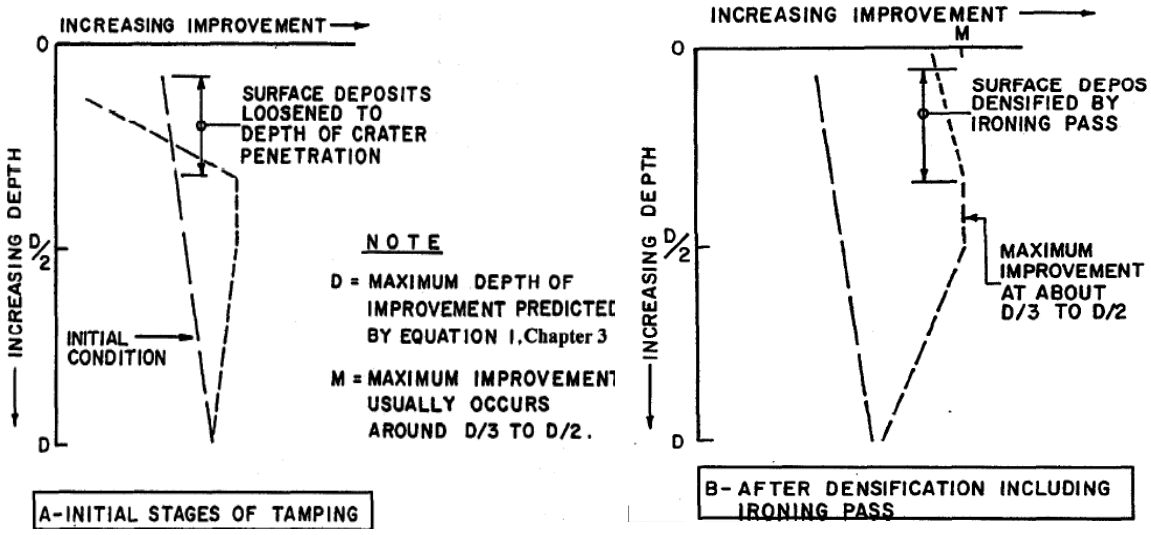

Figure 4.1 Variations in improvements with depth during dynamic compaction (Lukas, 1986)

4.2. COMPARISON OF VERTICAL STRAIN PROFILES

4.2.1. Elastic vertical strains

The ground improvement achieved by compaction must have a relation with the void ratio reduction, soil stiffness, density, and strain profiles at depth. This means that the soil volume changes are directly concerned with the soil improvement. According to the generalized Hook's law, the volume change is given as:

$$\Delta V = (1+\varepsilon_x)dx\cdot(1+\varepsilon_y)dy\cdot(1+\varepsilon_z)dz - dx\cdot dy\cdot dz \qquad (4.1)$$

Expanding the right side and neglecting higher-order terms involving ε_x^2 and ε_x^3, we obtain

$$\Delta V = \left[1 + (\varepsilon_x + \varepsilon_y + \varepsilon_z)\right] dx \cdot dy \cdot dz - dx \cdot dy \cdot dz = \varepsilon_x + \varepsilon_y + \varepsilon_z \qquad (4.2)$$

in which V_o is the initial volume $dx \cdot dy \cdot dz$ and ΔV is the volume change.

The unit volume change e is defined as

$$e = \frac{\Delta V}{V_o} = \varepsilon_x + \varepsilon_y + \varepsilon_z \qquad (4.3)$$

Equation 4.3 shows that the normal strains are more important than the shear strains in the compaction process.

From this perspective, Hansbo (1979) studied that the patterns of ground improvement and vertical strain change with static and dynamic compaction. He noted that the dynamic strain profile is deeper than the static profile as shown in Figure 4.2. He also observed the improved pattern that is the surface looser than the point of maximum compaction occurred.

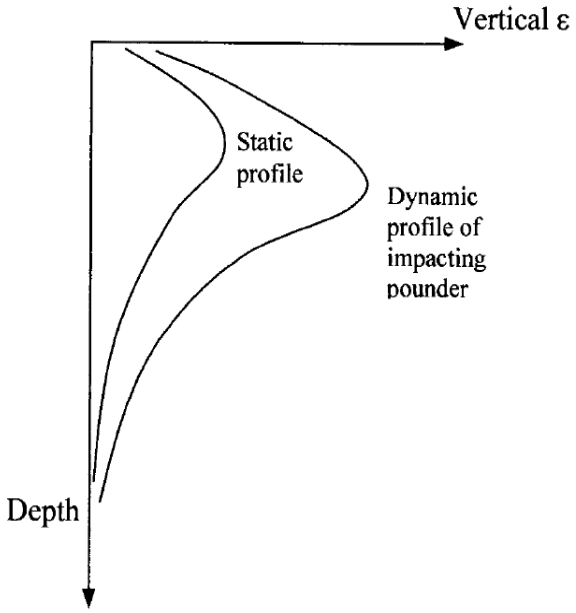

Figure 4.2 Compaction of static and dynamic strain profiles (Hansbo, 1979)

Moreover, Huang (1993) calculated the various strains using elastic equations under the center of a flexible plate loaded by a 25kJ impact compactor. Figure 4.3 shows the vertical strain profile that is similar to Hansbo's results. However, all of the elastic strain returns to zero when the applied loads are removed. It is not enough to understand what happens in the soil under the loads causing the permanent strains.

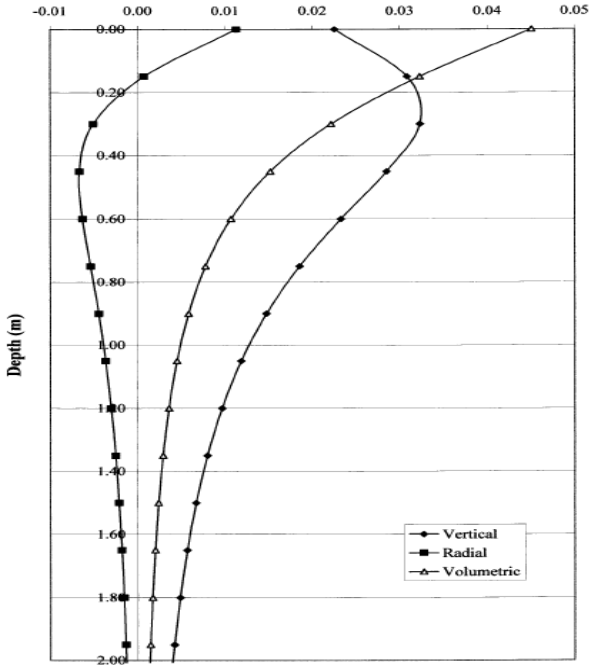

Figure 4.3 Elastic strain under an impact compactor (Huang, 1993)

4.2.2. Elastic-plastic vertical strains

To understand the behavior of soil more accurately, an elastic-plastic analysis was also conducted by using the FLAC (Fast Lagrangian Analysis of Contiuna) finite difference software that allows for the Mohr-Coulomb constitutive model (Berry, 2001). He predicted the vertical strain for various Mohr-Coulomb parameters as shown in Figure 4.4.

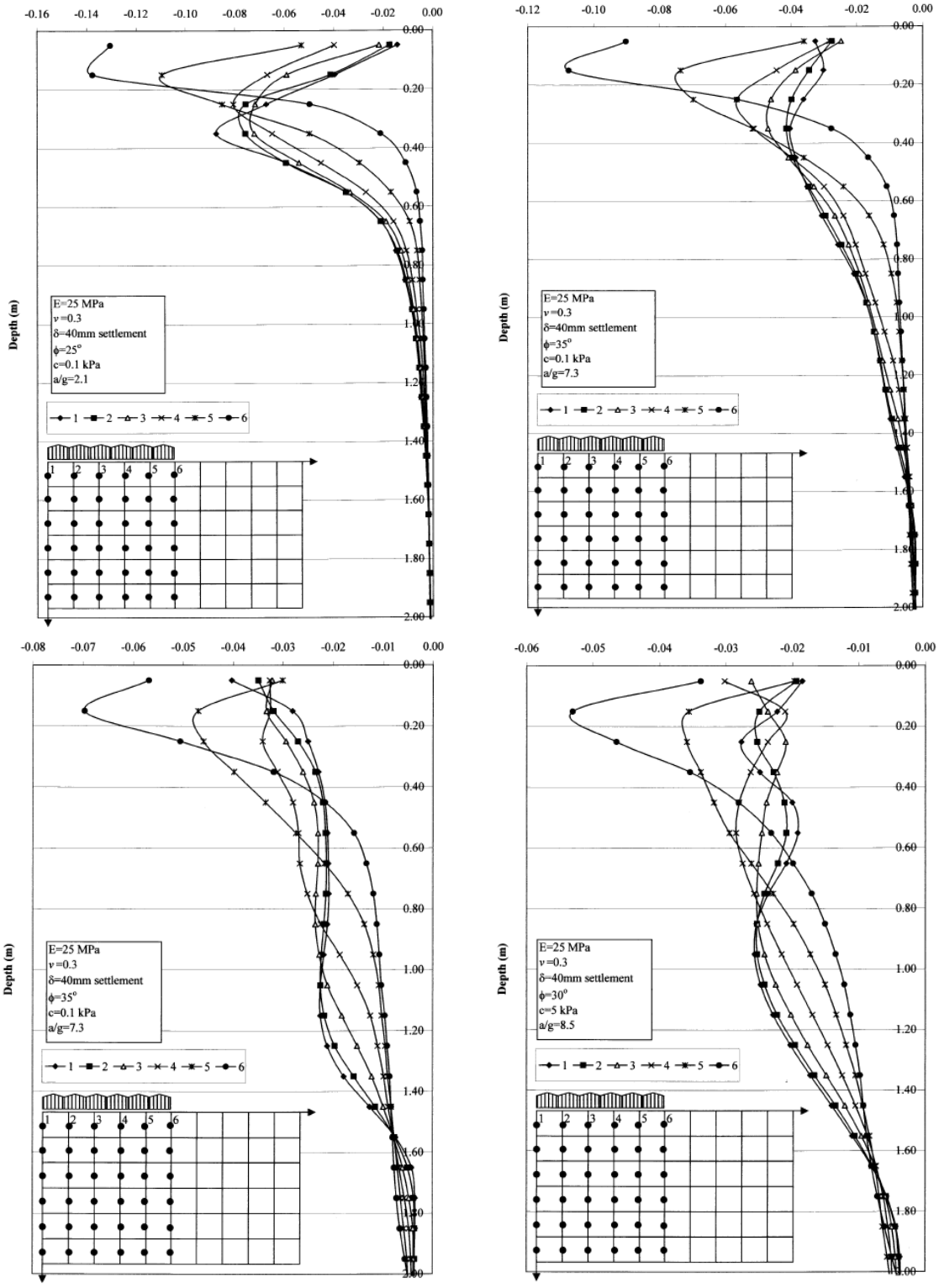

Figure 4.4 Elastic-plastic analysis of vertical strain (Berry, 2001)

4.2.3. Ground improvement profiles in situ

Field testing was also conducted by Wolfgang Wallrath (2004), a Bomag researcher. The test field was prepared for 30 m length and 3 m depth. After its water content was controlled, the excavated soil was mixed, and laid again. The soil properties used in the test bed were the following:

1. Soil type according to DIN 4022: gravel, extremely silty, sandy (DIN 18196),
2. Largest particle size: 90mm,
3. Proctor density: 1,958 g/cm^3,
4. Particle density: 2,685 g/cm^3,
5. Optimum water content: 11.4 %, and
6. Range of water content: 7.0 – 14.5 %.

Two similar types of Bomag rollers, a BW 225 DH-3 Variocontrol with smooth drum and a BW 225 DH-3 Variocontrol with polygonal drum, were used for evaluating ground improvement by measuring the dry density, surface settlement, and SPT N-value. After different numbers of passes, the following characteristics were found. The polygonal drum has a special compaction effect caused by the continuous exchange between the wedge introducing concentrated vertical force and the plate introducing high linear load and shearing force. The shearing forces shift the soil locally so the soil down to 0.5 m remained looser whereas the smooth drum always developed a denser surface than the polygonal one (See Figure 4.5).

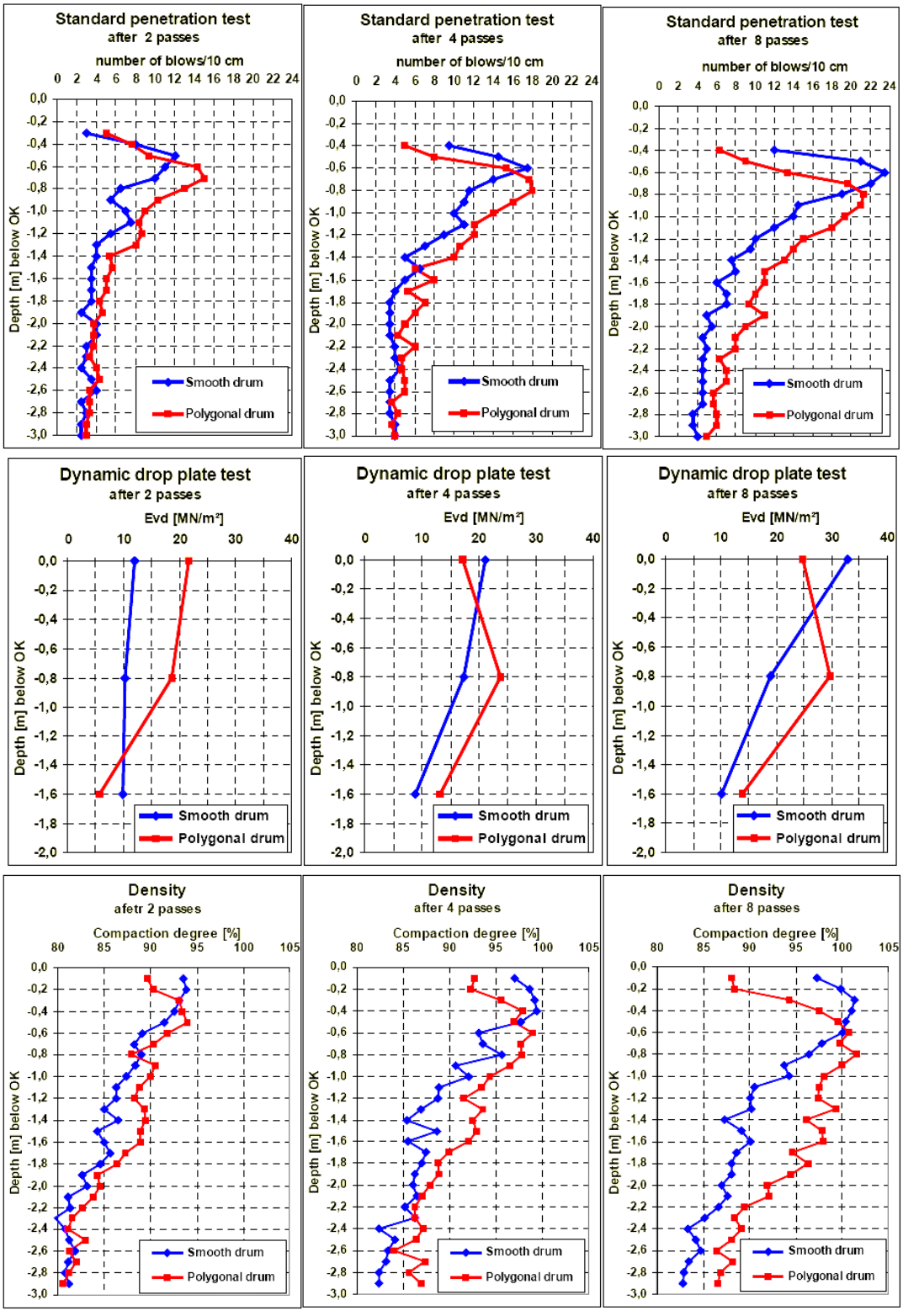

Figure 4.5 Ground improvement profile in-situ (Wallrath. W., 2004)

The other major impact roller manufacturer is Broons. Its roller is also fully used on many land reclamation projects in the world to obtain the necessary degree of compaction and uniformity of the soils. Figure 4.6 illustrates the density improvement, in terms of standard compaction, after 12 passes on a filled site comprising uniform fine sand.

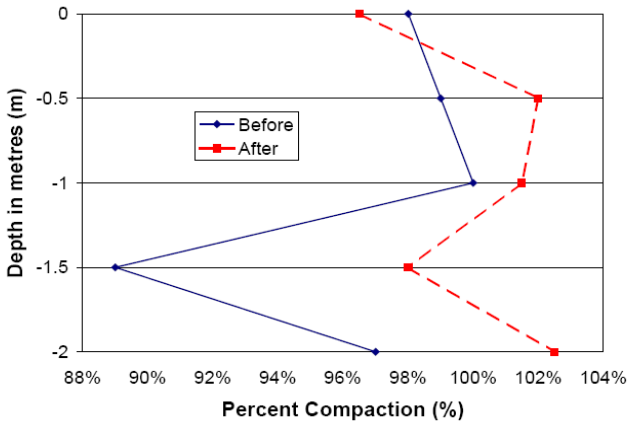

Figure 4.6 Density improvement in sand fill (Avalle, 2004)

In addition, Figures 4.7 and 4.8 show examples of the CPT tip resistance profiles conducted by the Broons researcher on the reclamation fill comprising calcareous sand.

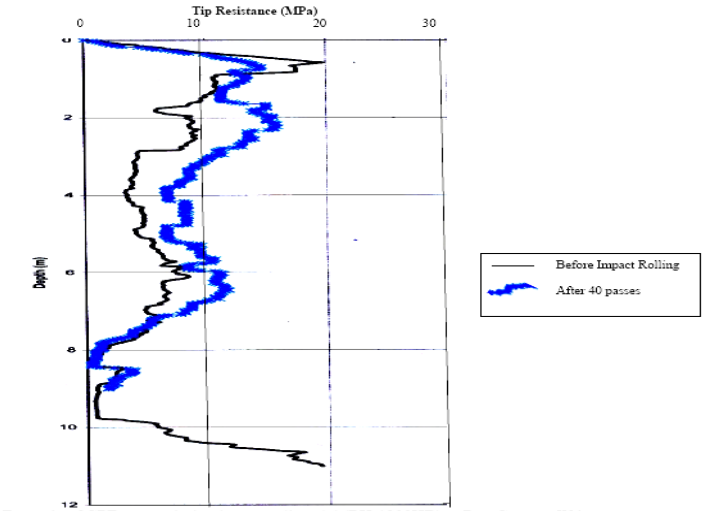

Figure 4.7 CPT test profile during impact rolling using Broons roller (Avalle, 2007)

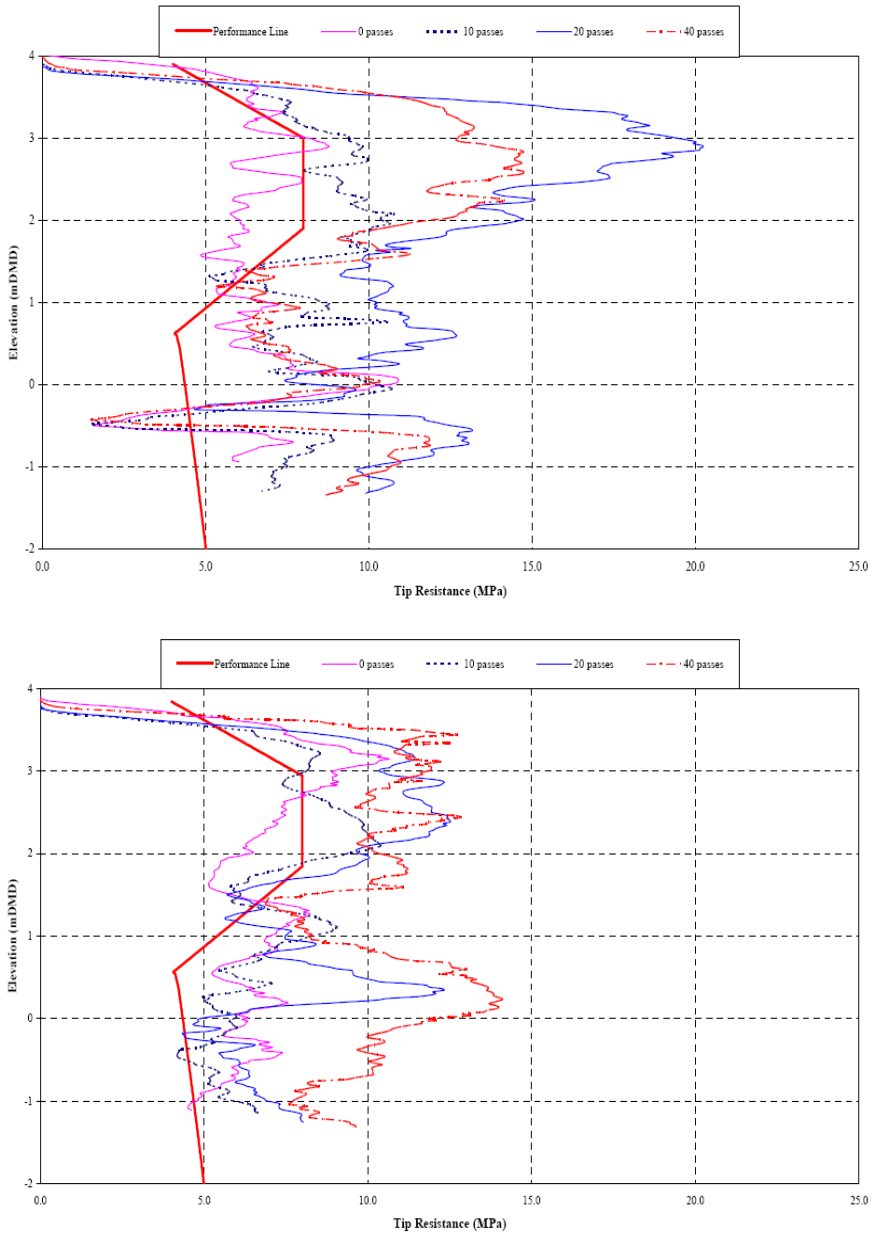

Figure 4.8 CPT test results from Broons compaction projects (Avalle, 2009)

The results show that there is a reduction of density at the surface and a significant improvement down to 0.5m-2m. This looks very similar to the Bomag field data, the pattern of impact compaction soil improvement (Lukas, 1986), and the vertical strain profiles.

4.2.4. Simulated vertical strain profiles

The vertical strain analysis was also undertaken to compare the features of the ground improvement profile beneath the contact area. It confirms that the pattern of compaction is fairly similar to the field measurements (i.e., Bomag, Broons, and Lukas field test results) as well as the behavior noted by Lukas. That is, the vertical strains at the surface achieved by both the impact rollers and the cylindrical roller are smaller than the maximum strain achieved by each one. It can explain why the area down to 0.2-0.5m remained looser. In addition, the depth of influence of strains achieved by the impact rollers is deeper than those by the cylindrical roller. It is clear evidence that the impact rollers are adequate for deep compaction. Figure 4.9 shows simulated vertical strain profiles.

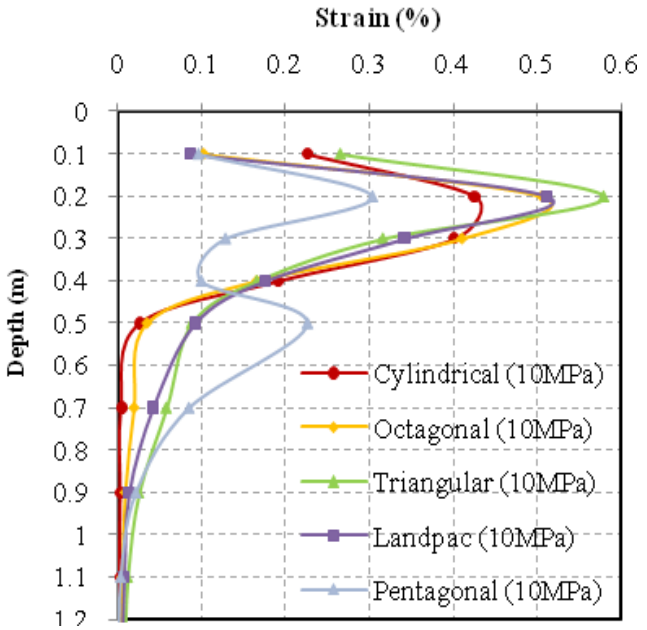

(a) Vertical strain after 1pass in soil = 10MPa

Figure 4.9 Simulated vertical strain profiles

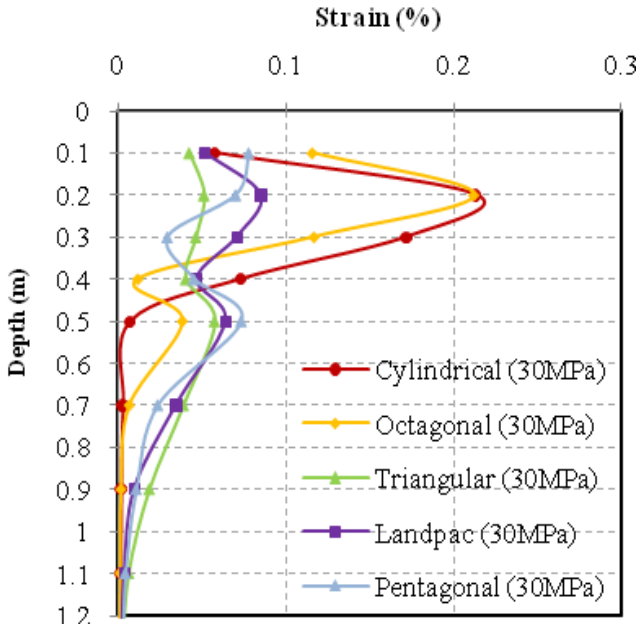

(b) Vertical strain after 1pass in soil = 30MPa

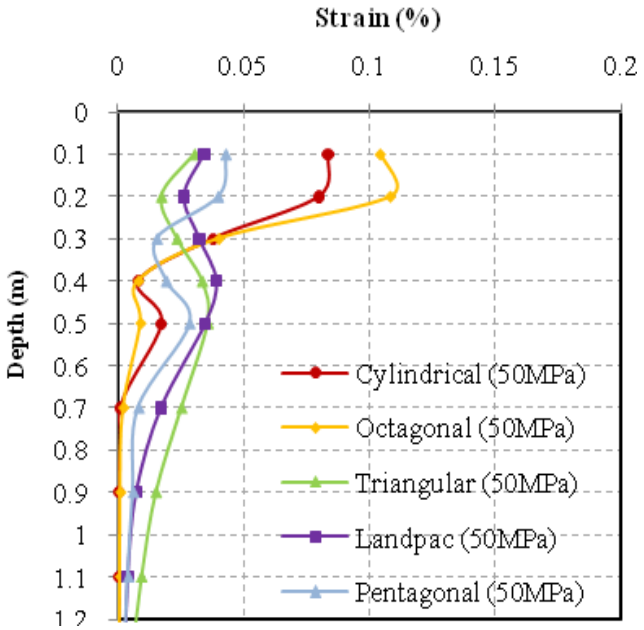

(c) Vertical strain after 1pass in soil = 50MPa

Figure 4.9 continued

From the above comparison, the following conclusions are clearly evident:

1. The numerical simulation shows reduced strain just below the drum due to the dilation of the horizontal direction and frictional restraint (See Figure 4.10). This results in a peak in the strain profile down to 0.2m-0.5m. This looks remarkably similar to the Bomag and Broons field data (See Figures 4.5 to 4.8) and the pattern of the dynamic compaction profile as shown in Figure 4.1. It is a common feature of impact compaction that requires final compaction with a cylindrical smooth roller.

2. The stronger material has a deeper peak in the strain profile.

3. The weaker material has a greater strain near the surface

Consequently, the vertical strain profile is valuable to evaluate the soil model and the key feature is found under the compaction load (i.e., "S" shape vertical strain profile) although the real behavior is complex.

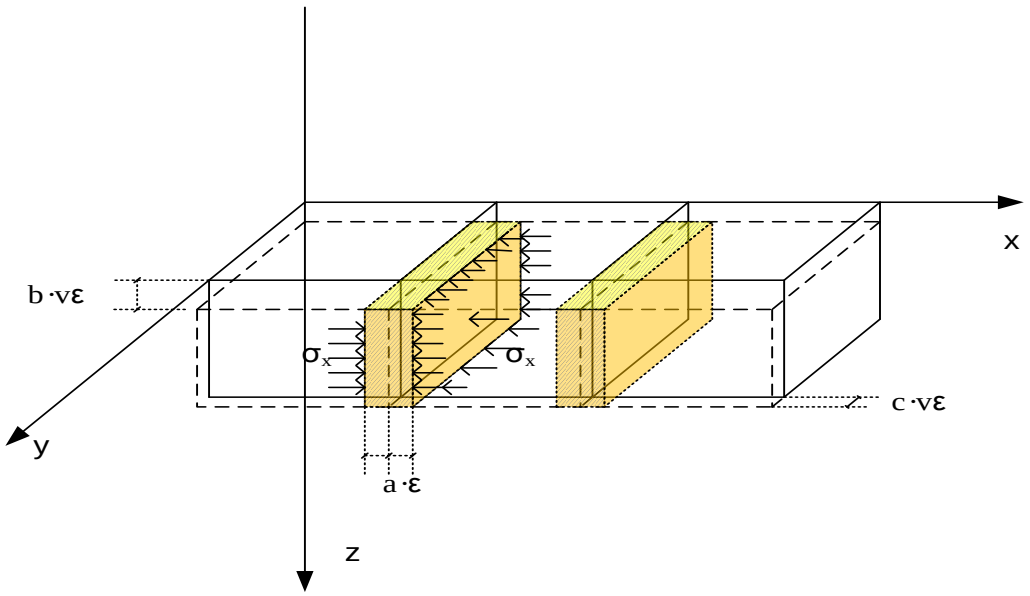

Figure 4.10 Soil dilations and frictional restraints of horizontal direction prevent compaction beneath the drum

4.3. COMPARISON OF SURFACE SETTLEMENTS

One of the main factors to figure out the ground improvement is settlement. The relationship between the surface settlements and soil density was found by Forssblad (1980). Figure 4.11, re-plotted by Berry (2001) with the x-axis on a natural scale instead of a log scale, illustrates this relation.

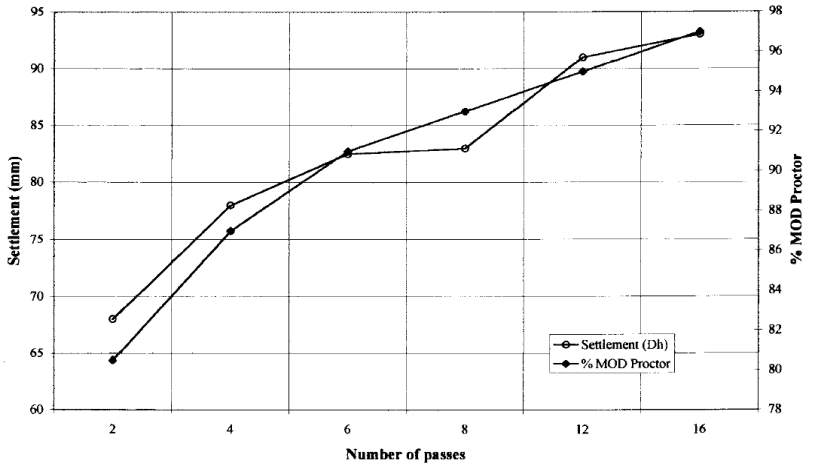

Figure 4.11 The relation between surface settlement and density (Berry, 2001)

From this relationship between the surface settlement and density, it is clear that the bigger settlement leads to the denser results. In this study, surface settlements are also compared with the field data. The Bomag company has the surface settlement data measured by Wolfgang Wallrath (2004), a Bomag researcher.

As a result, the polygonal drum has a greater depth effect and surface settlement. In the first pass, the settlement caused by the polygonal drum is higher than by the smooth drum. However, the increment of settlement gradually converged (See Figure 4.12).

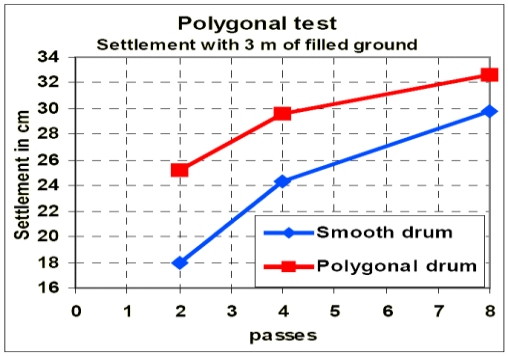

Figure 4.12 The comparison of settlement with polygonal and smooth rollers (Wallrath. W., 2004)

The Broons company also carried out the field test to evaluate the performance of their impact roller and develop the design and specification for earthworks on approximately 7m of filling site primarily comprising clay, sandstone, shale, and other material including metal, ash, glass, and concrete, etc. Figure 4.13 plots the average settlement versus the number of impact roller passes.

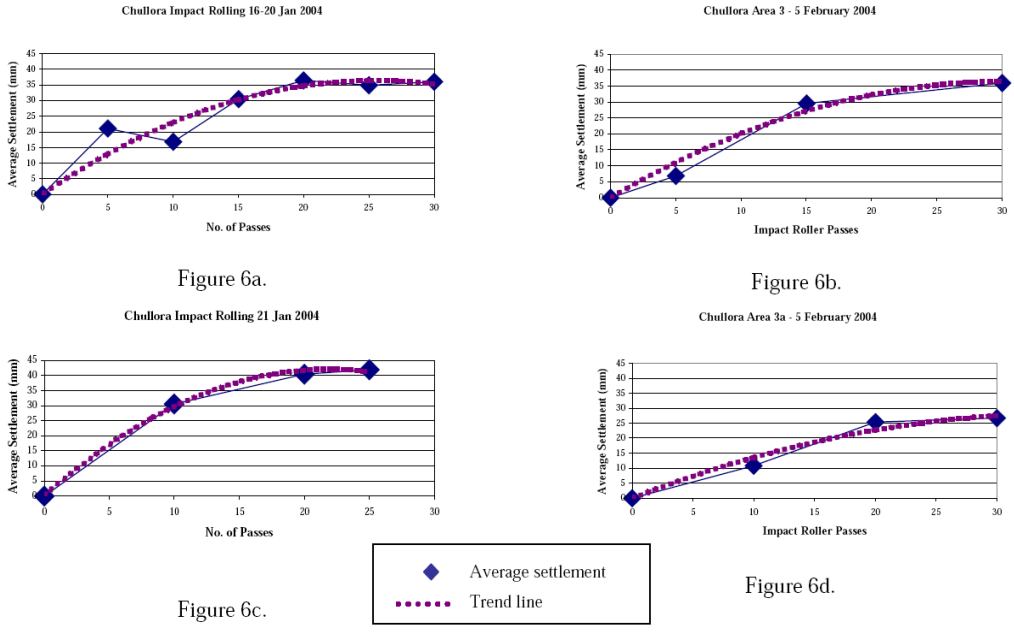

Figure 4.13 Surface settlement measurement using Boons impact roller (Avalle, D. and Young, G., 2004)

As can be seen in Figure 4.13, the polynomial trend lines illustrate the reduction in the rate of settlement. It is an evident trend that the settlement generally reduced significantly as the ground is getting harder.

The surface settlement analysis was also performed to compare the compaction results between the field data and the predicted simulation data. Accordingly, a higher settlement was achieved by the impact roller than by the static one, but the increment of settlement reduced when the ground is getting harder. Figure 4.14 shows the accumulated settlement results during simulation.

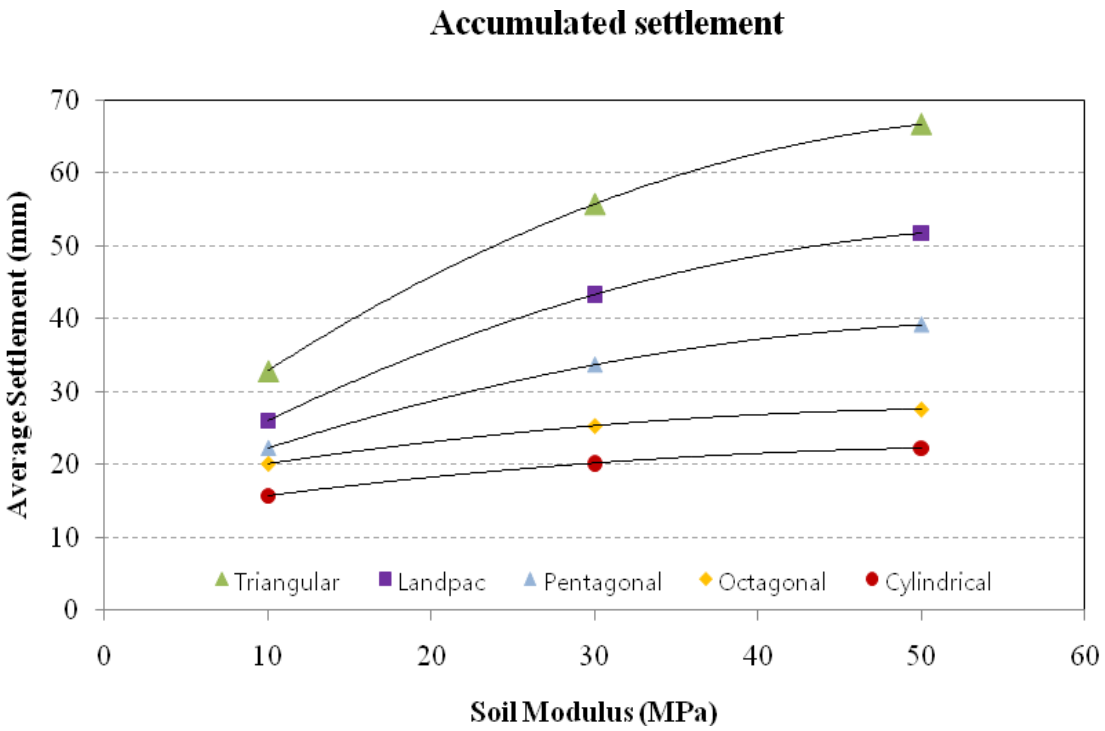

Figure 4.14 Comparison of simulated settlement results for different soil types

As can be seen in Figure 4.14, the cylindrical and octagonal rollers' efficiency were reduced significantly after the soil modulus is 50MPa. This pattern is also observed

in the Bomag field experiment data. It indicates that the impact rollers can get harder, denser, and/or stiffer compaction results, and these are more appropriate to heavier construction fields, such as land reclamation.

Consequently, these simulation results prove the advantage of impact rollers. The impact rollers can guarantee the sufficient compaction of the soil layer by dense, stiff, and hard compaction results.

4.4. COMPARISON OF VERTICAL STRESS PROFILES

In addition to the vertical strain and the surface settlement, the contact stress between the roller and the ground has a great influence on the ground improvement. Estimates of contact stress were the first things to evaluate the ground improvement. Unfortunately, there is no guidance found on how to calculate the applied impact stress for an impact roller.

However, Rinehart et al. (2008) stated that the vertical stress is only weakly influenced by constitutive parameters such as the modulus and Poissons ratio, and the Hertzian contact theory exhibits good agreement with the experimentally measured stress data. For that reason, the Hertzian contact solution for a cylinder in contact with homogeneous and isotropic material can be used to find the relationship between the vertical stress and depth. Theoretical Hertzian contact solutions are given by

$$\sigma_z = p_o \frac{a}{\sqrt{a^2+z^2}} \tag{4.4}$$

$$p_o = \frac{2P}{\pi a} \tag{4.5}$$

where, p_o is the maximum normal contact stress at the surface,

P is the load per unit drum length applied at the cylinder and soil interface,

a is the half contact width between the cylinder and the soil, and

z is the depth below the surface.

To obtain the theoretical vertical stress profiles, the unknown contact width 2a was calculated from the surface deformation of the simulation as shown in Figure 4.15.

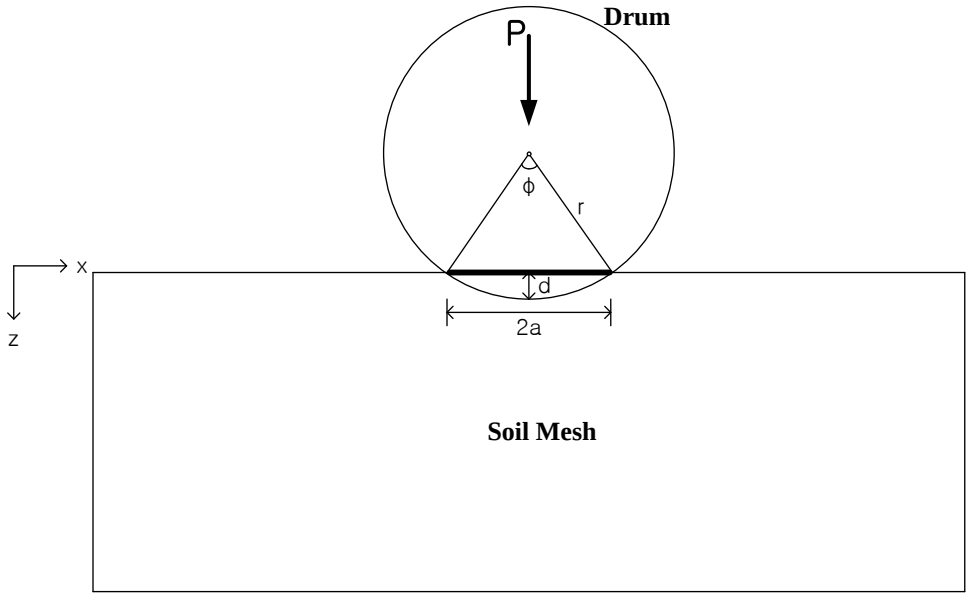

Figure 4.15 Hertzian contact theory

The relation between surface deformation d and contact width 2a is given by:

$$a = r \sin\frac{\phi}{2} \tag{4.3}$$

where $\phi = 2\cos^{-1}\left(\frac{r-d}{r}\right)$, and

d is the surface deformation and r is the radius of the drum.

The applied force P was set equal to the contact force between the drum and the soil in the model. After comparing the analytical solution and simulation results, the profiles of the vertical stress have good agreement during the roller passes. Figure 4.16 shows the comparison of the analytical solution using the Hertzian theory and simulation results.

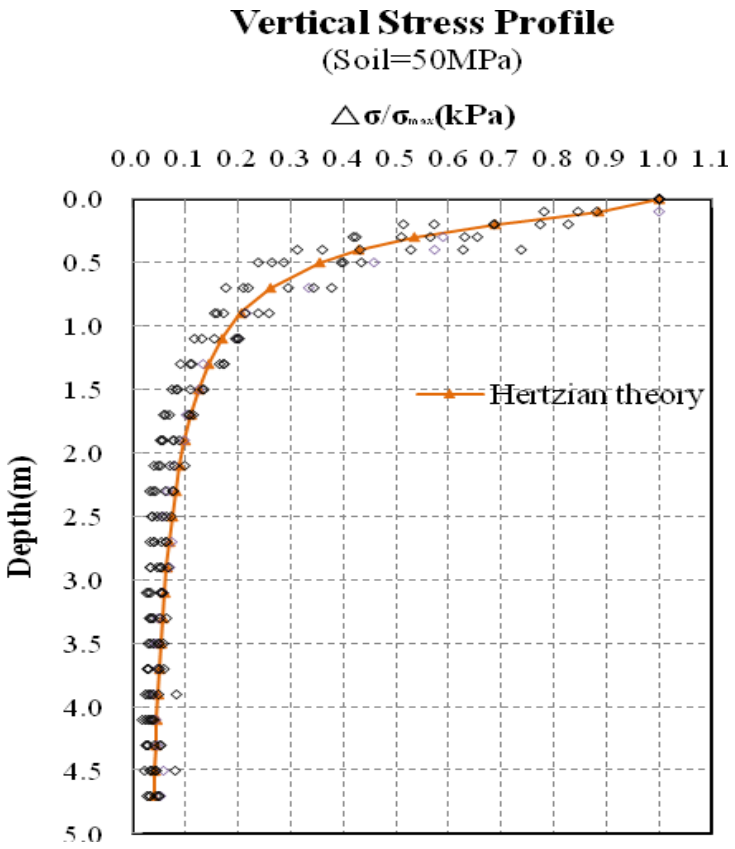

Figure 4.16 The comparison between the theoretical solution and simulation results for vertical stresses

On the other hand, there are few field data related to the vertical stress profile to study the ground improvement under the impact roller. Figure 4.17 shows the vertical stresses under the roller, which was measured by Bomag. These field data have a good

agreement with the simulation results. In other words, the maximum stress occurred just below the drum and then reduced gradually. It also has an agreement with elastic, pressure bulb, and Boussinesq's theories. Figure 4.17 illustrates the vertical stresses profile measured by Bomag. Details not presented below are attached in APPENDIX B.

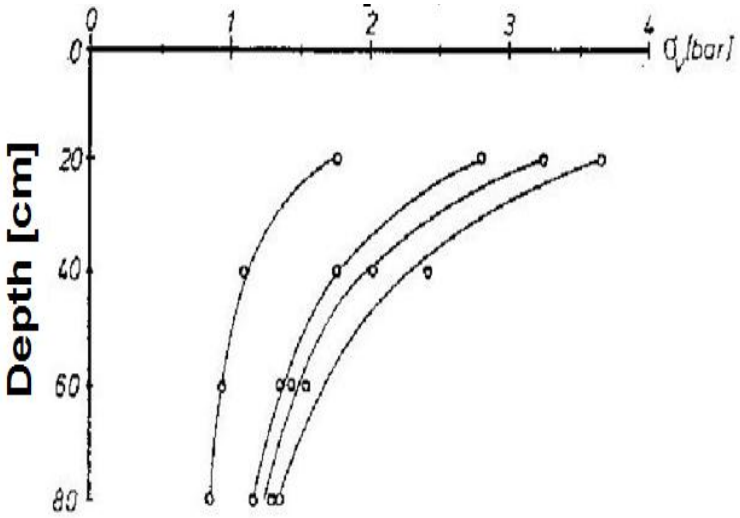

(a) Vertical stresses for increasing compaction

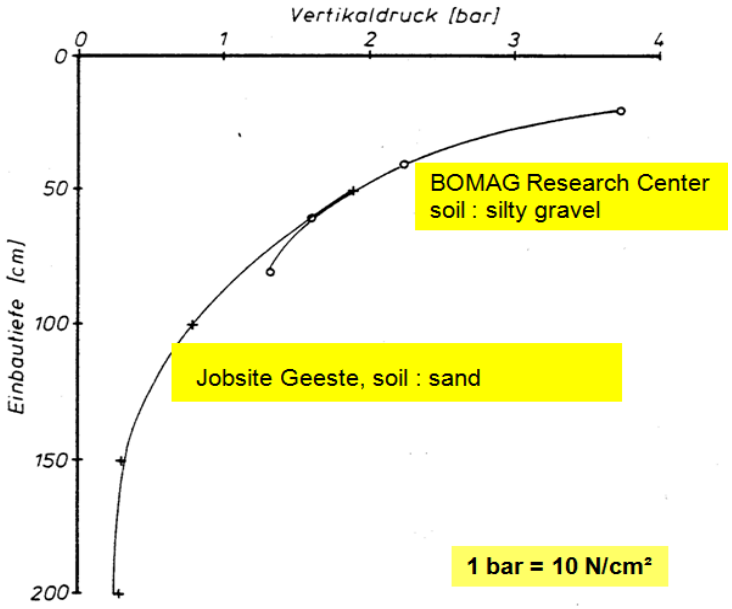

(b) Vertical stresses under the roller

Figure 4.17 Vertical stresses profile (Bomag research center-unpublished data)

5. CONCLUSIONS

In this study, the numerical simulation was conducted to characterize the behavior of the impact roller compaction and to demonstrate the impact rollers are suitable for thick lifts. To do so, the Druker-Prager constitutive model was applied to calculate the vertical stress profile (i.e., the depth of influence), the vertical strain, and surface displacements.

In developing such an impact compaction model, the effect of wave absorption and reflection, water table within the zone of influence of the compaction, and the effect of a layering would need to be considered. However, the purpose of this study is making the direct comparison between the impact roller shapes and the depths of influence; thus, these effects have not been considered in this model. The results obtained from this research are presented in the following conclusions:

1. The width of the contact area between the drum and the soil controls the depth of compaction. The softer the soil is, the deeper the roller sinks in the soil, the wider the contact area is, and the deeper the compaction is. Therefore, the depth of compaction depends on the stiffness of the soil.

2. The surface pressure controls the degree of compaction. This pressure is higher for the impact rollers than for the cylindrical rollers due to the dynamic effect. Yet, the distribution of the pressure is much more uneven for impact rollers than for cylindrical rollers.

3. The depth of compaction is larger for impact rollers because they impart

higher stresses which increase the penetration of the roller drum into the soil thereby increasing the width and therefore depth of influence.

4. It is also possible that the increase depth of influence is due to wave propagation during the impact. These waves can propagate much deeper than the typical depth of influence for static loading.

5. The loosening effect of the surface is more prominent for the impact rollers than for the cylindrical rollers.

Based on the conclusion reached, it appears optimum to;

Compact first with an impact roller and use several passes to minimize the extent of the areas between impacts. Finish by using a cylindrical smooth roller to optimize the compaction of the shallow layers. This process combines the benefits of both types of rollers: compaction of the deep layers (0.5 to 1.5 m) with the impact roller but loosening of the shallow layers (0 to 0.5 m) followed by compaction of the shallow layer (0 to 0.5 m) with the cylindrical roller without disturbing the deep layers.

For the above mentioned reasons, this research demonstrates that the impact rollers are appropriate for difficult to compact soils and thick layers even though these are required for final compaction with a cylindrical smooth roller.

REFERENCES

Adam, D. and Kopf F. (2000). "Sophisticated Compaction Technologies and Continuous Compaction Control." *European Workshop Compaction of Soils and Granular Materials*, Presses Ponts et Chaussées, Paris, France.

Ammann (http://www.ammann-group.com/Pneumatic-tyred-rollers.4677+M52087573ab0.0.html). Jan. 8th, 2010.

Avalle, D.L. (2004). "Ground improvement using the 'square' impact roller-case studies." *5th Int. Conf. on Ground Improvement Techniques*, Kuala Lumpiur., 3-4.

Avalle, D.L., and Young, G. (2004). "Trial programme and recent use of the impact roller in Sydney." *Australian Geomechanics Society Earthworks Seminar*. Adelaide. 2-4.

Avalle, D.L. (2007). "Trials and validation of deep compaction using the 'square' impact roller." *Austrian Geomechanics Society Sydney Chapter Mini-Symposium: Advances in Earthworks*. Sydney. 2-5.

BCD. (2008). User's manual. Texas A&M Univ., College Station, Texas, 3-14.

Berry A. (2001). "Development of a volumetric strain influence ground improvement prediction model with special reference to impact compaction." M.E. Dissertation, Pretoria Univ., Pretoria.

Bomag research center. (2009). *Unpublished field data on trial undertaken at the Geeste/Emsland*, Germany.

Bomag (http://www.bomag.com/ext_resource/americas/heavy/BW213D40_4pg.pdf). Jan. 8th, 2010.

Bowles, Josepth E. (1997). *Foundation analysis and design fifth edition.* McGraw-Hill, New York, pp 125.

Briaud, J.-L., Li,Y., and Rhee,K., (2006). "BCD: A soil modulus device for compaction control." *J. Geotech. Geoenviron. Eng.*, 132(1), 108-115.

Briaud, J.-L. (2001). *Introduction to soil moduli.* Geotech. News, BiTech Publisher, Richmond, B.C., Canada.

Broons (http://www.broons.com/impact/broons_impact.pdf). Jan. 8th, 2010.

Chen, W.F., and Baladi, G. Y. (1985). *Soil plasticity*. Developments in Geotechnical engineering, Volume 38. Elsevier, Amsterdam.

Chen, W. F., and Saleeb, A. F. (1982). *Constitutive equations for engineering materials. Volume 1: Elasticity and modeling*. John Wiley & Sons, New York, New York.

Dynapac (http://www.dynapac.com/en/Products/?cat=10&product=418). Jan. 8th, 2010.

Forssblad, L. (1980). "Compaction meter on vibrating rollers for improved compaction control." *Proc., Int. Conf. on Compaction*, Volume: II, Paris. 541-546.

Hansbo, S. (1979). "*Dynamic consolidation of soil by a falling weight. Ground Engineerin*g." Emap construct., 12(1), 27-36.

Landpac (http://www.landpac.co.uk/). Jan. 8th, 2010.

LS-DYNA. (2006). LS-DYNA Theory manual. Livermore Software Technology Corporation (LSTC). Livermore, California.

Lukas, R.G. (1986). "Dynamic compaction for highway construction. Volume1: Design and construction guidelines." Federal Highway Admin., *Rep. No. FHWA/RD86/133*.

Johnson, A. W. and Sallberg, J.R. (1960*).* " Factor that Influence Field Compaction of soils: Compaction Characteristics of Field Equipment," Bulletin 272. Highway Research Board, National Academy of Science – National Research Council. Washington, D.C.

NAVFAC DM 7.02. (1986). "Foundation and Earth Structures, design Manual DM 7.02." *Naval Facilities Engineering command, Department of the Navy*. Alexandria, VA.

Paige-Green P. (1998). "The use of impact compaction in ground improvement." *Report CR-97/098 (prepared for Landpac)*, CSIR, Pretoria.

Peurifoy, R.L. and Ledbetter, W.B. (1985). *Construction Planning, Equipment, and Methods,* 7th edition. McGraw-Hill. New York, New York. 20-56.

Proctor, R. R. (1933). "The Design and Construction of Rolled Earth Dams." *Engineering News Record*. 111: 245-248, 286-289, 348-351, 372-376

Rinehart, R.V., Mooney, M.A & Derger, J.R. (2008). "In-ground stress-strain beneath center and edge of vibratory roller compactor". Advances in Transportation Geotechnics: *Proc. 1st Int. Conf. Transport. Geotech.*, Nottingham, 737-741.

Turnbull, W.J. and Foster, C.R. (1956). "Stabilization of Materials by Compaction." *J. Soil Mechanics and Foundation Division*, ASCE, 82(SM2). 1-23.

Wallrath, W. (2004). "Depth effect of the POLYGONAL drum results from the compaction test on a 3 m filling." *Research Report*, BOMAG GmbH, Germany.

Wang, S et al. (2006). "Discussion on the use of parameters of Druker-Prager criterion." *J. the Key eng. materials,* vols. 306-308, 1449-1454

APPENDIX A

COMPACTION EQUIPMENT AND METHOD (NAVFAC DM-7.02 Table 5)

APPENDIX A. Compaction Equipment and Methods (NAVFAC DM-7.02 Table 5)

Equipment types	**Applicability**	**Requirements for compaction of 95 to 100 percent Standard Proctor maximum density**			**Possible variations in equipment**
		Compacted lift thickness. in	Passes or coverages	Dimensions and weight of equipment	
Sheepsfoot Rollers	For fine-grained soils or dirty coarse-grained soils with more than 20% passing No. 200 sieve. Not suitable for clean coarse-grained soils. Particularly appropriate for compaction of impervious zone for earth dam or linings where bonding of lifts is important.	6	4 to 6 passes for fine-grained soil. 6 to 8 passes for coarse-grained soil.	Soil type / Foot contact area(ft^2) / Foot contact pressures psf Fine-grained soil PI>30: 5 to 12: 250 to 500 Fine-grained soil PI<30: 7 to 14: 200 to 400 Coarse-grained soil: 10 to 14: 150 to 25- Efficient compaction of soils wet of optimum requires less contact pressure than the same soils at lower moisture contents.	For earth dam, highway and airfield work, articulated self propelled rollers are commonly used. For smaller projects, towed 40 to 60inch drums are used. Foot contact pressure should be regulated so as to avoid shearing the soil on the third or fourth pass.
Rubber-tire Roller	For clean, coarse-grained soils with 4 to 8% passing the No. 200 sieve. For fine-grained soils or well graded, dirty coarse-grained soils with more than 8% passing the No. 200 sieve.	10 6 to 8	3 to 5 coverages 4 to 6 coverages	Tire inflation pressure of 35 to 130 psf for clean granular material or base course and subgrade compaction. Wheel load 18,000 to 25,000lbs. Tire inflation pressure in excess of 65 psi, for fine-grained soils of high plasticity. For uniform clean sands or silty fine sands, use large size tires with pressures of 40 to 50 psf.	Wide variety of rubber tire compaction equipment is available. For cohesive soils, light-wheel loads, such as provided by wobble-wheel equipment, may be substituted for heavy-wheel load if lift thickness is decreased. For granular soils, large-size tires are desirable to avoid shear and rutting.
Smooth wheel Rollers	Appropriate for subgrade or base course compaction of well-graded sand-gravel mixtures. May be used for fine-grained soils other than in earth dams. Not suitable for clean well-	8 to 12 6 to 8	4 coverages 6 coverages	Tandem type rollers for base course or subgrade compaction 10 to 15 ton weight, 300 to 500 lbs per lineal in. of width of rear roller. 3-wheel roller for compaction of fine-grained soil; weights from 5 to 6 tons for materials of low plasticity to 10 tons for materials of high plasticity.	3-wheel rollers obtainable in wide range of sizes. 2-wheel tandem rollers are available in the range of 1 to 20 ton weight. 3-axle tandem rollers are generally used in the range of 10 to 20 tons weight. Very heavy rollers are used for proof rolling of subgrade or base course.

APPENDIX A (continued) Compaction Equipment and Methods

Equipment types	Applicability	Requirements for compaction of 95 to 100 percent Standard Proctor maximum density			Possible variations in equipment
		Compacted lift thickness. in	Passes or coverages	Dimensions and weight of equipment	
Vibrating sheetsfoot rollers	For coarse-grained soils sand-gravel mixtures	8 to 12	3 to 5	1 to 20 tons ballasted weight. Dynamic force up to 20 tons.	May have either fixed or variable cyclic frequency.
Vibrationg smooth drum rollers	For coarse-grained soils san-gravel mixture-rock fills	6 to 12 (soil) to 36 (rock)	3 to 5 4 to 6	-do-	-do-
Vibrating baseplate compactors	For coarse-grained soils with less than about 12 % passing No. 200 sieve. Best suited for materials with 4 to 8 % passing No. 200 sieve placed thoroughly wet	8 to 10	3 coverages	Single pads or plates should weigh no less than 200 lbs. may be used in tandem where working space is available. For clean coarse-grained soil, vibrations frequency should be no less than 1,600 cycles per minute.	Vibrating pads or plates are available, hand-propelled, single or in gangs, with width of coverage form 1-1/2 to 15 ft. various types of vibrating-drum equipment should be considered for compaction in large areas.
Crawler tractor	Best suited for coarse-grained soils with less than 4 to 8 % passing No. 200 sieve, placed thoroughly wet.	6 to 10	3 to 4 coverages	Vehicle with “standard” tracks having contact pressure not less than 10 psf.	Tractor weight up to 85 tons
Power tamper or rammer	For difficult access, trench backfill. Suitable for all inorganic soils	4 to 6 in. for silt or clay, 6in. for coarse-grained soils.	2 coverages	30-lb minimum weight. Considerable range is tolerable, depending on materials and conditions.	Weighs up to 250 lbs., foot diameter 4 to 10 in.

APPENDIX B

BOMAG UNPUBLISHED FIELD DATA

BOMAG
FAYAT GROUP

Stress measurements for increasing compaction depending on depth; BOMAG compaction research center

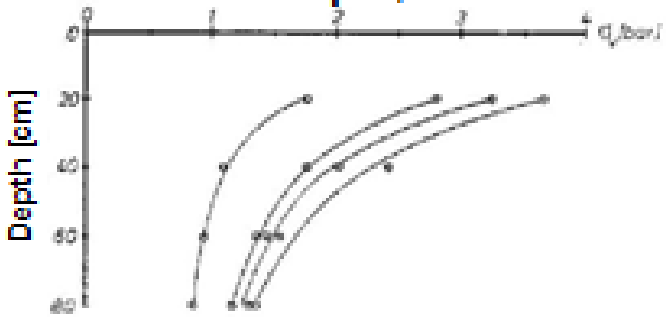

Vertical stresses for increasing compaction

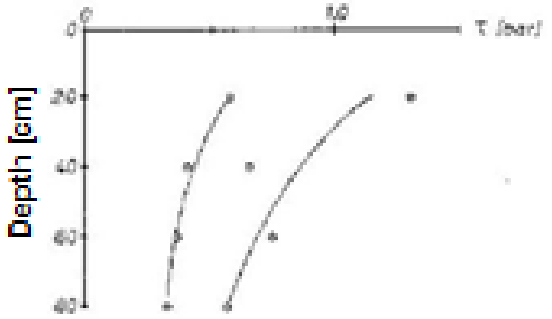

Shearing stresses for increasing compaction

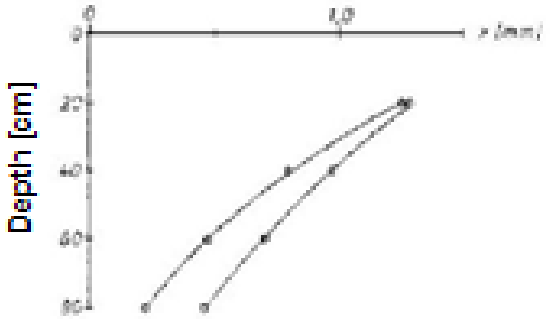

Vertical amplitude for increasing compaction

Compaction equipment: BW 212 D,
(10 t single drum roller ; 1,9mm amplitude)

soil : silty gravel

BOMAG
FAYAT GROUP

Jobsite measurement , sand , U < 5

Geeste / Emsland, Germany

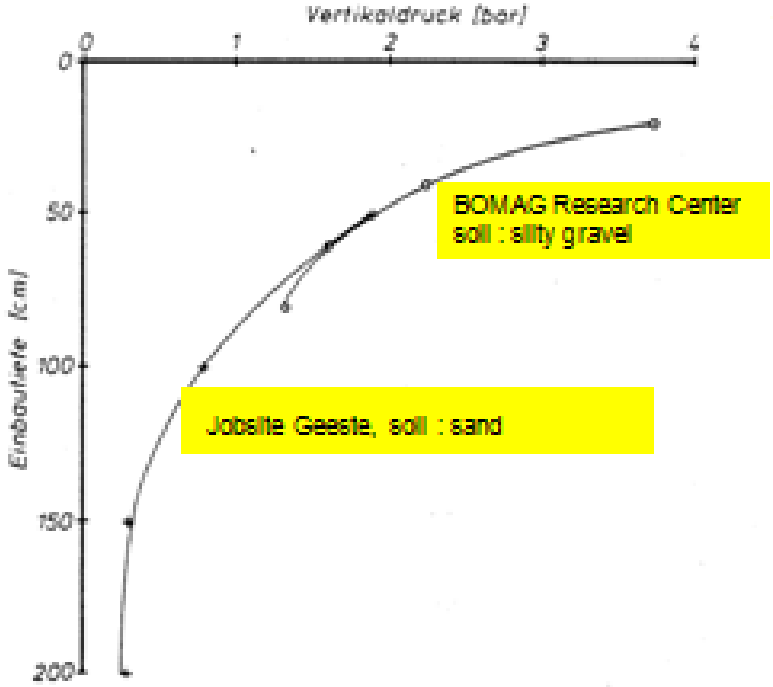

depth cm			
300	21 12	0,22 0,20	0,022 0,021
120	21 12	0,22 0,22	0,042 0,029
100	21 12	0,20 0,19	0,044 0,031
20	21 12	- 1,89	- 0,128
(cm)	(mm) (in)	(psf)	(mm)

measurement values taken from Geeste jobsite

roller: BW 212 D, 10 t
(single drum roller)

Vertical stresses at for increasing compaction

1 bar = 10 N/cm²

VITA

Kukjoo Kim received a Bachelor of Engineering degree in the Department of Civil Engineering from the Korea Military Academy, Korea, in March 2001. He was then commissioned as an Engineering Officer in 2001. He further served as a Platoon Leader as well as a Construction Officer in the 51st Division Engineering Battalion. After training for the O.A.C. (the Officer Advanced Course), while in service as a logistic officer in the Engineering Battalion, Division 1, he volunteered to be dispatched in Iraq and served as a project manager in a Civil - Military Cooperation, set up to rebuild the area in Erbil. After that, he joined the Zachry Department of Civil Engineering at Texas A&M University in August 2008 and received his M.S. degree in August 2010. His research interests are intelligent compaction, specializing in impact rollers.

He can be reached at

Name: Kukjoo Kim, P.E.

Address: Department of Civil Engineering Texas A&M University 3136 TAMU
College Station, Texas 77843-3136

Email Address: Klaus.jkim@gmail.com

Education: B.E., Civil Engineering, Korea Military Academy, 2001
M.S., Civil Engineering, Texas A&M University, 2010